CHARACTERIZING CORNEAL BIOMECHANICAL PROPERTIES USING DYNAMIC OPTICAL COHERENCE ELASTOGRAPHY

By

Srilatha Vantipalli, B.S.

DISSERTATION

In partial satisfaction of the requirements for the degree of

DOCTOR OF PHILOSOPHY

in

PHYSIOLOGICAL OPTICS

Presented to the Graduate Faculty of the

College of Optometry
University of Houston

August, 2016

Approved:

Michael Twa, O.D, Ph.D. (Chair)

Alan Burns, Ph.D.

Jason Marsack, Ph.D.

Kirill Larin, Ph.D.

William Miller, O.D, Ph.D.

Committee in Charge

Dedication

My family

Acknowledgements

I would like to acknowledge everyone who has assisted me throughout my doctoral studies over the past 5 years. I would like to start by thanking my advisor, Dr. Michael Twa for being the best mentor I could ever ask for. When I first started out with Dr. Twa, I did not know something as basic as to where to begin and what to look for, while reading a scientific paper. I am grateful you took me in as your student despite that. From being able to think independently and critically, conduct experiments, perform analyses, write abstract, grants, manuscripts, while the list is never ending, I truly appreciate you teaching me everything. At the end of these five years, I can say that everything I know I owe it to you. You have set an example of excellence as a scientist and a role model. Your positive energy and passion towards science is beyond amazing and infectious. I admire your way of instigating students to think independently but also being there whenever help was needed. I thank you for being most patient with me throughout this journey and for your insightful feedback at every step of the way.

I would like to thank Dr. Laura Frishman for your continuous support throughout the program. I will always be in awe of the number of things you handle and still keep track of every graduate student at all times. I particularly admire your ability to pat on the back while also giving the nudge to do better at the same time.

I would like to extend my special thanks to Dr. Kirill Larin and all his lab members. I started working with Dr. Shang Wang but I would like to particularly thank Jiasong Li and Manmohan Singh for helping me through all the long experiments often exceeding 24 hrs. The light atmosphere in your lab made performing long experiments a fun experience. I thank you for all your inputs and feedback with the experiments and manuscripts.

I would like to thank Dr. Alan Burns for teaching and helping me with experiments involving the electron microscope and the deconvolution microscope. I thank you for your inputs and valuable feedback at different stages of my dissertation.

I would like to thank Dr. Jason Marsack and Dr. William Miller for agreeing to serve on my dissertation committee. I truly appreciate all of their time and assistance as I navigated this process.

I would also like to extend my thanks to Dr. Diana Lozano, who was my first and only lab mate. You taught me several little things in the beginning that turned out to be really important and helpful in the long run. I really enjoyed working alongside you, Diana and missed you immensely towards the end. I would also like to mention that through this program I have made some friends for life whom I would like to thank too: Aubrey Hargrave, Sri Magadi, Elda Rueda. We started at the same time, made the journey together and it gives me immense happiness to take the graduation walk together with all of you to commemorate our journey. I would like to thank our summer research students: Brodie S DeJernett, Betty Zhang and Kevin Soong for their help with my work.

I wish to thank Chris Keuther, Charles Neff, John Bauer and Margaret Gondo for helping me with their technical expertise at several stages during this journey. I would also like to thank the UHCO graduate student managers who helped manage all my administrative aspects: Michele Stafford, Diana Davis and Renee Armacost and the librarians: Suzanne Ferimer and Pamela Forbes for their ever-ready assistance through the years.

I would like to thank my parents for giving me the confidence, support and faith to let me follow my dreams. I will forever be indebted to my brother, Ravi for believing in me and encouraging me to move across countries to pursue graduate studies in the US. You have assisted me every step of the way, from preparing applications to the PhD program until the extra nudge to complete at the very end. I thank you for everything,

especially for telling me what I needed to hear to get me through my moments of doubt. Finally, I want to thank my husband, Raja for always being there as a buffer and facilitating every little thing I needed, particularly giving me the space and abundant time required to complete his arduous journey, while being patient throughout. I would like to mention a special thanks to my in-laws for their constant support through these years from the time they knew me.

I could not have completed my research without the support of all these wonderful people!

The work presented in this dissertation was supported by: NIH/NEI R01-EY022362, NIH/NEI P30 EY07551, NIH/NEI T35EY00708 and University of Houston College of Optometry Student Vision Research Support Grant-2014.

CHARACTERIZING CORNEAL BIOMECHANICAL PROPERTIES USING DYNAMIC OPTICAL COHERENCE ELASTOGRAPHY

By

Srilatha Vantipalli

An Abstract of a Dissertation Presented to the Faculty of the College of Optometry

University of Houston

Submitted in Partial Fulfillment of the requirements for the Degree of

Doctor of Philosophy

August, 2016

Abstract

Purpose: Optical coherence elastography (OCE) quantifies the tissue's biomechanical properties through mechanical loading and imaging the tissue response using optical coherence tomography (OCT). Current techniques evaluating corneal stiffness do not account for the influence of key physiological factors on the measured corneal biomechanical properties and either require contact, or create global deformations masking the localized variations: the hallmark of corneal ectasias, e.g., keratoconus. To implement OCE in the cornea, we developed a micro air-pulse stimulator that provides non-contact, dynamic, spatially localized, tissue stimulation. This dissertation determines **a)** the acute effects of tissue hydration and UV riboflavin cross-linking (CXL) treatment on the corneal ultrastructure, and evaluates the corneal biomechanical properties determined using OCE due to the effect of **b)** hydration and CXL treatment, **c)** deep stromal cross-linking treatments and **d)** *in vivo* application.

Methods: a) *Ex vivo* de-epithelialized rabbit corneas (n=11) were cross-linked instilling 0.1% riboflavin solution for 30min across the whole cornea and UV irradiation (365nm, 3mW/cm^2) to only the temporal half-region for 30min while instilling riboflavin and processed for light and transmission electron microscopy. Corneal thickness and collagen fibril separation computed as the average radial inter-fibrillar distance from the sampled fibril cross-sectional electron micrographs were recorded. **b)** OCE imaging was performed using phase-sensitive OCT imaging to quantify the tissue deformation dynamics resulting from a spatially discrete, low-force air-pulse (150μm spot size; 0.8ms duration; <10Pa (<0.08mmHg)). The time-dependent surface deformation is characterized by a viscoelastic tissue recovery response, quantified by an exponential decay constant—*relaxation rate* (RR). Higher RR is consistent with increased stiffness. Hydration influence was determined (n=10) instilling 0.9% saline every 5min for 60min

and 20% dextran for another 60min. Measurements were made every 20min to determine central corneal thickness (CCT) and RR. Hydration and CXL effects were determined by obtaining OCE measurements on cross-linked corneas using isotonic (n=6) and hypertonic (n=7) riboflavin. **c)** OCE measurements were performed (n=10) at: the de-epithelialized stromal surface, 2/3rd corneal depth post-trephination, and after deep stromal cross-linking treatment. Rose bengal green light cross-linking (RGX) using 0.1% rose bengal solution for 20min (n=5) and 10min green light irradiation (565nm, 0.25W/cm^2) and CXL treatment (n=5) was performed in the deep stroma. **d)** *In vivo* OCE was performed on anesthetized Dutch belted rabbits (n=20) recording within-session (IOP: 10, 20, 30, 40mmHg) and between sessions RR measurements before and after animal re-positioning (10mmHg).

Results: a) Corneal thickness decreased significantly (−56%) after CXL treatment. Anterior collagen fibril spacing decreased significantly in the paired CXL treated region (−23%) showing that acute CXL treatment-induced changes are not only tonicity-driven. **b)** Corneal thickness was positively correlated (R^2=0.9) with stiffness. CXL treatment using isotonic riboflavin (CCT: −1%) produced stiffer corneas (higher RR: +10%). However, CXL treatment using hypertonic riboflavin (reduced CCT: −31%) produced a tonicity-driven stiffness decrease that offset the expected stiffer material properties due to CXL treatment, resulting in no significant change in corneal material properties (RR: +6%). **c)** Deep stromal RGX (RR: +22%) and CXL (RR: +44%) treatments showed significantly stiffer corneas. **d)** *In vivo* RR showed excellent measurement precision for within and between session measures.

Conclusion: OCE is a promising technique to quantify the corneal biomechanical properties while preserving the intact corneal shape and structure. We demonstrate the influence of hydration, and the modifications due to cross-linking treatments on the

corneal ultrastructure and biomechanical properties using OCE methods. The observed excellent measurement precision is critical for *in vivo* application of OCE in clinical settings. Further development and future application of OCE to derive corneal material properties will allow us to quantify the magnitude of ectatic diseases, the effectiveness of CXL treatment and follow changes over time.

Table of Contents

List of Figures

Chapter One

Chapter Two

Chapter Three

Chapter Four

Chapter Five

Chapter Six

List of Tables

Chapter One

Chapter Four

Chapter Five

Chapter Six

CHAPTER ONE

BACKGROUND AND INTRODUCTION

Background

1. Tissue biomechanics

Measurement of tissue biomechanical properties refers to quantifying the tissue's stiffness or other fundamental material properties using a number of evolving testing methods. Palpation is a subjective way of obtaining information on tissue stiffness by applying tactile pressure to sense tissue abnormalities e.g., heat, stiffness, swelling etc. However, palpation is based on experience and is qualitative. Quantitative measurement of a material's mechanical properties is typically performed through mechanical testing methods and many of these methods have been adapted for measurements with soft tissues.

i. Basic Mechanical Properties

Mechanical properties of materials are evaluated to understand their strength, resistance to external pressure and assess their wear and tear. This involves deforming the material by application of precisely known external forces to quantify their mechanical properties. The force applied to deform the material is quantified as stress (σ). The induced deformation due to the stress applied on the material is quantified as strain (ε). Any material that returns back to its original dimensions, after the force exerted to deform is removed is known to be elastic. In elastic materials, the deformation is reversible. This elastic stress-strain relationship between the force applied and the deformation caused due to the force exerted is quantified by Hooke's law. Hooke's law is defined over a specific range of a material's stress-strain response function and only for isotropic and homogeneous materials. A material is defined as isotropic, when it exhibits the same properties in all directions, and homogeneous when the material properties are the same throughout. According to Hooke's law, for isotropic and homogenous materials, the stress applied is linearly proportional to the induced strain up to a certain

limit and the slope of the linear portion of the stress-strain curve gives the elastic moduli ($\sigma = E\varepsilon$). Depending on the method of measurement of stress and strain, the moduli of elasticity (E) primarily include: Young's modulus, Shear modulus and Bulk modulus. These moduli are used to describe the stiffness of the material. Based on the size, shape, material composition, several methods are employed to quantify these moduli.

ii. *Mechanical Testing Methods in Ideal Materials*

Elasticity testing methods can have either a static or a dynamic force applied to induce deformation (strain). Static loads are defined as loads that exert a constant amount of force while dynamic loads exert varying amounts of force intermittently. Tensile or tension testing is a technique, wherein the material's resistance to elongation is tested by gripping it tightly and pulling apart. Compression testing is performed to test the material's resistance to compressive loading, e.g., squeezing force applied by bringing two platforms closer together. Torsion or shear test is performed to test the material's resistance to twisting forces wherein one end of the material is gripped and torsional force is applied to rotate it about its axis. In all cases, a known stress is applied and the strain induced is measured at all points during testing. From the linear portion of the resulting stress-strain function, the elastic moduli can be determined.

iii. *Issues with Mechanical Testing of Soft Tissues*

Most soft biological tissues do not behave like linear elastic materials. Instead, many exhibit non-linear hyper-elastic responses to deforming forces, consequently quantitative mechanical testing methods like extension, compression or shear testing employed in quantifying ideal materials (isotropic and homogeneous) are of limited use for quantifying soft tissue material properties. These methods are destructive to the soft tissue, wherein the tissue is dissected out of its surrounding environment and testing is performed on excised materials. Soft tissues are multi-layered composed of various components (cells, extra-cellular matrix constituents like collagen, elastin, and ground

substance, e.g. proteoglycans, glycosaminoglycans, etc.) usually forming a complex structure. Because of this, the measurement of mechanical properties is not the same in all positions (inhomogeneous). The measured material properties of soft tissue are influenced by the physical and chemical environmental factors such as temperature, hydration, osmotic pressure, pH, etc. Therefore, the measured material properties also vary depending on the testing conditions (*ex vivo* or *in vivo*). As a result, evaluating soft tissue material properties requires less invasive, but highly robust techniques that can preserve the key structural and morphological features of the tissue.

2. The cornea and its unique features contributing to the material properties

This dissertation is focused on characterizing corneal biomechanical properties. The cornea has several key structural features that enable its function and contribute to its mechanical properties. The human cornea is composed of 5 layers: epithelium, anterior limiting lamina, stroma, posterior limiting lamina and endothelium. The stroma forms the bulk of the cornea, accounting for 90% of corneal thickness. The stroma is primarily made up of collagen fibrils (heterotypic fibrils predominantly Type I and Type V) with a network of keratocytes surrounded by ground substance composed mainly of proteoglycans with glycosaminoglycan side-chains and glycoproteins. The collagen fibrils are arranged as a pseudo hexagonal lattice,[1, 2] and uniaxial, parallel collagen fibrils are organized into flat, elongated sheets of collagen lamellae with a network of stellate keratocytes interspersed between the lamellae.[3] Elastin-free extracellular fibrillin-containing microfibrils are also present in minor quantities interspersed between the lamellae providing structural support to the stromal architecture.[4]

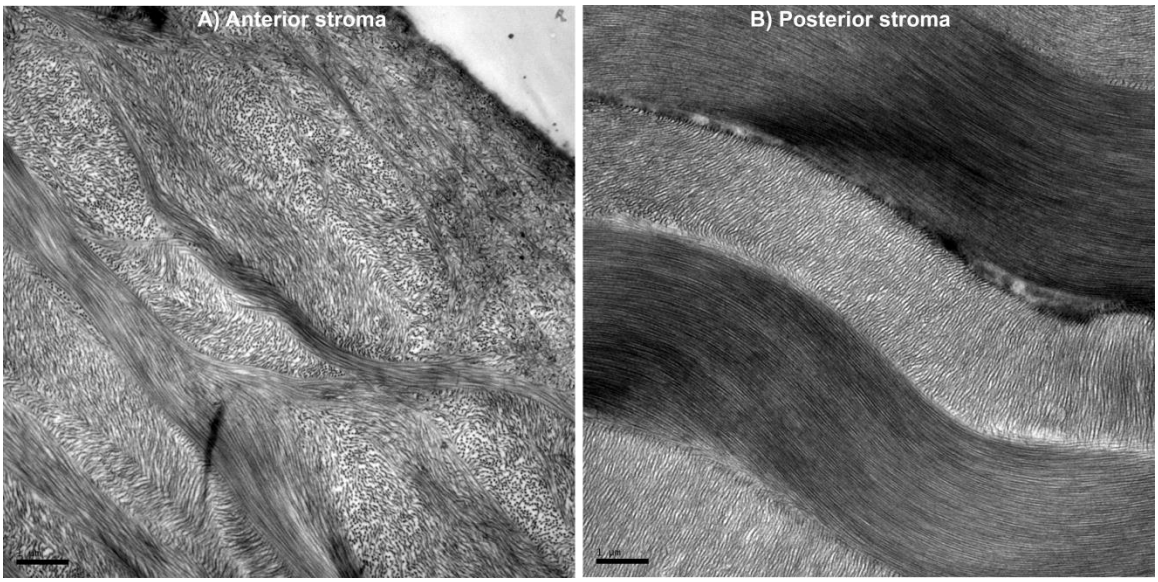

Figure 1.1: Electron micrographs showing anterior and posterior rabbit corneal stroma. Stromal architecture varies with depth: **A)** anterior lamellae are thinner, narrower and branch obliquely forming an intricate anterior lamellar inter-woven network, **B)** posterior lamellae are thicker, wider and arranged parallel to each other. Scale bar: 1µm.

The cornea is inhomogeneous as the composition across its depth is not the same. Stromal architecture varies structurally with depth (**Figure 1.1**).[5-7] The anterior lamellae are thinner, narrower than the posterior lamellae and branch obliquely into each other, forming a well-interwoven collagen lamellar network,[5, 7] while the posterior lamellae are thicker and wider,[8] and arranged parallel to each other and parallel to the corneal surface.[3] The cornea is anisotropic because of the collagen lamellar organization with vertically and horizontally preferred collagen fibril orientation at the corneal apex.[9, 10] The intricate anterior lamellar interweaving is responsible for providing structural stability.[11]

Proteoglycans are bottlebrush-like macromolecules made up of a protein core molecule with covalently attached glycosaminoglycans side chains (predominantly dermatan sulfate and keratan sulfate in the human corneas) having different biochemical composition anterior to posterior.[12] Keratocan and lumican are the major keratan sulfate proteoglycans present in the corneal stroma, while decorin is the major dermatan sulfate

proteoglycan. The proteoglycan-collagen fibril interaction is believed to be responsible for maintaining the matrix assembly, ordering, and spacing between collagen fibrils.[13, 14] The proteoglycans are negatively charged macromolecules exerting a swelling pressure of about 50 mmHg, drawing fluid into the corneal stroma.[15-18] The fluid influx into the corneal stroma represents the "leak" which is counterbalanced by the active transport function of the endothelial cells in the pump-leak mechanism.[19] The presence of proteoglycans with attached glycosaminoglycan side chains contribute to the viscoelastic properties exhibited by the cornea.[3]

3. Measuring Corneal Biomechanical Properties: Current techniques

Although several techniques exist to determine corneal biomechanical properties, most require contact and all but a few techniques are limited to *ex vivo* use. A brief description of techniques used for deriving corneal biomechanical properties along with their drawbacks is reviewed below.

i. Available In Vitro Techniques to Measure Corneal Stiffness

Early studies implemented traditional destructive biomechanical testing methods like strip extensiometry[20-23] or rheometry[24] to characterize corneal stiffness. However, the cornea is excised and flattened to make measurements. Excising the cornea disturbs the intricate stromal architecture and disrupts hydration control, which could lead to either tissue swelling or thinning. All these factors modify the tissue from *in vivo* physiological conditions and affect the measured corneal material properties[25] .

Strip extensiometry studies are a form of tangential testing to characterize the in-plane tensile properties of the cornea (extension either vertically (x axis) or horizontally (y axis) in the plane of the cornea). However, the in-plane tensile properties of the cornea will be very different from its out-of plane mechanical properties (perpendicular to the cornea along its anterior to posterior direction (z axis)) owing to the arrangement of

the collagen lamella and any inter-lamellar bonds. Out-of-plane mechanical properties can have important implications for the normal functioning of the cornea, as the cornea may be subjected to normal day-to-day loads in that dimension *in vivo*, e.g. while blinking, rubbing the eyes, etc. The key limitation with strip extensiometry is also the sample boundary conditions, which changes with the location and orientation from where the strip is cut from and how the ends of the tissue are gripped during testing. As a consequence of these limitations, the repeatability and reliability of the elastic moduli obtained are notoriously variable for soft tissues.[26]

Pressure inflation studies performed to quantify corneal biomechanical properties on whole globes[27] or corneal buttons with scleral border[26] are less destructive than extensiometry. However with whole globes when the corneal buttons are still held at the limbus, the cornea and sclera can together contribute to the measured material properties, modifying the measured corneal material properties.

Brillouin microscopy captures the frequency shift in scattered light from the interaction between the light and sound inherent within the tissue. The frequency shift is quantified as brillouin modulus and this shift is proportional to the material's elastic modulus. Scarcelli and colleagues[28] applied brillouin microscopy in the cornea and demonstrated the depth-resolved effects of UV riboflavin[28] and rose bengal green light[29] cross-linking techniques in the cornea. Although, the brillouin modulus is proportionally related to the elastic moduli, equating it with a universally accepted unit of measure (e.g., Young's modulus) is still a challenge.

ii. *Available In Vivo Techniques to Measure Corneal Stiffness*

The Ocular Response Analyzer (ORA)[30] is a modified air-puff tonometer that creates a global corneal deformation for a period of 8 ms with incremental pressure until the corneal shape becomes flat (applanated) followed by a decrease in pressure to return back to baseline. Corneal biomechanical properties are quantified from the dynamics of

the corneal deformation response in ORA as corneal hysteresis and corneal resistance factor. Corneal Visualization Scheimpflug Technology (CorVis ST)[31] also creates a global corneal deformation for a period of 35 ms with constant pressure across a horizontal width of 8 mm. A scheimpflug camera records the corneal images from the air-pulse deformation until maximum corneal displacement and recovery back to baseline. The CorVis provides about ten different parameters describing corneal material properties. Air pulse stimulation in ORA and CorVis ST creates a global corneal deformation utilizing an air pulse of high volume, large amplitude and long duration (8 ms and 35 ms respectively). Using either of these methods, the resulting global corneal deformation can mask the localized focal spatial variations in the corneal biomechanical properties.

iii) Optical Coherence Elastography imaging in the cornea

Elastography, first described by Ophir, is an emerging biomedical imaging technique used to derive soft tissue material properties as a less invasive alternative to destructive testing methods.[32] In general, elastography involves baseline tissue imaging using either ultrasound, computed tomography (CT), magnetic resonance imaging (MRI) or optical coherence tomography (OCT). Following imaging, tissue stimulation methods like acoustic force, mechanical indentation, vibration, air pulse, etc., are used to perturb the tissue. The response to stimulus is re-imaged during deformation. The tissue mechanical properties are derived from image analysis and mathematical modeling of the tissue response, to relate the observed tissue's structural deformation to the underlying biomechanical properties. Elastography has been implemented as a clinical diagnostic tool[33, 34] for detecting liver cirrhosis,[35] breast cancer,[36, 37] prostate cancer[38] and thyroid cancer[39] with a goal of reducing the need for invasive procedures, e.g., fine-needle aspirations and biopsies.

Imaging techniques like scanning probe microscopy, scanning acoustic microscopy etc. provide nanometer-scale resolution but low penetration depth. On the other hand, ultrasound, CT, MRI imaging techniques have higher penetration depth; however, their resolution is limited (cm to mm-scale). Optical coherence tomography has the capacity to provide higher resolution than CT or MRI and also the capability to measure at micron-level penetration depth. Schmitt first described optical coherence elastography (OCE) methods by using OCT imaging to determine tissue biomechanical properties.[40] Combining OCT imaging with various tissue stimulation methods (bulk compression,[41] mechanical indentation,[42] magnetic nanoparticles,[43] ultrasound,[44] acoustic radiation,[45, 46] air puff[47, 48]) has gained success in the disease diagnosis of different tissues.[49]

Dupps,[25] Ford and colleagues[42] first applied optical coherence elastography methods to the cornea as a non-destructive way to determine corneal biomechanical properties using static mechanical compression as the tissue stimulation method and demonstrated the techniques capability to resolve sub-micron displacements in corneal tissue. Supersonic shear imaging[44] quantifies corneal stiffness by measuring the shear wave's propagation speed generated in the anterior stroma using focused ultrasound. Young's modulus is derived from the shear wave speed. However, these techniques are too powerful for *in vivo* application.

To address the issues of contact and global characterization of corneal material properties with the existing techniques, we built a custom micro air-pulse stimulator that dynamically perturbs the cornea at a focal location non-invasively for a short time period (< 1ms) and combined it with a phase-sensitive optical coherence tomography as part of the optical coherence elastography imaging system (OCE).[50]

Introduction

Biomechanical properties are influenced by corneal structure and function. Corneal pathologies like keratoconus or refractive surgeries alter the tissue's microstructure, while simultaneously impacting the corneal mechanical behavior and vision.[51] Treatments like collagen cross-linking slow down the cornea's structural degradation and vision deterioration by strengthening a mechanically unstable cornea.[52, 53] Determining and quantifying the corneal mechanical behavior will aid in understanding the etiology of keratoconus and other ectasias, and help in monitoring and improving the efficacy of current treatment modalities. Current techniques evaluating corneal stiffness do not account for the influence of key physiological factors, e.g., hydration, on the measured corneal biomechanical properties and either require contact, or create global deformations masking the localized variations: the hallmark of corneal ectasias, e.g., keratoconic corneas have weaker material properties at the cone versus peripherally.[54-56] Optical coherence elastography (OCE) quantifies the tissue's biomechanical properties through mechanical loading and imaging the tissue response using optical coherence tomography (OCT). To implement OCE in the cornea, we developed a micro air-pulse stimulator that provides non-contact, dynamic, spatially localized, tissue stimulation. This dissertation determines the air pulse stimuli characteristics, the acute effects of tissue hydration and UV riboflavin cross-linking (CXL) treatment on the corneal ultrastructure, and evaluates the corneal biomechanical properties determined using OCE due to the effect of hydration and CXL treatment, deep stromal collagen cross-linking treatments and *in vivo* application.

The first part of this dissertation evaluates the stimuli characteristics of a custom-built micro air pulse stimulator and adapting the device for dynamic optical coherence elastography imaging of the cornea. This novel approach for tissue stimulation will enable non-invasive application of elastography for the measurement and quantification

of corneal biomechanical properties. We specifically determine the spatial, temporal features of the air pulse required for corneal stimulation. This fundamental work on tissue stimulation characteristics is critical for the development of OCE imaging in the eye.

The second part of the dissertation determines the acute effects of tissue hydration and collagen cross-linking treatment on the corneal ultrastructure and biomechanical properties. UV riboflavin cross-linking (UV CXL) is an emerging treatment for keratoconus[53] and post-refractive surgery ectasia[57] that can slow disease progression by increasing corneal stiffness.[58, 59] The mechanism of UV CXL treatment[60, 61] is suggested to be similar to non-enzymatic glycation seen with aging[62] or diabetes.[63] However, the exact ultrastructural locations where cross-links are induced in the cornea due to the CXL treatment are still unclear.[64, 65] We evaluate the acute ultrastructural and global morphological changes produced by UV riboflavin cross-linking in the rabbit cornea.

Changes in the corneal hydration state are known to affect the measured biomechanical properties by influencing the underlying tissue mechanical strength.[66, 67] The riboflavin used in the conventional cross-linking treatment protocol is dissolved in dextran which is a hyperosmotic agent and can create in a tonicity-driven corneal thickness change during treatment.[68] Therefore, the corneal material properties after cross-linking are also influenced by corneal hydration. We evaluate the individual and combined effects of hydration and UV riboflavin cross-linking treatment on the corneal biomechanical properties measured using OCE. The results from this work help determine the acute effects of cross-linking treatment and the influence of a key physiological factor (hydration) on the treatment effect.

The third part of this dissertation evaluates the depth dependent tissue properties of the stromal bed and to implement a cross-linking treatment in the deep cornea. UV

riboflavin cross-linking treatment effect is confined to the anterior stroma (~200um).[52, 54, 69] Combining collagen cross-linking treatment in the deep stroma with emerging corneal transplantation procedures to treat keratoconus like anterior lamellar keratoplasty and refractive surgeries like LASIK or photorefractive keratectomy (PRK) is being proposed as a prophylactic measure to increase the posterior corneal stiffness and prevent future ectasia.[65] However, UV CXL treatment is not safe for use in the deep corneal stroma due to endothelial cell UV toxicity.[70] Cherfan et al.[29] and Wang et al.[71] showed an increase in corneal stiffness using a non-UV cross linking based on rose bengal stain and green light (RGX). We specifically quantify the deep stromal biomechanical properties and demonstrate the effect of cross-linking treatments in the deep stroma. The results from this work shows promise for future applications in lamellar keratoplasty and refractive surgery through modification of deep corneal biomechanical properties.

The fourth part of this dissertation investigates the feasibility of performing *in vivo* dynamic OCE imaging to obtain rabbit corneal biomechanical properties and to evaluate the repeatability and short-term reproducibility of *in vivo* dynamic OCE measurements on rabbit corneas. While adapting dynamic OCE for *in vivo* imaging, the subtle tissue displacement induced by air-pulse stimulation may be influenced by pre-existing motion due to ocular pulse, physiological respiration or cardiac cycle or due to the alignment of the cornea. It is, therefore, important to know if their influence is substantial enough to degrade our tissue response and obstruct reproducible dynamic OCE imaging. The results from this work help quantify the *in vivo* sensitivity of the OCE imaging technique.

All experiments are conducted in rabbit eyes, as the rabbit corneas are dimensionally closest to the human corneas. However, there are several structural exceptions which are laid out in the following table.

Table 1.1: Comparison between Human and Rabbit Corneas

Structural feature	Human Cornea	Rabbit Cornea
Corneal thickness[72, 73]	500-550 µm	400-450 µm
Stromal anterior lamellar interweaving[5]	68% stromal depth	34% stromal depth
Corneal contour[74]	Thinner center; Thicker periphery	Uniformly thick all across
Anterior limiting lamina[72, 75, 76]	Present	Absent
Endothelial cells regeneration[77]	No	Yes

The physiologically normal baseline corneal thickness is higher in human corneas than in rabbit corneas.[72, 73] Mechanically, thicker materials (due to more mass) are more resistant to deformation and exhibit a higher elastic modulus. We expect the measured biomechanical properties of human corneas to be higher in magnitude than in rabbit corneas. The anterior lamellar interweaving in the human corneal stroma is to a greater depth than in rabbit corneas,[5] indicating perhaps a higher structural stability of human corneas over the rabbit corneas. The structural variability in the lamellar organization across the corneal depth can affect the measured corneal depth dependent biomechanical properties between the human and rabbit corneas dissimilarly; however, the effects of hydration and crosslinking reported from rabbit corneas in this work will still be applicable to human corneas as the basic structural composition and physiological functions carried out by corneas in the two species are similar. Although a higher magnitude of changes can be expected for human corneal samples, the direction of the effects of hydration and/or crosslinking will remain the same.

Organization of Dissertation

The dissertation is organized as follows. Chapter 2 discusses the development and adaptation of air pulse stimulator for dynamic optical coherence elastography of the cornea. Chapter 3 and 4 together address the second objective of determining the acute effects of corneal collagen cross-linking treatment on the rabbit corneal ultrastructure and its biomechanical properties and the influence of hydration on the treatment effect. Chapter 3 focuses on the acute global and ultrastructural changes due to UV riboflavin cross-linking treatment in rabbit corneas after isolating hydration driven effects and Chapter 4 investigates the effect of hydration and UV riboflavin cross-linking treatments individually and together in rabbit corneas using dynamic OCE.

Chapter 5 evaluates the depth dependent corneal biomechanical properties using dynamic optical coherence elastography methods and implements rose bengal green light cross-linking and UV riboflavin cross-linking treatments in the deep stroma of the rabbit cornea. Additional collagen cross-linking treatments on the full thickness corneal stroma are also performed for comparison. Chapter 6 investigates the feasibility of performing *in vivo* dynamic OCE imaging to obtain rabbit corneal biomechanical properties and to evaluate the repeatability and short-term reproducibility of *in vivo* dynamic OCE measurements on rabbit corneas. Chapter 7 presents our conclusions and directions for future research in this area.

CHAPTER TWO

DEVELOPMENT AND ADAPTATION OF MICRO AIR-PULSE STIMULATOR FOR DYNAMIC OPTICAL COHERENCE ELASTOGRAPHY OF THE CORNEA

Srilatha Vantipalli, [1] Shang Wang, [2] Kirill V. Larin, [2] Michael D. Twa[3]

[1]College of Optometry, University of Houston, 505 J. Davis Armistead Bldg., Houston, TX 77204; [2]Department of Biomedical Engineering, University of Houston, 3605 Cullen Blvd, Houston, TX 77204; [3]School of Optometry, The University of Alabama at Birmingham, 1716 University Blvd, Birmingham, AL 35233

Preface

Optical coherence elastography was first described in 1998[40] to quantify soft tissue biomechanical properties. Dynamic optical coherence elastography (OCE) involves quantifying tissue biomechanical properties using a dynamic loading mechanism and an imaging system (optical coherence tomography) to capture the response to loading. We are adapting elastography imaging for the eye by developing a micro air-pulse stimulator that creates a localized short-duration focal stimulation. Current techniques (Ocular Response Analyzer[78] (ORA) and the Corneal Visualization Scheimpflug Technology[79] (CorVis ST) used for air pulse stimulation create a global deformation which cannot distinguish the spatially localized variations in the cornea, which is the hallmark of disease conditions like keratoconus and other post-refractive surgery ectasias. This novel approach for tissue stimulation will enable application of elastography for the measurement and quantification of spatially localized corneal biomechanical properties in a non-invasive manner. The purpose of this chapter is to evaluate air pulse stimuli characteristics i.e., force, time of flight, spatial characteristics etc., a key component that enables optical coherence elastography imaging in the eye.

Abstract

Purpose: Dynamic optical coherence elastography (OCE) involves quantifying tissue biomechanical properties using a loading mechanism and an imaging system (optical coherence tomography) to capture the response to loading. This study characterizes the air pulse stimulator parameters to enable the adaptation and application of dynamic OCE imaging for the cornea.

Methods: The force, time of flight and spatial air pulse characteristics were assessed using a high-resolution pressure transducer. The force was recorded by varying the external air source input (5 to 88psi). The incident angle (varying from 90° to 0°) and the distance (0mm to 20mm away) effect on the output excitation pressure were measured. The excitation pressure profiles were recorded by the pressure sensor. The time of flight between the air pulse trigger and response was obtained from high-speed photography images captured following air pulse stimulation of a water surface at increasing delay periods (0.05ms steps from 0.1 to 20ms) at various input pressures (10 to 50psi) and increasing distance (0 to 20mm away). The air pulse perturbed surface diameter was obtained at 10psi input pressure from the high-speed photography images using a calibrated scale obtained from imaging a reference grid having known dimensions.

Results: The air pulse stimulus is an impulse response with a localized Gaussian profile with stimulus duration of ~ 1ms for input pressures less than 10psi. Excitation pressure increases linearly ($R^2 = 0.99$) with an increase in the external air source input pressure. Excitation pressure decreases with a cosine function as the delivery port was angled away from the pressure sensor surface normal position ($R^2 = 0.97$). Excitation pressure decreases exponentially with an increase in the distance between the delivery port and the pressure sensor ($R^2 = 0.95$). Time of flight from trigger to excitation was 0.5 ± 0.1ms (mean ± standard deviation) and the air pulse stimulated region diameter was 150 µm at 10psi input pressure.

Conclusion: We obtained the air pulse characteristics required for corneal stimulation. The ability to stimulate the cornea non-invasively with discrete localized pulses will enable *in vivo* application of dynamic optical coherence elastography imaging and aid in the spatial characterization in corneal ectatic diseases like keratoconus or after post-refractive surgeries where the tissue mechanical properties are altered unevenly across the corneal surface.

Introduction

Elastography is a medical imaging technique to measure the tissue biomechanical properties. Elastography is successfully implemented in place of invasive tissue biopsy procedures for early diagnosis of breast cancer[80] based on tissue stiffness (hard or soft). This research aims to measure and quantify corneal biomechanical properties using elastography imaging in the eye. Elastography involves baseline imaging, perturbing the tissue using a loading mechanism and imaging the tissue's response to stimulation. The loading mechanism can be static (continuous) or dynamic (pulse). Current loading mechanisms include using ultrasound waves,[44] acoustic waves,[81] or indentation.[42, 82] However, these require direct contact that may alter the tissue material properties. Current *in vivo* techniques like the Ocular Response Analyzer[78] (ORA) and the Corneal Visualization Scheimpflug Technology[79] (CorVis ST) use air pulse stimulation to derive corneal material properties. However, they create global corneal deformation by utilizing an air pulse of high volume, large amplitude and long duration (8 ms and 35 ms respectively). To address the issues of contact and global characterization of corneal material properties with existing techniques, we built a custom micro air-pulse stimulator that dynamically perturbs the cornea at a focal location non-invasively for a short time period (< 1ms). We combined the micro air-pulse stimulator with a phase-sensitive optical coherence tomography (OCT), as part of the optical coherence elastography imaging system (OCE).[50] This chapter evaluates the spatial, temporal features of the air pulse required for corneal stimulation to enable the application of dynamic OCE imaging in the eye.

Air pulse stimulation to perturb the cornea will enable *in vivo* application of dynamic optical coherence elastography imaging. The ability to stimulate the cornea with discrete localized pulses enables the spatial variation detection in material properties e.g. in ectatic diseases like keratoconus where localized thinning induces focal structural

weakening[83] (cone vs. surrounding region) or after post-refractive surgeries where the tissue mechanical properties altered unevenly across the corneal surface is the hallmark of the disease.[84] The ability to obtain spatially localized tissue material properties will enable customized treatments possible of targeting the locally affected region during surgeries or cross-linking treatments in the future.

Dynamic air pulse stimulation generates localized mechanical waves in tissues which disperse internally (compressive waves) and orthogonal waves propagating tangential to the corneal surface much like the ripples on the pond surface (shear waves). This dynamic tissue response to the air pulse stimulus is a complex viscoelastic response that is captured using a high-speed phase sensitive OCT imaging system. The purpose of this chapter is to evaluate and understand the air pulse stimuli characteristics by assessing the spatial and temporal dynamics of the air pulse, excitation force and time of flight characteristics.

Methods

Air pulse stimulator

An electromechanically operated solenoid valve driven device provides the air pulse stimulus. An external air source with a pressure gauge provides the input for the air pulse and the output is through a delivery port having a diameter of 0.15 mm.

Air pulse stimuli characteristics

The force, time of flight and spatial characteristics of the air pulse were assessed using a high-resolution analog pressure transducer (ATM 1st; STS) linked to an oscilloscope (DPO3014; Tektronix, Inc.).

a) Force

    i) Output excitation pressure

The distance between the output port and the pressure transducer was fixed and the output port was positioned to be normal to the pressure transducer. The excitation pressure delivered by the air pulse output port that is incident on the pressure transducer was measured repeatedly (5 measurements) and obtained with increasing external input air source pressure from 5000 Pa to 88000 Pa.

The air pulse duration was obtained by computing the full width at half maximum value from the Gaussian fit applied to the averaged air pulse profile obtained, when the external input air source pressure was 10 psi.

ii) Effect of delivery angle

The distance between the output port and the pressure transducer was fixed (~200 µm away) and the output excitation pressure was maintained constant (5000 Pa). The excitation pressure incident on the pressure transducer was recorded (5 measures) and obtained with change in the delivery angle from normal to parallel position of the output port with respect to the pressure transducer (10 degree steps).

iii) Effect of distance

The output excitation pressure was maintained constant (5000 Pa) and the output port was positioned to be normal to the pressure transducer. The excitation pressure incident on the pressure transducer was recorded (5 measures) and obtained with increasing distance of the output port from 0 mm to 20 mm away from the pressure transducer (2 mm steps).

The excitation pressure profile was recorded by the pressure sensor. A Gaussian fit was applied to the averaged oscilloscope's signal using the curve fitting tool in MATLAB. The peak amplitude from the Gaussian fit oscilloscope signal was obtained as the output excitation pressure.

b) Time of flight:

High-speed photography of the air pulse stimulation was performed to capture the time of flight. Time of flight was the time delay between the air pulse trigger and response of the air pulse stimulus. The air pulse output port was positioned normal to the water surface in a beaker about ~200 µm distance away. A thin layer of talcum powder was sprinkled on the water surface for better visualization. In a dark room, a camera (Nikon SB 900) was set-up on a tripod after framing and focus. The trigger for the air pulse stimulator was linked to the oscilloscope and the delay timer in the oscilloscope was linked to the camera flash. Once the air pulse stimulator was triggered, the oscilloscope triggered the flash after the set time delay. The flash triggered the camera to capture the image at that moment. The images were captured at increasing delay periods (0.05 ms steps from 0.1 ms to 20 ms) set on the oscilloscope. From the images captured, the point where the first disturbance on the water surface was observed was recorded, as the time delay from trigger to excitation (**Figure 2.1**). The delay was obtained at various input pressures (10 to 50 psi) and with the delivery port's increasing distance (0 to 20 mm) away from the water surface.

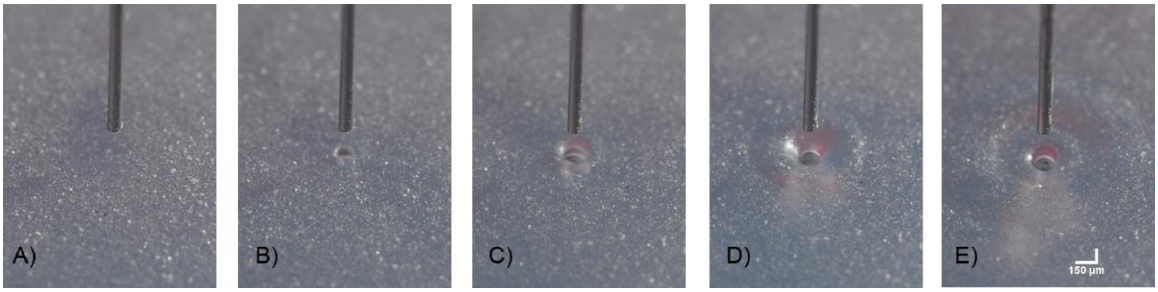

Figure 2.1: High speed photography set-up inset showing a series of air-pulse stimulated images. Images show the delivery port and the disturbance on the talcum powder sprinkled water surface created by the air pulse stimulus after a time delay of A) 0.5 ms, B) 0.7 ms, C) 0.9 ms, D) 1.5 ms, E) 3 ms following the air pulse trigger. Scale bar = 150 µm.

c) Space:

The diameter of the perturbed water surface was determined for the input pressure of 10 psi at the closest possible distance (~ 200 µm) between the output port and the water surface by using a calibrated scale obtained from imaging a reference grid of known dimensions.

Results

The air pulse stimulus is an impulse response shown as a localized Gaussian profile with stimulus duration of 1.04 ms (full width at half maximum) for 10 psi input pressure. **Figure 2.2** shows the impulse responses created by the air pulse stimulus at input pressures increasing from 10 psi to 88 psi.

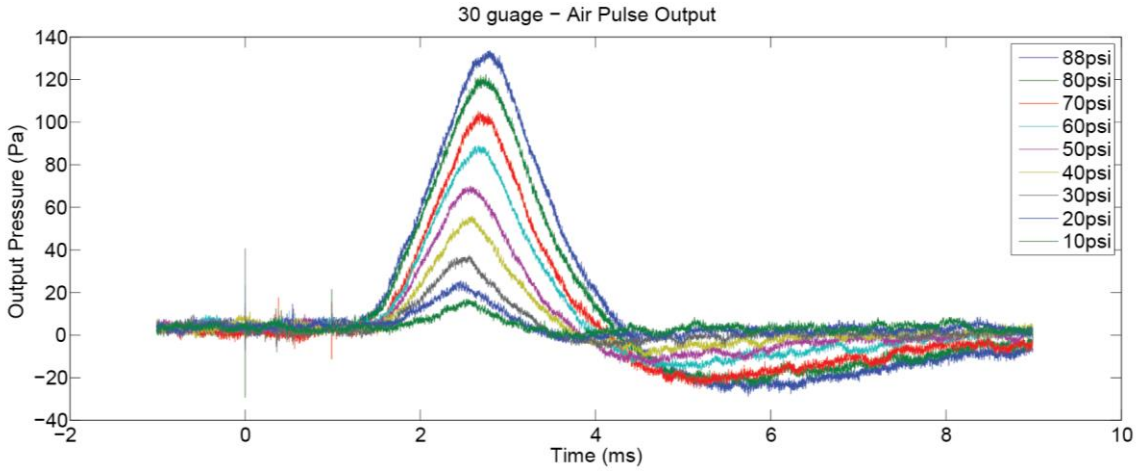

Figure 2.2: Air-pulse stimuli impulse responses. Each line shows the impulse responses as localized Gaussian profiles created by the air pulse stimulus at input pressures increasing from 10 psi to 88 psi. The stimulus duration is ~1 ms for input pressures less than 10 psi.

i. Force

i) Output excitation pressure

A linear increase in the excitation pressure ($R^2 = 0.99$; Slope: $\sim 1.5 \times 10^{-4}$) is recorded with an increase in the external air source input pressure **(Figure 2.3)**.

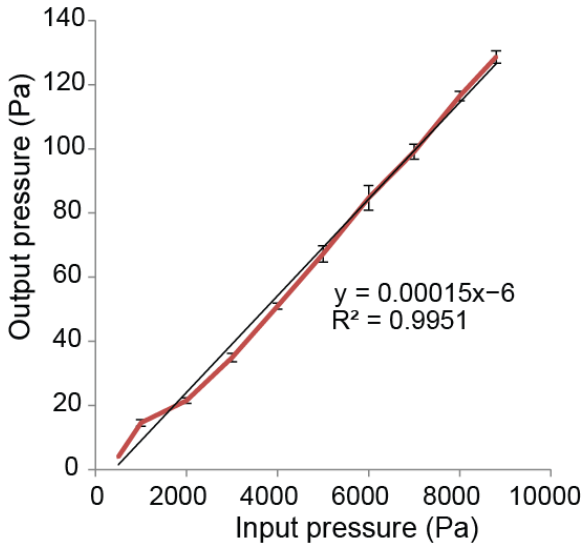

Figure 2.3: Excitation output pressure variations with increasing external air source pressure. The excitation output air pulse pressure increases linearly with increasing input pressure from 0 psi to 88 psi, keeping the distance from the pressure transducer constant and the delivery port at an angle normal to the sensor.

ii) Effect of delivery angle

A decrease in the excitation pressure with a cosine fit is observed as the delivery port is angled away from the pressure sensor surface normal position (R^2 = 0.97) as shown in **Figure 2.4**.[50]

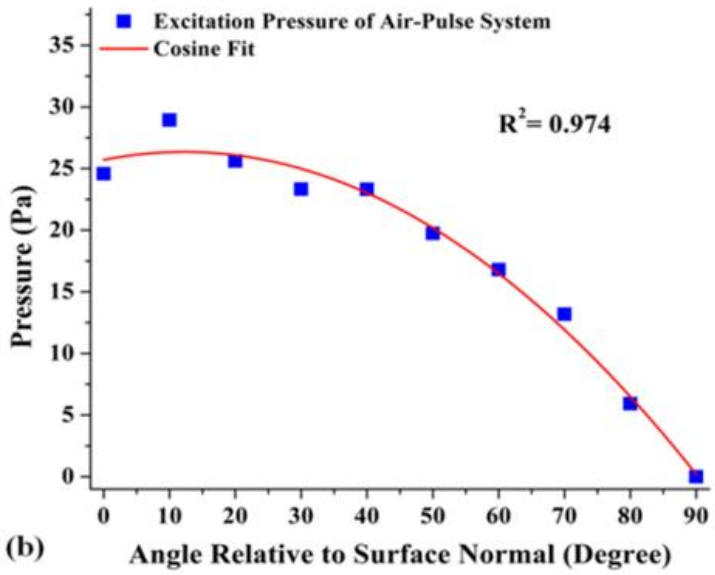

Figure 2.4: Excitation output pressure variations with angle of incidence of delivery port (re-published from Wang and colleagues).[50] The excitation pressure decreases with a cosine function as the delivery port is angled away from the surface normal position, keeping the input pressure constant and the distance between them constant.

iii) Effect of distance

A decrease in the excitation pressure with an exponential fit is observed with an increase in the distance between the delivery port and the pressure sensor (R^2 = 0.95) as shown in **Figure 2.5**.[50]

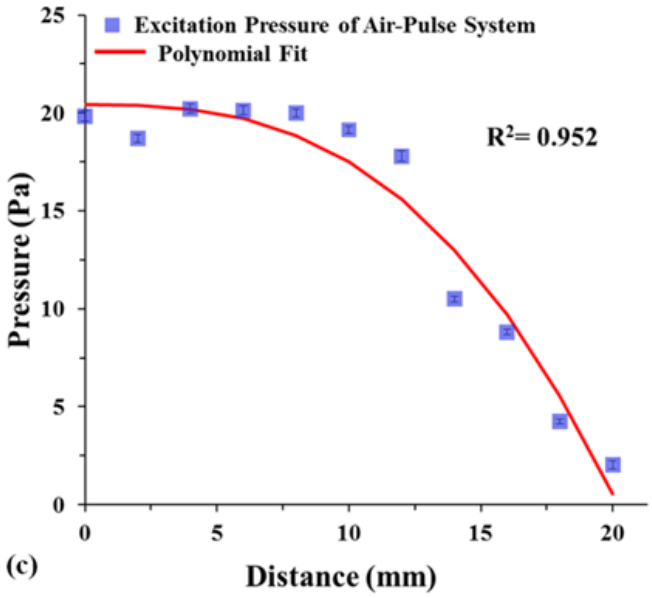

Figure 2.5: Excitation output pressure variations with delivery port distance (re-published from Wang and Colleagues).[50] The excitation pressure decreases exponentially with increase in the distance between the delivery port and the pressure sensor, keeping the input pressure constant and the delivery port at an angle normal to the sensor

b) Time of flight

The time of flight for various input pressures with increasing distance between the air pulse port and the water surface is shown in **Figure 2.6.** At the closest possible distance (~200 µm), the time of flight is 0.5 ± 0.1 ms (mean ± standard deviation) for all the measured input pressures. This delay will be accounted for while making OCE measurements.

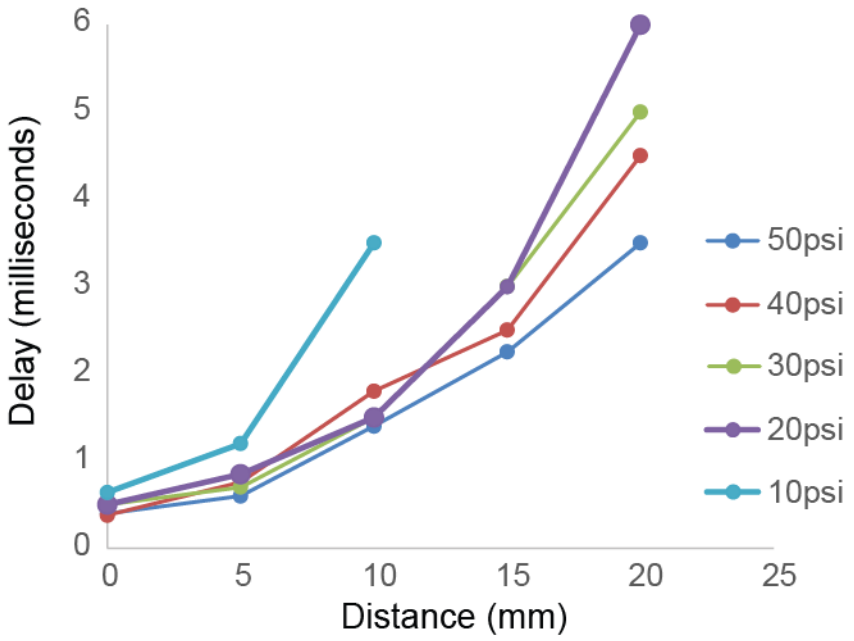

Figure 2.6: Time of flight for different excitation output pressures with delivery port distance. Time of flight is the delay from the time of trigger to excitation by the air pulse stimulus captured with high speed photography. At closest possible distance (~200 µm), the delay is ~0.5 ms for all the measured input pressures.

c) Space

The diameter of the air pulse stimulated region on the water surface was measured to be 150 µm for 10psi input pressures at closest possible distance (~200 µm) from the high-speed photography images.

Discussion

The air pulse characteristics demonstrate that the magnitude of the air pulse can be well-predicted and easily controlled based on the external air source pressure, the angle of delivery and distance of excitation. From these experiments, we can conclude that maximal excitation will be when the distance between the air pulse delivery port and the corneal surface is as close as possible and the angle of delivery is normal to the corneal surface. The duration of the air pulse is ~1 ms impacting a region of 150 µm

diameter. The time lag (0.5 ms) between time of trigger and the response is accounted for during OCE imaging. These fundamental characteristics of the air pulse stimulus will be used for perturbing the corneal surface in all the future experiments described in this dissertation.

Current techniques for tissue stimulation in optical coherence elastography imaging of the cornea includes compression/indentation using a gonioscopy lens by Ford et al.[42] However, this technique requires contact. Air pulse stimulation in ORA[30] creates a global corneal deformation for a period of 8 ms with incremental pressure large enough to change the corneal shape from convex to slightly concave, followed by a decrease in pressure to return to baseline. Air pulse stimulation in CorVis ST[31] also creates a global corneal deformation for a period of 35 ms with constant pressure across a horizontal width of 8 mm. The micro air-pulse excitation stimulus is different from both the ORA and the CorVis ST stimuli, creating a focal controlled discrete deformation (as opposed to a global deformation) for a short-time period of ~1 ms having a localized spatiotemporal Gaussian profile with a force amplitude ranging 2 to 10 Pa (0.02 to 0.08 mmHg) delivered through a 150 µm diameter port.

Air pulse stimulation will enable the adaptation and implementation of dynamic optical coherence elastography imaging *in vivo* to aid in the detection of spatially variable corneal biomechanical properties in ectatic conditions like keratoconus[83] or post-refractive surgeries[84] or to devise customized treatments protocols targeting the locally affected region during surgeries or cross-linking treatments in the future. The air pulse stimulation characteristics are flexible and can be modified for future applications in other ocular tissues to stimulate and obtain biomechanical properties of the sclera [85] (myopia), lens[86] (cataract), extra-ocular muscles,[87] and lamina cribrosa and optic nerve[88] (glaucoma) by re-configuring the required excitation air pulse characteristics suitable for the tissue.

CHAPTER THREE

ACUTE ULTRASTRUCTURAL EFFECTS OF UV RIBOFLAVIN CROSS-LINKING IN RABBIT CORNEAS

Srilatha Vantipalli[1], Brodie S DeJernett[1], Michael D. Twa[2]

[1]College of Optometry, University of Houston, 505 J. Davis Armistead Bldg., Houston, TX 77204

[2]School of Optometry, The University of Alabama at Birmingham, 1716 University Blvd, Birmingham, AL 35233

Preface

This chapter investigates the acute ultrastructural and morphological changes in the cornea produced by UV riboflavin cross-linking treatment. Previous studies suggest tissue hydration[89] as the driving force for the acute ultrastructural changes measured after cross-linking treatment. We will compare the control and treated regions from the same cornea to account for the influence of hydration effects. We will also implement microwave tissue processing techniques as an attempt to better preserve tissue morphology throughout the processing stages. The information from evaluating the acute anterior ultrastructural and morphological changes after corneal cross-linking can potentially aid in understanding the cross-linking mechanism with a goal to improve the efficacy of the cross-linking treatment and reduce the variability in the treatment outcomes.

Abstract

Purpose: To determine the acute ultrastructural and morphological changes produced by UV riboflavin cross-linking (CXL) in rabbit corneas after isolating hydration driven effects.

Methods: UV riboflavin cross-linking was performed on *ex vivo* rabbit corneas after epithelial debridement by instilling riboflavin solution every 5min for 30min across the whole cornea (hypertonic riboflavin: 0.1% riboflavin in 20% dextran in 0.9% saline; n=5; or hypotonic riboflavin: 0.1% riboflavin in 0.9% saline; n=6). UV light (365nm, 3mW/cm^2) was used to irradiate only the temporal half-region of the cornea for 30min while instilling riboflavin every 5min. After microwave processing, transmission electron micrographs (TEM) of collagen fibril cross-sections were obtained from the anterior stroma (~10-20µm depth), sampling five regions at 6800x magnification. Collagen fibril separation was computed as the average radial distance between the collagen fibrils in the sampled TEM and obtained from the dominant peak of a radial distribution function fit to the electron micrographs. Central corneal thickness (CCT) was determined to track the hydration changes throughout the experiments using a non-contact Spectral Domain RTVue Optical Coherence Tomography (SD-OCT) (RTVue) before tissue processing and from light microscopy images of fixed tissues.

Results: Collagen fibril spacing decreased significantly from 83.4 nm in the control region (only riboflavin) to 64.3nm in the paired CXL treated region (riboflavin+UV) obtained from the same corneas using hypertonic riboflavin (−23%; Mean difference: −19nm; 95% Confidence Interval (CI): −15 to −23 ; *P*=0.01) and from 68.2nm (controls) to 59.2nm (treated) using hypotonic riboflavin (−13%; −9nm; 95% CI: −5 to −13; *P*=0.01). Corneal thickness decreased significantly in the CXL treated regions compared to the CCT of untreated regions at baseline when using either hypertonic riboflavin

(−56%; −356µm; 95% CI: −281 to −431; *P*=0.01) or using hypotonic riboflavin (−29%; −198µm; 95% CI: −131 to −265; *P*=0.01).

Conclusion: Although UV riboflavin cross-linking treatment produced an acute overall decrease in corneal thickness, no thickness difference is observed between the controls (hypertonic riboflavin only) and the paired CXL treated region (hypertonic riboflavin + UV irradiation) post-tissue processing. However, anterior collagen fibril spacing reduction is observed in the CXL treated region (−23%). This implies cross-linking treatment induced the observed acute anterior collagen fibril spacing decrease in the treated region that is not only tonicity driven.

Introduction

Corneal collagen cross-linking (CXL) is an emerging treatment for conditions like keratoconus or post-refractive surgery ectasias, wherein riboflavin is administered with UV radiation to increase corneal strength. Andreassen et al.[90] used traditional uniaxial tensile testing to show decreased stiffness in keratoconic corneas. Spoerl[60], Wollensak and colleagues[58] pioneered the first application of UV riboflavin cross-linking treatment for halting or slowing disease progression in keratoconic corneas and demonstrated corneal stiffening.[59] However, the exact ultrastructural locations where cross-links are induced in the cornea due to the CXL treatment are still unclear.[64, 65] In this study, we evaluate the acute ultrastructural and global morphological changes produced by UV riboflavin cross-linking in the rabbit cornea. This information can potentially aid in understanding the mechanism of CXL treatment with the goal to improve the efficacy of the cross-linking treatment and reduce the variability in the treatment outcomes.

Several studies proposed the possible locations of cross-links caused by CXL treatment in the corneal stromal ultrastructure involving the collagen fibrils,[61, 91, 92] the surrounding proteoglycan core proteins, and their covalently attached glycosaminoglycan side chains. Non-enzymatic glycation with the formation of advanced glycation end products similar to that seen with aging[62] or diabetes[63] is suggested with CXL treatment, resulting in stiffer tissue properties.[60, 61, 93] Glycation in rat tail tendons showed collagen fibril diameter increase and collagen fibril spacing decrease with the formation of covalent cross-links.[94] Wollensak and colleagues documented a similar increase in corneal collagen fibril diameter from transmission electron micrographs following CXL treatment in rabbit corneas.[95] The results from transmission electron micrographs obtained by Wollensak can be secondary to tissue processing methods and artifacts, e.g., tissue shrinkage/swelling. In addition, because acute tonicity changes can influence the collagen fibril separation,[96] measuring corneal collagen fibril separation

following CXL treatment *ex vivo* while accounting for the effect of hydration is a challenge and needs to be addressed. Hayes et al.[89] measured the collagen fibril separation changes using X-ray crystallography methods and demonstrated the observed decrease in collagen fibril separation to be driven by hydration only and not due to the CXL treatment. However, it is possible the effect of hydration may have masked the change caused due to CXL treatment.

This study addresses the acute morphological changes induced after UV riboflavin cross-linking treatment by investigating both the effects of hydration and the effect of cross-linking treatment. A within-tissue paired control condition was accomplished by administering the riboflavin solution (hypertonic/hypotonic) to the whole cornea but applying UV irradiation to only half of the cornea. This way any change driven by hydration is observed in the non-UV irradiated region, which was exposed to only the riboflavin solution, while the combined effect of hydration and CXL treatment was observed in the other half (riboflavin solution + UV irradiation). Corneal tissue fixation protocols previously described by Hanlon et al. that were optimized for the murine cornea were adapted for the rabbit cornea, and used to process the corneal tissue samples for transmission electron microscopy (TEM).[97]

The purpose of this study is to determine the effect of UV riboflavin cross-linking treatment on the collagen fibril separation in rabbit corneas and evaluate the changes in corneal thickness from baseline to post tissue processing.

Methods

Freshly enucleated mature albino rabbit eye globes (n = 11; age: >6 months) were obtained within 12 hours from Pel-Freeze Biologicals stored in Dulbecco's Modified Eagle's Medium. All experiments were conducted within 36 hours after enucleation.

Experimental procedure

The anatomical orientation of the whole globes was identified, marked and maintained throughout the study by first locating the nictitating membrane location (nasal-inferior), optic nerve orientation, extra-ocular muscles insertion location, and rabbit corneal shape (horizontal axis wider than vertical axis). Epithelium was debrided using a blunt spatula. De-epithelialized central corneal thickness (CCT) was obtained before and after cross-linking treatment using a non-contact Spectral Domain RTVue Optical Coherence Tomography (SD-OCT) (RTVue). UV riboflavin cross-linking was performed by instilling 0.1% riboflavin solution every 5 minutes for 60 minutes across the whole cornea [either hypertonic riboflavin solution (n = 5; 0.1% riboflavin in 20% dextran (Dextran T500 dissolved in 0.9% phosphate buffered saline (PBS; pH = 7.4) or hypotonic riboflavin solution (n = 6; 0.1% riboflavin dissolved in 0.9% saline)]. In order to include a control (only riboflavin) and treated region (riboflavin+UV) within the same eye, the temporal half of corneal tissues were exposed to UV radiation (365 nm, 3 mW/cm^2) by split field illumination for the last 30 minutes (**Figure 3.1**). This ensured comparable baseline thickness and morphology in the non UV-irradiated and paired treated regions.

After treatment, the corneas were dissected from the enucleated whole globes along with a narrow scleral tissue rim. To track the anatomical orientation, a V-shaped notch and an incision were cut into the scleral rim superiorly and nasally respectively (nasal region: control; temporal region: treated).

Microwave fixation processing for electron microscopy and imaging

Whole corneas were fixed in 2.5% glutaraldehyde in 25 mM sodium acetate buffer (pH = 5.7), 0.1 M magnesium chloride ($MgCl_2$) with 0.05% cuprolinic blue and microwaved for 4 repeated three-minute cycles (1 min vacuum on—1 min vacuum off—1 min vacuum at 150 W) using a PELCO BioWave Pro microwave tissue processor (Ted Pella, Inc., Redding, CA) and stored overnight in fresh fixative at room temperature.

Following storage in fixative, the cornea was cut in half along the treatment line (vertical meridian) into nasal and temporal halves using a single-edged razor blade. Under a stereomicroscope, another cut was made along the horizontal meridian. Small nasal (untreated) and temporal (treated) pieces (~1 mm x 0.75 mm) were cut along the central horizontal meridian (as depicted in **Figure 3.1**). These samples were placed in separate glass vials and processed for electron microscopy.

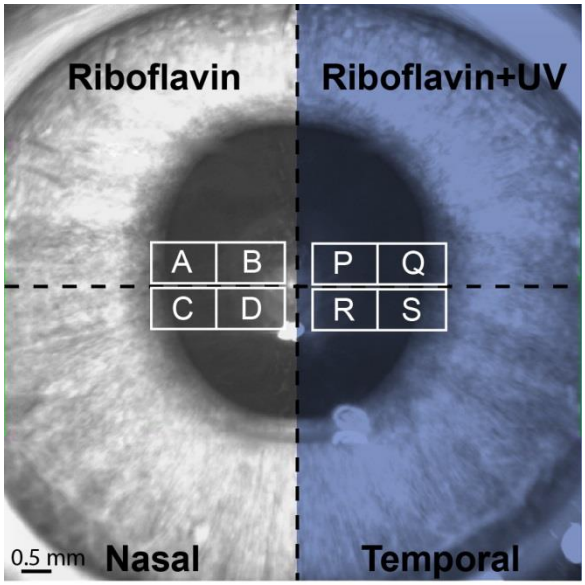

Figure 3.1: Schematic showing the enface OCT image of a rabbit cornea. UV Riboflavin cross-linking treatment was performed by administering the riboflavin solution (hypertonic/hypotonic) to the whole cornea but applying UV irradiation to only the temporal-half region. The cornea was cut in half along the treatment line (vertical meridian: black dash line) into nasal and temporal halves. Another cut was made along the horizontal meridian (black dash line). Small nasal (control: A, B, C, D)) and temporal (treated: P, Q, R, S)) pieces (~1 mm x 0.75 mm) cut along the central horizontal meridian were processed for electron microscopy.

Microwave fixation processing was preferred over conventional fixation protocol as it shortens the fixation time, allows fixation avoiding heat and associated damage, enables faster and better tissue penetration of the reagents used and can maintain the tissue quality without swelling, shrinking, or other processing artifacts. These advantages are

possible as the microwave utilizes a temperature controlling heat sink, upon which the tissues are placed in a vacuum chamber making it possible to enable fixation avoiding heating of the tissue samples. The vacuum combined with microwave energy reduces the boiling point of solutions and increases the rate of diffusion of the fixative and the reagents, thus enhancing the tissue penetration in a short time.[98] Microwave processing is also preferred for corneal tissues as the short fixation duration minimizes tonicity changes and greatly aides in maintaining the corneal ultrastructure without leading to morphological distortions and inter-lamellar separations. Microwave fixation processing involves a buffer rinse followed by three-minute cycles in 0.5% aqueous sodium tungstate and 0.5% sodium tungstate in 50% ethyl alcohol, dehydration in a graded ethyl alcohol series, embedding in Araldite 502/Embed 812 media and baking overnight in an oven at 60^0C. Embedded corneal tissues were cut into 400 nm ultrathin sections, suspended on formvar grids and stained using 3% Uranyl Acetate and Reynold's Lead Citrate.

Orthogonal profiles of the collagen fiber cross-sections were imaged using a Transmission Electron Microscope (FEI TECNAI G2 Spirit) equipped with a Gatan First Light 2000 x 2000 digital CCD camera at ~10-20 μm depth from the anterior stromal surface, sampling five regions at 6800x magnification to obtain the collagen fibril separation for all corneas. Light microscopy (LEICA) images of 0.5 μm thick corneal sections stained with toluidine blue were taken at 10x magnification to obtain corneal thickness. Corneal thickness was measured from the photographs of light microscopy images using a stage calibrated micrometer.

Image Analysis

Collagen fibril separation (inter-fibril spacing or nearest neighbor distance) was quantified as the average radial distance between the collagen fibrils in the sampled electron micrographs. [99] A distribution function of these radial distances was fit to the

electron micrographs to compute the collagen fibril separation using ImageJ software (**Figure 3.2**). The dominant peak from a radial distribution function provides the average collagen fibril separation of the electron micrograph.[100] All statistical comparisons were performed by conducting two-tailed paired t-tests using STATA 13.

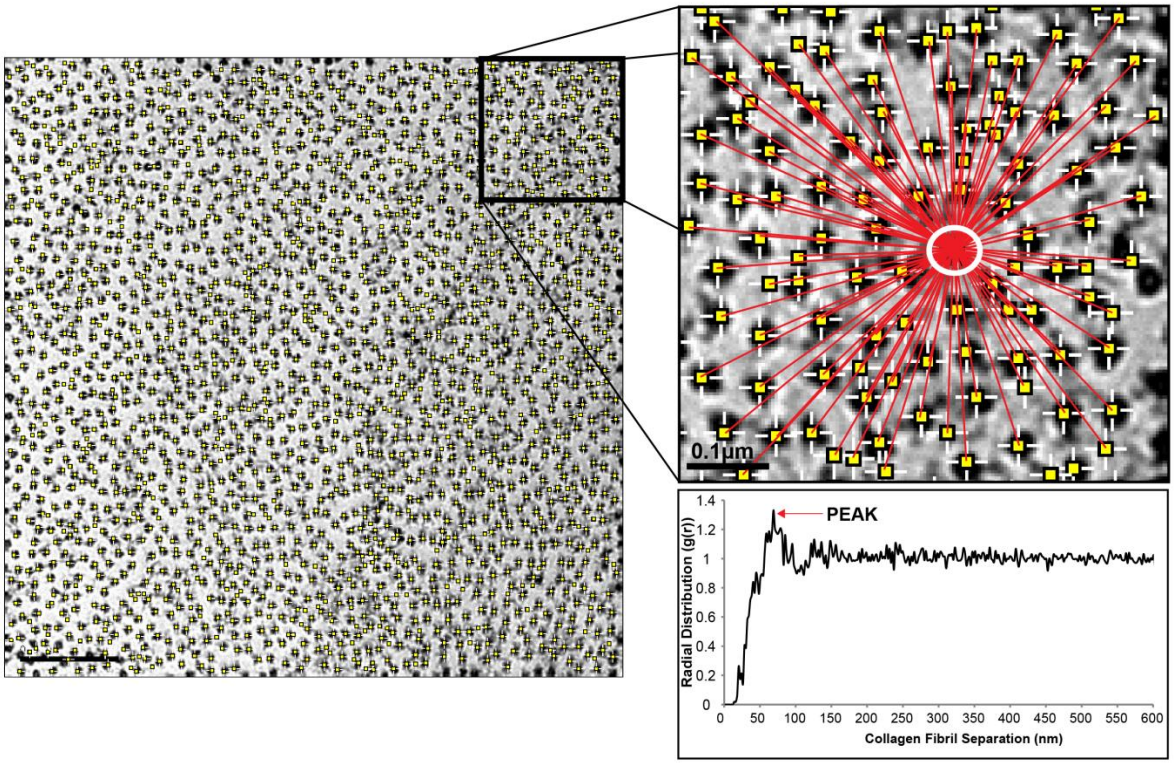

Figure 3.2: Illustration shows how collagen fibril separation was quantified by fitting a radial distribution function to the transmission electron micrograph of a rabbit cornea in the treated region after UV Riboflavin cross-linking treatment. Scale bar represents 0.5 µm. Inset shows collagen fibrils spacing from a reference fixed fibril (located in the white circle) obtained as a frequency distribution plot. An average of the cumulative frequency distribution plots obtained from all the individual fibrils in the electron micrograph gives the radial distribution function. The dominant peak from the radial distribution function provides the average collagen fibril separation (inter-fibril spacing or nearest neighbor distance) of the electron micrograph.

A vapor pressure osmometer (Vapro 5520, Wescor, Logan, UT) was used to obtain the measured osmolality of the hypertonic, hypotonic riboflavin solutions and the fixative (2.5% glutaraldehyde in 25 mM sodium acetate buffer (pH = 5.7), 0.1 M $MgCl_2$ with 0.05% cuprolinic blue). An initial calibration of the osmometer was performed by applying 10 µL of 290 mmol/kg osmolality standard solution (Optimol: OA-029, Wescor, Inc.) into a solute-free paper disc in the sample holder. Osmolalities of each solution (10 µL) were then measured five times separately, each time on fresh solute-free paper discs.

Results

Collagen fibril separation obtained from the radial distribution function peaks plotted for the transmission electron micrographs showed a significant decrease from 83.4nm in the untreated samples to 64.3 nm in their paired CXL treated region (64.3 nm) obtained from the same cornea when using hypertonic riboflavin (−23%; Mean Difference: −19 nm; 95% Confidence Interval (CI): −15 to −23; $P = 0.01$). Collagen fibril separation decreased significantly from 68.2 nm (control region) to 59.2 nm (treated region) when using hypotonic riboflavin (−13%; −9 nm; 95% CI: −5 to −13; $P = 0.01$). **Figure 3.3** shows typical electron micrographs of the rabbit anterior stromal collagen fibril spacing in the paired control (left) and CXL treated (right) sampled regions obtained from the same cornea after UV Riboflavin cross-linking treatment. **Figure 3.4** shows the anterior stromal collagen fibril spacing obtained from the peaks of radial distribution functions plotted for corneal electron micrographs of the paired control and CXL treated regions of the same rabbit cornea after cross-linking using hypertonic (A) and hypotonic (B) riboflavin solutions.

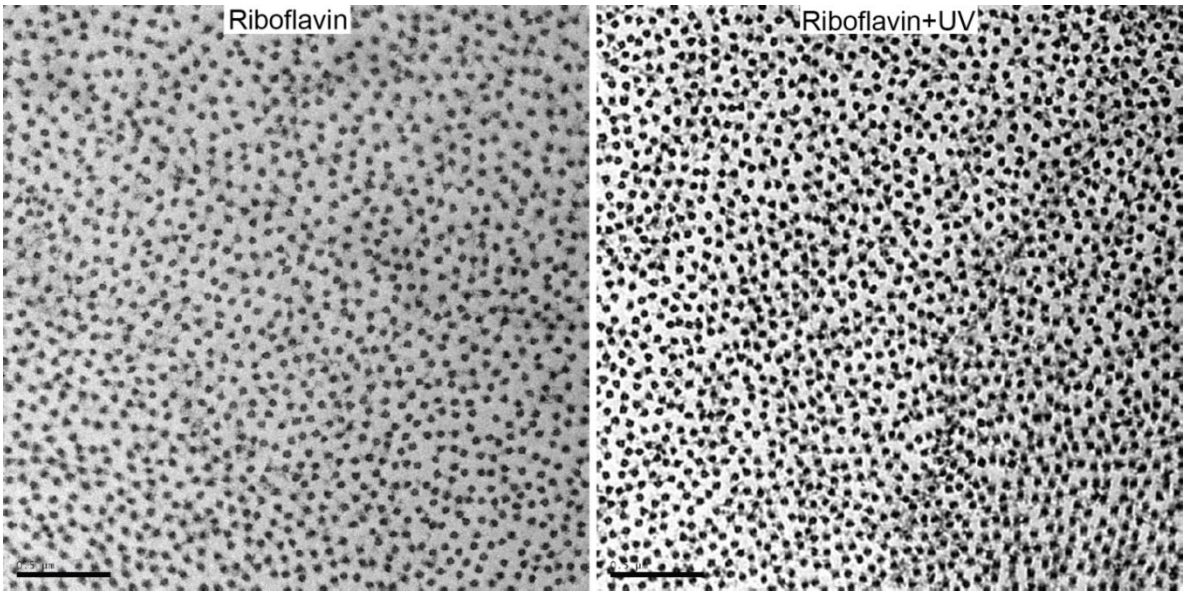

Figure 3.3: Transmission Electron Micrographs of rabbit corneas showing the collagen fibril spacing in the paired control (left) and treated (right) tissue regions from the same cornea with and without UV exposure. Scale bar represents 0.5 µm. The treated tissue region shows reduced collagen fibril separation compared to the control obtained from the same cornea. These samples are obtained from adjacent regions on either side of central treatment line in the hypertonic riboflavin treated group.

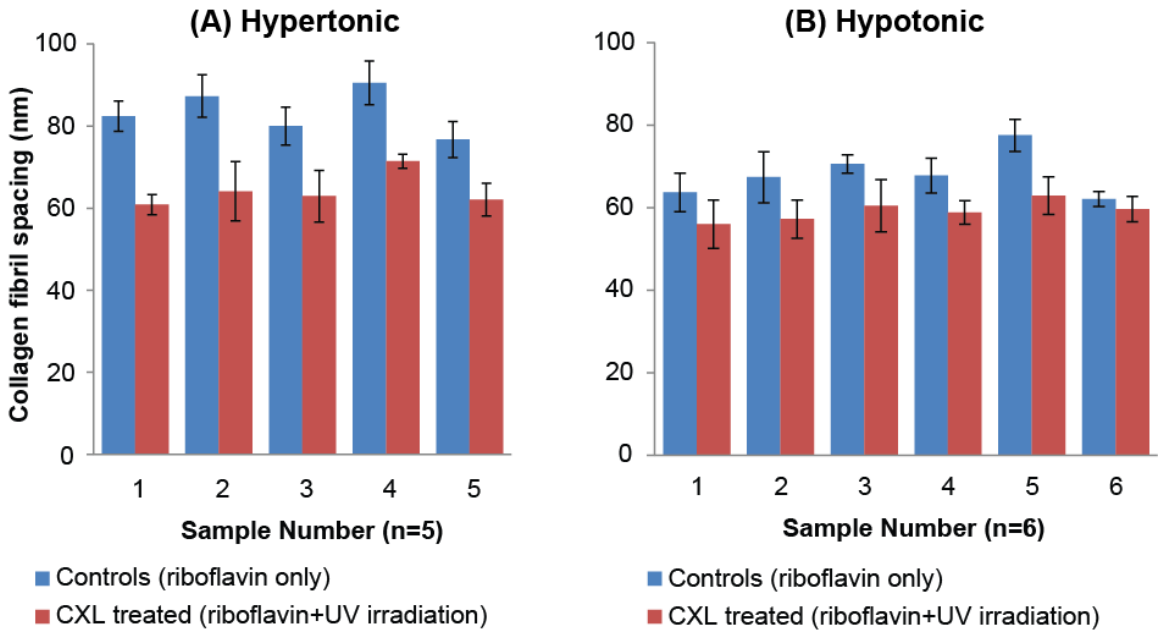

Figure 3.4: Anterior stromal collagen fibril spacing obtained from corneal electron micrographs in the control and CXL treated regions of the same rabbit cornea after cross-linking. Collagen fibril spacing is obtained from the dominant peaks of radial distribution functions plotted for electron micrographs after cross-linking using (A) hypertonic and (B) hypotonic riboflavin solutions. Significant decrease in fibril spacing is noted in the CXL treated region compared to their paired control region when cross-linked using both hypertonic (n=5; −23%; From 83.4 (control) to 64.3 nm (CXL treated); P = 0.01) and hypotonic (n = 6; −13%; From 68.2 (control) to 59.2 nm (CXL treated); P = 0.01) riboflavin solutions.

Mean baseline CCT was 641 µm in the corneas treated with hypertonic riboflavin solution (n=5) and 676 µm with hypotonic riboflavin solutions (n=6) measured *ex vivo* on de-epithelialized rabbit corneas using SD-OCT. UV riboflavin cross-linking treatment showed an overall significant decrease in the treated sample's corneal thickness measured from light microscopy after tissue fixation compared to the CCT obtained from SD-OCT images taken before cross-linking when treated using hypertonic riboflavin solution (−56%; −356 µm; 95% CI: −281 to −431; P = 0.01) (**Figure 3.5A**) and hypotonic riboflavin solution (−29%; −198 µm; 95% CI: −131 to −265; P = 0.01) (**Figure 3.5B**).

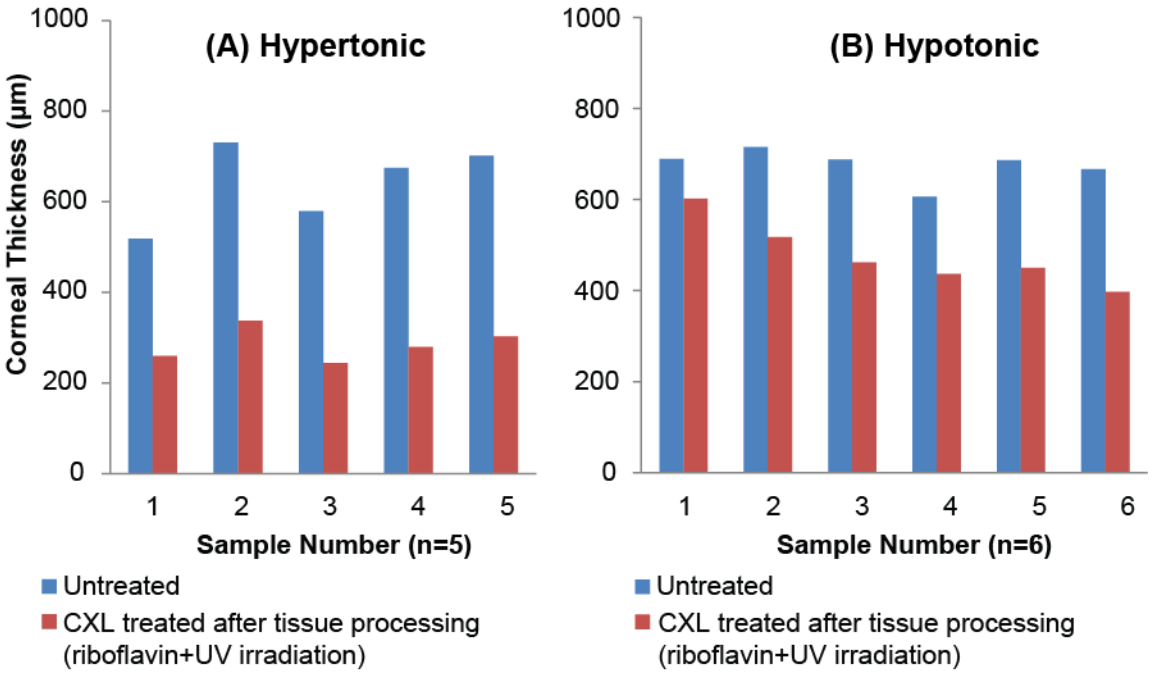

Figure 3.5: Distribution of ex vivo rabbit corneal thickness obtained using SD-OCT before cross-linking treatment and CXL treated sample's corneal thickness using hypertonic (A) and hypotonic (B) riboflavin solutions measured from light microscopy after tissue processing. UV riboflavin cross-linking treatment showed an overall significant thickness decrease when using hypertonic riboflavin solution (−56%; −356 µm; 95% CI: −281 to −431; *P* = 0.01) and hypotonic riboflavin solution (−29%; −198 µm; 95% CI: −131 to −265; *P* = 0.01).

Mean measured osmolality of the hypertonic, hypotonic riboflavin solutions and fixative solution (2.5% glutaraldehyde in 25 mM sodium acetate buffer (pH = 5.7), 0.1 M $MgCl_2$ with 0.05% cuprolinic blue) was 621.6 mmol/kg, 319.6 mmol/kg and 345.4 mmol/kg respectively as obtained using the osmometer.

Effect of riboflavin solution tonicity

Acute riboflavin tonicity driven changes comparing CCT obtained from SD-OCT imaging before and after cross-linking treatment showed a significant decrease (−57%; −363 µm; 95% CI: −279 to −448; *P* = 0.01) from 641 to 278 µm using hypertonic

riboflavin solution (**Figures 3.6A**) and a significant increase (+7%; +46 µm; 95% CI: +7 to +85; *P* = 0.03) from 676 to 721 µm using hypotonic riboflavin solution (**Figures 3.6B**). The higher tonicity of riboflavin diluted in 20% Dextran solution (Measured Osmolality: 621.6 mmol/kg) caused a decrease in corneal thickness and the lower tonicity of riboflavin diluted in 0.9% saline solution (Measured Osmolality: 319.6 mmol/kg) caused an increase in corneal thickness after treatment.

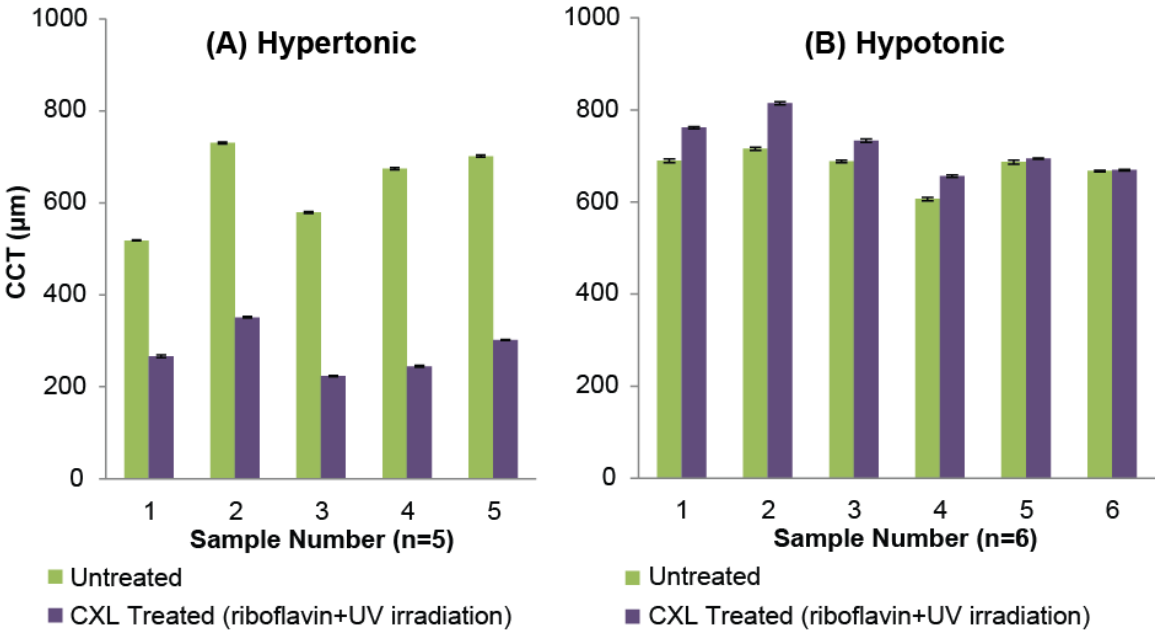

Figure 3.6: Distribution of central corneal thickness (CCT) in ex vivo rabbit eyes measured using SD-OCT before and after UV Riboflavin crosslinking using hypertonic (A) and hypotonic (B) riboflavin solutions. There is a significant decrease (n=5; −57%; −363 µm; 95% CI: −279 to −448; *P* = 0.01) with hypertonic riboflavin and a significant increase (n=6; +7%; +45 µm; 95% CI: +7 to +85; *P* = 0.03) in thickness after cross-linking with hypotonic riboflavin). The higher tonicity of riboflavin diluted in 20% Dextran solution (Measured Osmolality: 621.6 mmol/kg) caused a decrease in corneal thickness and the lower tonicity of riboflavin diluted in 0.9% saline solution (Measured Osmolality: 319.6 mmol/kg) caused an increase in corneal thickness after treatment.

Effect of tissue shrinkage/swelling due to tissue processing

The corneal thickness post-CXL treatment prior to tissue processing obtained using SD-OCT showed no significant change after tissue processing in the controls (+5%; +15 µm; 95% CI: −28 to +57; *P* = 0.39) and CXL treated (+3%; +7 µm; 95% CI: −32 to +18 ; *P* = 0.48) paired regions as measured from the corneal light microscopy images, when hypertonic riboflavin was used in the cross-linking procedure. No significant change was observed between the corneal thickness of the control and CXL treated paired regions measured from rabbit corneal light microscopy images when treated using hypertonic riboflavin solution (−3%; −8 µm; 95% CI: −28 to 13; *P* = 0.35) (**Figures 3.7A**). No change in corneal thickness after tissue processing for electron microscopy in both the control and CXL treated paired region obtained from the same cornea demonstrates no tissue shrinkage or swelling induced due to tissue processing.

The corneal thickness obtained post-CXL treatment prior to tissue processing obtained using SD-OCT decreased significantly after tissue fixation as measured from light microscopy images in the control (−18%; −131 µm; 95% CI: −37 to −225; *P* = 0.02) and CXL treated (−34%; −243 µm; 95% CI: −192 to −295; *P* = 0.01) paired region when hypotonic riboflavin was used for the cross-linking procedure. Significant decrease (−19%; −113 µm; 95% CI: −16 to −209; *P* = 0.03) was observed from 590 µm in the control region to 478 µm in the paired CXL treated region measured from rabbit light microscopy images when treated using hypotonic riboflavin solution (**Figures 3.7B**). Tissue processing for electron microscopy showed tissue shrinkage when using hypotonic riboflavin solution, resulting in reduced corneal thickness in the control (18%) and CXL treated (34%) paired regions obtained from the same corneas.

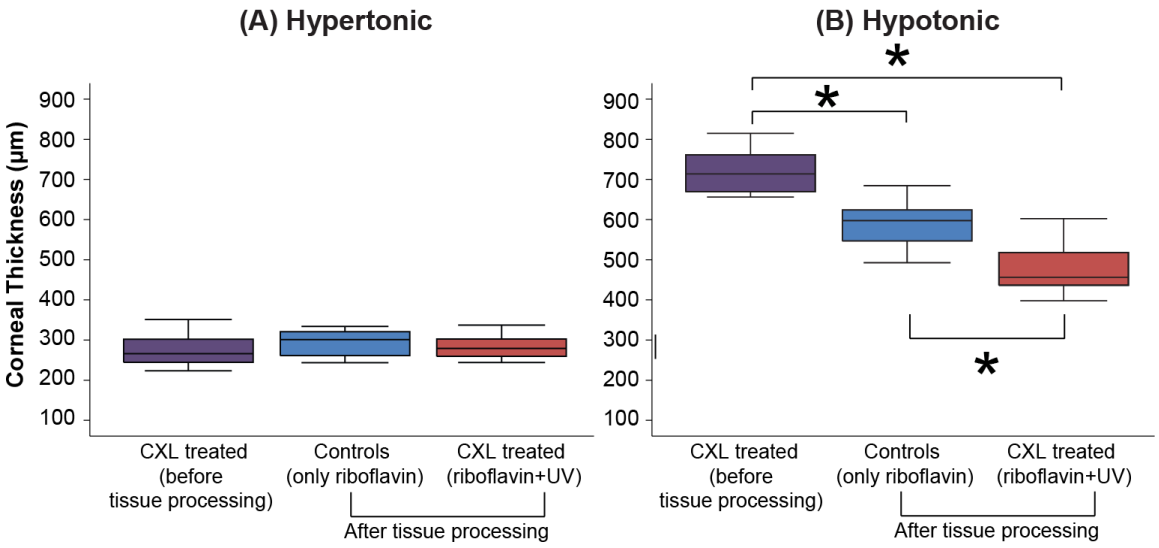

Figure 3.7: Distribution of corneal thickness measured from SD-OCT prior to tissue processing and from the light microscopy images of fixed rabbit corneal tissues in the control and CXL treated paired regions from the same cornea when using (A) hypertonic and (B) hypotonic riboflavin solution. With hypertonic riboflavin, there is no change in corneal thickness after tissue fixation in both the control and CXL treated paired regions obtained from the same cornea resulting in no tissue shrinkage or swelling due to electron microscopy tissue processing. Tissue processing for electron microscopy showed tissue shrinkage when using hypotonic riboflavin solution, resulting in reduced corneal thickness in the control (18%) and CXL treated (34%) paired region obtained from the same corneas.

Discussion

Using hypertonic riboflavin solution in the cross-linking treatment resulted in an acute tonicity driven corneal thickness decrease (–57%). Higher osmolality of hypertonic riboflavin solution (measured osmolality: 621.6 mmol/kg) compared to the fixative solution (measured osmolality: 345.4 mmol/kg) aided in maintaining the tissue thickness post-processing. The fixation protocol implemented to process the corneal tissue for electron microscopy helped preserve the corneal morphology by maintaining corneal thickness without shrinkage, swelling or distortion artifacts, as a preferred technique over

conventional tissue fixation methods. Although, no corneal thickness difference is observed between the controls (riboflavin only) and the CXL treated paired region (riboflavin + UV irradiation) post-tissue processing, there is reduced anterior collagen fibril separation in the CXL treated region (−23%). This implies cross-linking treatment induced the observed acute anterior collagen fibril spacing decrease in the treated region and it is not only driven by the tonicity (hydration) changes within the samples.

On the other hand, using hypotonic riboflavin solution in the cross-linking treatment resulted in a tonicity driven corneal thickness increase (+7%). Following this during electron microscopy tissue processing, tissue shrinkage occurred inducing reduced corneal thickness in the control (−18%) and treated (−34%) paired regions. If tonicity is the sole driving force behind the observed effects due to cross-linking treatment, the thickness reduction should ideally be the same in both the control and CXL treated paired regions because they are derived from the same cornea. However, the treated region reduced more—post-processed corneal thickness in the CXL treated regions reduced by 19% compared to their paired control regions. This shows that the corneal thickness decrease is also because of the cross-linking treatment and not only tonicity driven.

Our results show an acute anterior collagen fibril spacing decrease and an overall corneal thickness reduction due to the effect of tonicity and UV riboflavin cross-linking treatment. Including a control and CXL treated paired sample from the same cornea in the study helped capture the effects due to cross-linking treatment and the effects induced by tonicity.

The anatomical location where the cross-links can be induced with CXL treatment is still an open question. Brummer et al.[61] described six possible cross-linking mechanisms at the molecular level involving the proteoglycan core protein, glycosaminoglycans, and

collagen fibrils. There might be partial or even no participation of proteoglycans in the cross-linking mechanisms in *ex vivo* whole globes as there is neutralization of the negatively-charged proteoglycans with an increase in corneal swelling[101, 102] (baseline corneal thicknesses are higher *ex vivo*). However, *in vivo,* magnitude of the cross-linking treatment can be expected to be higher due to the involvement of proteoglycans in forming additional cross-links (described by Brummer et al.[61] and Hayes et al.[92]) between two proteoglycan core proteins, proteoglycan core protein and collagen fibril, glycosaminoglycan and collagen fibril surface. There is also the possibility of inducing cross-links between collagen fibrils (inter-fibril interaction), inter-molecular, and intra-molecular interaction within the collagen fibrils within or at their surface[92] with CXL treatment. The increased resistance to *in vitro* enzymatic digestion in CXL treated corneas[103] also supports the idea of the cross-link formation within and between collagen fibrils.

Variability in mean total corneal thickness across the different samples can be due to sample-related factors like health at the time of death, time of death/excision time, storage conditions, preservation techniques, the effect of hydration, room temperature, humidity, etc. Baseline corneal thicknesses (669 µm) recorded in this study are higher than previously known physiologically normal rabbit corneal thickness (~400 µm)[104] because of using *ex vivo* corneas from enucleated globes. Because of this, even though the electron microscopy processing methods used in this study preserved the tissue morphology, preventing tissue shrinking/swelling using hypertonic riboflavin, the collagen fibril separation in the control region is higher (hypertonic group: 83 nm; hypotonic group: 68 nm) than previously published values.[2, 105] Giraud et al.[105] measured inter-fibrillar distances in rabbits to be 54 nm and Meek et al. measured the spacing to be 59 nm using x-ray crystallography. Therefore, future studies should include additional steps for

hydration control prior to the experiments to reduce the corneal thickness to its physiologically normal range.

To conclude, this study demonstrates the acute effects of UV riboflavin cross-linking on the anterior corneal ultrastructure in rabbit corneas. At the ultrastructural level, a decrease in anterior collagen fibril spacing is demonstrated with UV riboflavin cross-linking treatment. UV riboflavin cross-linking treatment globally causes an acute decrease in corneal thickness. Future work should be towards understanding the long-term effects of cross-linking on the corneal ultrastructure.

CHAPTER FOUR

EFFECT OF TONICITY AND UV RIBOFLAVIN CROSS-LINKING TREATMENT ON CORNEAL BIOMECHANICAL PROPERTIES USING OPTICAL COHERENCE ELASTOGRAPHY

Srilatha Vantipalli, [1] Jiasong Li, [2] Manmohan Singh, [2] Salavat R Aglyamov, [3] Kirill V. Larin, [2, 4] Michael D. Twa[5]

[1]College of Optometry, University of Houston, 505 J. Davis Armistead Bldg., Houston, TX 77204; [2]Department of Biomedical Engineering, University of Houston, 3605 Cullen Blvd, Houston, TX 77204; [3]Department of Biomedical Engineering, University of Texas at Austin, Austin, TX, 78712; [4]Interdisciplinary Laboratory of Biophotonics, Tomsk State University, Tomsk 634050, Russia ; [5]School of Optometry, The University of Alabama at Birmingham, 1716 University Blvd, Birmingham, AL 35233

Preface

Collagen cross-linking is an emerging treatment for keratoconus that can slow disease progression by increasing corneal stiffness using riboflavin and UV light.[53] The riboflavin used in the conventional cross-linking treatment protocol is dissolved in dextran which is a hyperosmotic agent. Current techniques deriving corneal biomechanical properties do not consider the influence of tissue hydration when measuring the effect of cross-linking. This chapter evaluates a) the influence of hydration state on the corneal biomechanical properties and b) the influence of hydration on the acute treatment effects due to UV riboflavin crosslinking treatment using OCE imaging.

Abstract

Purpose: Current techniques to derive corneal biomechanical properties do not consider the influence of tissue hydration or its effect on collagen cross-linking. Here we investigate the effects of hydration alone and the combined acute effect of hydration and UV riboflavin cross-linking (CXL) treatment on measured rabbit corneal biomechanical properties.

Methods: Dynamic elastography imaging was performed using phase-sensitive optical coherence tomography (OCT) imaging (30 kHz A-scan rate) to quantify the tissue deformation dynamics resulting from a spatially discrete, low-force air-pulse (150µm spot size; 0.8 ms duration; 4Pa (0.03mmHg)). The time-dependent surface deformation at the corneal apex is characterized by a viscoelastic tissue recovery response, quantified by an exponential decay constant—*relaxation rate*. Out of a total of 23 fresh ex vivo globes with fixed IOP (15mmHg), 10 eyes were instilled 0.9% saline every 5min for 60min and 20% dextran every 5min for another 60min. Measurements were made every 20min for 120min to determine the central corneal thickness (CCT) and the relaxation rates. CXL treatment was performed on the remaining 13 eyes, by applying isotonic riboflavin solution (n=6; 0.1% riboflavin in 2.5% dextran dissolved in 0.9% saline) and hypertonic riboflavin solution (n=7; 0.1% riboflavin in 20% dextran dissolved in 0.9% saline) every 5min for 30min, followed by UV irradiation (365nm, 3mW/cm^2) for 30min while instilling riboflavin. CCT and relaxation rates were obtained before and after CXL treatment.

Results: Applying 0.9% saline showed no significant change in CCT (−1%; mean difference: −5µm; 95% Confidence Interval: −35 to +25; P=0.70) or the relaxation rates (−6%; −0.18ms^{-1}; 95% CI: −0.03 to +0.40; P=0.08), but instilling 20% dextran showed a significant decrease in CCT (−44%; −303µm; 95% CI: −269 to −336; P=0.01) and the relaxation rates (−21%; −0.57ms^{-1}; 95% CI: −0.37 to −0.76; P=0.01). Corneal thickness was positively correlated (R^2=0.9) with relaxation rates**.** In the CXL treated eyes, isotonic

riboflavin did not affect CCT (−1%; −5µm; 95% CI: −21 to +32; P=0.62) while hypertonic riboflavin showed a significant CCT decrease (−31%; −189µm; 95% CI: −127 to −252; P=0.01) from 618µm to 429µm after treatment. Isotonic CXL treatment showed significantly greater relaxation rates (+10%; +0.24ms^{-1}; 95% CI: +0.08 to +0.40; P = 0.01) after treatment (2.53ms^{-1}) than in untreated tissue (2.29ms^{-1}). However, hypertonic CXL treatment showed little change in relaxation rates (+6%; +0.11ms^{-1}; 95% CI: −0.04 to +0.27; P=0.12)

Conclusions: Corneal thickness and stiffness are correlated positively. Higher RR implies stiffer corneal material properties after isotonic CXL treatment. Hydration (tonicity) driven corneal thinning using hypertonic riboflavin produced a stiffness decrease that offset the expected stiffer material properties due to CXL treatment, resulting in no net change in acute corneal material properties after hypertonic CXL treatment. This demonstrates corneal hydration is an important factor in the measurement of corneal biomechanics that can confound short-term effects due to CXL treatment.

Introduction

Current techniques to derive corneal biomechanical properties i.e., extensiometry,[59] inflation testing,[27] optical coherence elastography (OCE),[106-109] ultrasound elastography,[110] Brillouin spectroscopy,[28] etc., are largely performed *ex vivo* and do not consider the influence of tissue hydration on the measured material properties. Previous studies show steps taken to preserve or restore physiological corneal thickness prior to the experiments by storing at 4^0C with cotton soaked in 0.9% saline,[111] or immersing in 20% dextran overnight,[66] etc. or using commercial preservative solutions (e.g. Optisol),[112] oils,[113, 114] etc., to control corneal thickness. However, maintaining thickness over time is still a problem. Changes in the corneal hydration state are known to affect the measured biomechanical properties by influencing the underlying tissue mechanical strength.[66, 67] Here, we evaluate the influence of tissue hydration state on the corneal biomechanical properties by OCE. In general, 0.1% riboflavin solution dissolved in 20% dextran is used in the UV riboflavin cross-linking (CXL) treatment performed to slow disease progression by increasing corneal stiffness[58, 59] for keratoconus[53] and post-refractive surgery ectasias.[57] However, the riboflavin used in the conventional cross-linking treatment protocol is often dissolved in dextran, which is a hyperosmotic agent resulting in a tonicity-driven corneal thickness change during treatment.[68] Therefore, the corneal material properties after cross-linking are also acutely influenced by corneal hydration. This study evaluates the influence of hydration on the acute treatment effects due to UV riboflavin crosslinking treatment.

Corneal stroma forms the bulk of the cornea and is ultrastructurally comprised primarily of heterotypic collagen fibrils[12] (predominantly type I and type V) arranged as a *pseudo-hexagonal* lattice[115] and organized into collagen lamellae with a network of keratocytes interspersed between the lamellae,[3] surrounded by ground substance composed mainly of proteoglycans (predominantly dermatan sulfate and keratan sulfate

with small amounts of heparin sulfate) with glycosaminoglycan side-chains. Epithelial barrier function, stromal imbibition pressure due to the negative charges on proteoglycan-glycosaminoglycan complexes, endothelial pump function, the osmolality of the tears and the aqueous, closed-eye (hypoxia) or open-eye, evaporation due to room environmental conditions (humidity, temperature) are all factors that play a role in influencing *in vivo* corneal thickness.[19, 116-118] However *ex vivo*, the globe is enucleated, the endothelial pump function slowly declines while the negative charge on the proteoglycans creates an imbibition force driving water into the stroma, altering corneal hydration.

Previous studies show tissue hydration changes affecting the measured biomechanical properties. Dias et al.[66] performed atomic force microscopy on *ex vivo* excised porcine corneas and showed increased Young's modulus in swollen corneas immersed in balanced salt solution and 0.9% saline media. A similar increase in hysteresis was shown by Kling et al.,[67] wherein whole globe inflation testing was performed on *ex vivo* porcine corneas after treating with Optisol, 8% dextran, 20% dextran and 0.1% riboflavin dissolved in 20% dextran for 30 minutes. Previous histology studies by Hayes et al.[89] investigating the short term effects of CXL treatment question whether the observed changes are due to the treatment alone or due to the hydration state altered by the osmotic effects driven by the presence of dextran. We investigate the effects of hydration alone and the combined acute effect of hydration and UV riboflavin cross-linking (CXL) treatment on measured rabbit corneal biomechanical properties.

In this study, we will implement optical coherence elastography (OCE) methods that allow us to non-destructively quantify stiffness in the cornea in an almost *in vivo*-like setting wherein an intact cornea without any incisions or excisions is used with controlled intra-ocular pressure inside the enucleated globe. We developed a micro air pulse

stimulator that creates a localized short-duration focal stimulation. This approach is non-contact and provides the capability to obtain spatially localized corneal material properties. Optical coherence elastography (OCE) involves dynamically loading the tissue using an air pulse to create a focused mechanical stimulation and imaging the induced microscopic tissue motion using a high-resolution optical coherence tomography (OCT) to derive the tissue's material properties.[50, 107, 119] The purpose of this study is two-fold: 1) develop a way to control and maintain corneal thickness over a period of 200 minutes in controlled environmental conditions in *ex vivo* rabbit corneas and then apply optical coherence elastography imaging methods to quantify the influence of corneal hydration state on the tissue biomechanical properties and 2) evaluate the influence of hydration on the treatment effects due to UV riboflavin crosslinking treatment using OCE imaging.

Methods

Freshly enucleated mature albino whole rabbit eyes (age > 6 months) were obtained from Pel-Freeze Biologicals within 12 hours stored in Dulbecco's Modified Eagle's Medium and used within 36 hrs after enucleation.

A) Effect of tonicity

i. Effect of tonicity on corneal thickness

A total of five groups (each group n = 3) were instilled 5 solutions of different osmolalities respectively: 0.9% saline solution (pH = 7.4), 2.5% dextran, 5% dextran, 10% dextran and 20% dextran solutions (all diluted in 0.9% saline). Each cornea was de-epithelialized using a blunt spatula. One drop of the solution was applied every 5 minutes for 200 minutes to the exposed stromal surface. Central corneal thickness (CCT) was measured every 5 minutes using a non-contact Spectral Domain RTVue Optical Coherence Tomography (SD-OCT) (RTVue) for 200 minutes. Rate of change of

CCT per minute was calculated for each group in room environmental conditions (temperature: ~23^{0}C, relative humidity: ~60%). Measured Osmolality was obtained for all the solutions using a vapor pressure osmometer (Vapro 5520, Wescor, Logan, UT). An initial calibration of the osmometer was performed by applying 10 µL of 290 mmol/kg osmolality standard solution (Optimol: OA-029, Wescor, Inc.) into a solute-free paper disc in the sample holder. Osmolalities of each solution (10 µL) were then measured five times separately, each time on fresh solute-free paper discs.

ii. Effect of tonicity on corneal biomechanical properties

Anatomical orientation of the fresh whole rabbit globes (n = 10) was identified, placed in a holder, and the globes were cannulated at the equator to control the intra-ocular pressure (IOP) using two 19 mm gauge needles placed perpendicular to each other. One needle was connected to a pressure sensor (Model 41X; Keller Instruments) to continuously monitor the internal pressure and fed into the computer. The other needle was attached to an automated computer-controlled micro infusion/withdrawal syringe (filled with 0.9% saline solution) pump (NE-500 programmable syringe pump, New Era Pump Systems, Inc.) that adjusted the pressure on a closed feedback loop to maintain the desired IOP inside the eyes, throughout the experiments. Corneal epithelium was manually debrided using a blunt spatula. Baseline structural OCT imaging of the debrided cornea was performed to obtain the CCT prior to OCE measurements.

Baseline optical coherence elastography was performed using a high resolution, home-built phase-stabilized swept source optical coherence tomography imaging system and a micro air pulse stimulator that produced focal tissue surface stimulation. **Figure 4.1** shows the schematic of the OCE set-up. Our previous publications[50, 120, 121] provide a detailed description of the imaging system. The imaging system utilizes a swept source laser illuminator (HSL2000, Santec, Inc., Torrance, California) with a central wavelength

of 1310 ± 75 nm, A-scan rate of 30 kHz, and an output power of 36 mW. The system enables axial spatial resolution of ~11 µm, lateral spatial resolution of ~16 µm and high phase stability of ~16 milliradians, corresponding to a displacement sensitivity of ~3 nm in air.[121] The home-built air pulse stimulator gives a focal controlled air pulse with a localized spatiotemporal Gaussian profile having a force amplitude ranging 2 to 10 Pa (0.02 to 0.08 mmHg) delivered over 0.8 ms duration through a 150 µm diameter port at an angle of incidence of 45° to the apical surface. The distance between the air-pulse stimulator and the cornea was maintained constant (~200 µm) by manually controlling the z-axis stage.

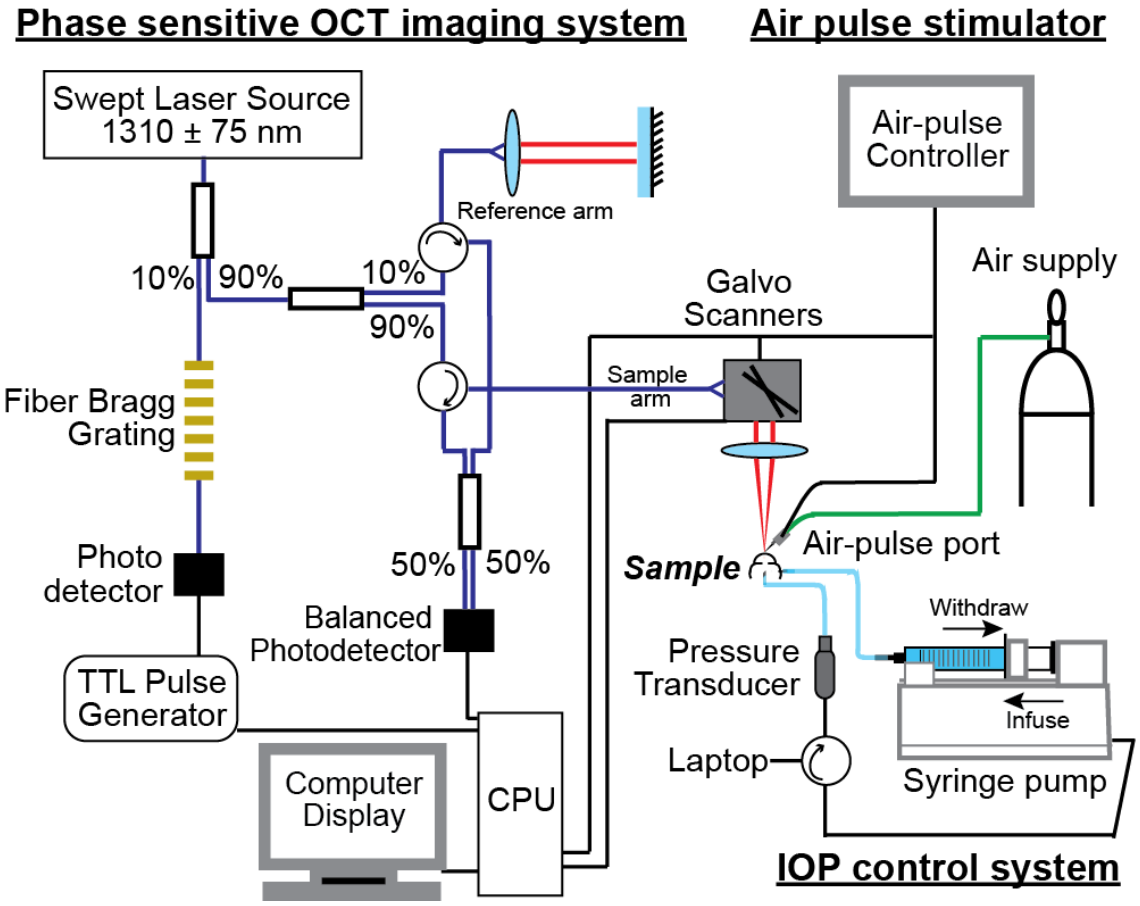

Figure 4.1: Optical Coherence Elastography Imaging System schematic shows the phase stabilized swept source OCT imaging system, micro air pulse stimulator, and IOP control system. The OCT imaging axis was coincident with the air pulse stimulator's port to obtain a co-

localized response during in vivo measurements of rabbit corneal tissue material properties. IOP was maintained throughout the experiment using a closed–loop micro infusion syringe pump.

Air pulse stimulation at the corneal apex was used to produce localized mechanical waves which dispersed internally as an axial compressive force and had tangential lateral propagation (shear waves). This low-amplitude (micrometer-scale) localized tissue displacement was a complex viscoelastic response to the air-pulse stimulation. The OCT system was used to record the time-dependent surface response at the corneal apex,[120] and placed such that the OCT imaging axis was coincident with the air pulse stimulator's port to obtain a co-localized response. The phase profile of the recorded-localized point response was made up of an initial negative deformation to maximal displacement of the corneal surface, followed by a time-dependent corneal surface recovery back to its original position. This phase profile was unwrapped and converted from phase displacement to amplitude using

$$d(t) = \frac{\lambda}{2\pi n} \times \varphi(t), \qquad (1)$$

where d was the amplitude (µm), λ was the central wavelength of the OCT system (µm), n was refractive index ($n_{air} = 1$), and φ was phase (radians). **Figure 4.2** shows a typical displacement recorded at the corneal apex using the imaging system. A variance-weighted Fourier fit was applied to filter the low-frequency oscillations.

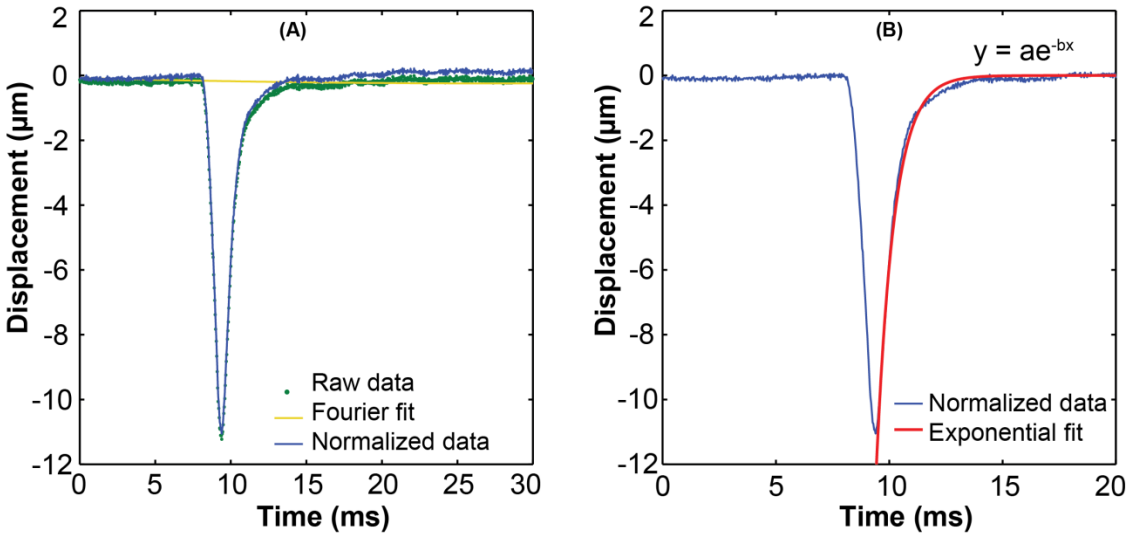

Figure 4.2: Optical coherence elastography of rabbit corneal surface shows A) the phase profile from point response during dynamic corneal surface stimulation and B) an exponential fit to the observed tissue deformation recovery response. A typical displacement signal recorded at the corneal apex demonstrates an initial negative surface deformation response to the air pulse force, peak deformation amplitude, and a prolonged viscoelastic recovery response (green dots). Low frequency sinusoidal noise in the phase signal is filtered using a Fourier fit to the raw data (yellow line). The relaxation rate (b) is obtained from an exponential fit, starting at the point of maximum deformation amplitude until the end of the observed phase response (~10 ms).

The rate, at which the corneal anterior surface recovered back to its initial position from the point of maximum displacement, captured the complex viscoelastic behavior displayed by the cornea in response to mechanical stimulation. The exponential decay function was calculated by fitting an exponential function using

$$y(t) = \left(a\, e^{(-bt)}\right) + c \qquad (2)$$

where *a* was amplitude (µm), and *b* was decay constant (ms^{-1}) starting at the point of maximum displacement amplitude until the surface recovery back to its original position. The primary outcome measure was the exponential decay constant (*b*) termed Relaxation Rate (RR).

Following the baseline OCE measurements, a hypotonic solution (0.9% saline) was instilled on the corneal surface every 5 minutes for 60 minutes to induce corneal swelling and then, a hypertonic solution (20% dextran solution diluted in 0.9% saline) was instilled every 5 minutes for another 60 minutes to induce corneal thinning. Structural images and point responses were captured every 20 minutes for 120 minutes at a fixed IOP of 15 mmHg. At each time point, CCT was determined from structural OCT images and relaxation rates were determined from the OCE recorded viscoelastic recovery responses.

The relationship between the corneal thickness and the relaxation rates were assessed by calculating the correlation coefficient while instilling 0.9% saline and 20% dextran over a period of 120 minutes in rabbit corneas Two-tailed paired t-tests were conducted to assess the change in corneal thickness and relaxation rates before and after instilling 0.9% saline and 20% dextran.

B) Effect of CXL on corneal biomechanical properties

Ex vivo rabbit globes (n = 6) were prepared as described above. After epithelial debridement, baseline structural OCT and dynamic OCE measurements were obtained with fixed IOP (15 mmHg). UV riboflavin cross-linking treatment was performed by instilling isotonic riboflavin solution (0.1% riboflavin dissolved in 2.5% dextran) every 5 minutes for 30 minutes on the exposed stromal surface, followed by UV irradiation (365 nm, 3 mW/cm^2) for 30 minutes while instilling riboflavin solution. Structural and point responses were measured again post-treatment.

C) Effect of tonicity and CXL on corneal biomechanical properties

Ex vivo rabbit globes (n = 7) were prepared and treated as described above. However, instead of isotonic riboflavin solution, hypertonic riboflavin solution (0.1% riboflavin in 20% dextran (T500) dissolved in 0.9% saline; Dresden protocol)[58] was used for the UV riboflavin cross-linking treatment. CCT was determined from structural OCT

imaging and relaxation rates were determined from the OCE-recorded viscoelastic recovery responses before and after CXL treatment. Two-tailed paired t-tests were performed to compare the corneal thickness and relaxation rates before and after CXL treatment.

Results

A) Effect of tonicity

i. Effect of tonicity on corneal thickness

The baseline mean CCT measured by OCT imaging was 749 ± 108 µm (n = 15 eyes). **Figure 4.3** shows the CCT change in ex vivo rabbit eyes with the application of different osmolality solutions over a period of 200 minutes. Corneal swelling was observed with the application of 0.9% saline and 2.5% dextran, while corneal de-swelling was seen with 5% dextran, 10% dextran and 20% dextran. Minimal change in thickness per minute was caused by 2.5% dextran and maximal change was seen with 20% dextran. **Table 4.1** shows the rate of change in corneal thickness per minute for the osmotic agents applied on de-epithelialized corneas along with their measured osmolality.

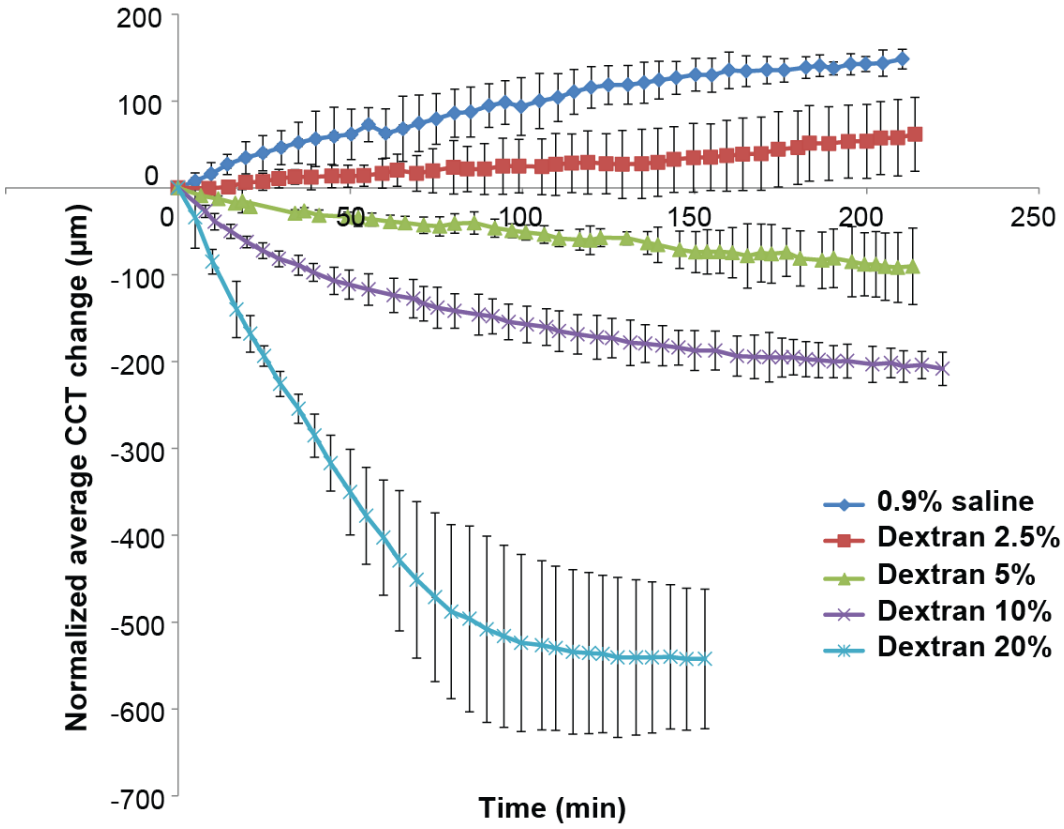

Figure 4.3: Central corneal thickness change in ex vivo rabbit eyes with the application of different osmolality solutions over a period of 200 minutes measured using an OCT. Corneal thickness of rabbit corneas is best controlled by 2.5% dextran solution when used *ex vivo* within 36 hrs after enucleation and epithelial debridement.

Table 4.1: Influence of osmotic agents on corneal thickness

S.No	Osmotic agents	Rate of change in CCT per min	Measured Osmolality
		µm/min	mmol/kg
1	0.9% saline	+0.70 ± 0.06	318.4 ± 1.34
2	2.5% dextran	+0.29 ± 0.20	312.8 ± 1.30
3	5% dextran	−0.42 ± 0.20	314.4 ± 1.14
4	10% dextran	−0.94 ± 0.08	327.4 ± 2.10
5	20% dextran	−3.54 ± 0.60	394.8 ± 4.00

ii. Effect of tonicity on corneal biomechanical properties

The baseline mean CCT of the rabbit corneas measured by structural OCT imaging was 671 ± 54 µm (n = 10 eyes) at 15 mmHg and the baseline mean relaxation rates measured by OCE imaging was 2.88 ± 0.31 ms^{-1}. **Figure 4.4** shows the relationship between relaxation rates and corneal thickness obtained using OCE while instilling 0.9% saline and 20% dextran over a period of 120 minutes in rabbit corneas. After 60 minutes of instilling PBS on the stromal surface, no significant change was noted in their CCT (−1%; mean difference: −5 µm; 95% CI: −35 to +25; P = 0.7) and relaxation rates (−6%; −0.18 ms^{-1}; 95% CI: −0.03 to −0.4; P = 0.08). After treatment with 20% dextran for the next 60 minutes, a significant decrease in CCT (−44%; −303 µm; 95% CI: −269 to −336; P = 0.01) and relaxation rates (−21%; −0.57 ms^{-1}; 95% CI: −0.37 to −0.76; P = 0.01) was observed. A significant positive linear correlation (R^2 = 0.91; P = 0.01; 95% CI: 0.001 to 0.003) is observed between corneal thickness and relaxation rates. There is a decrease in relaxation rates consistent with decreased stiffness with a decrease in corneal thickness.

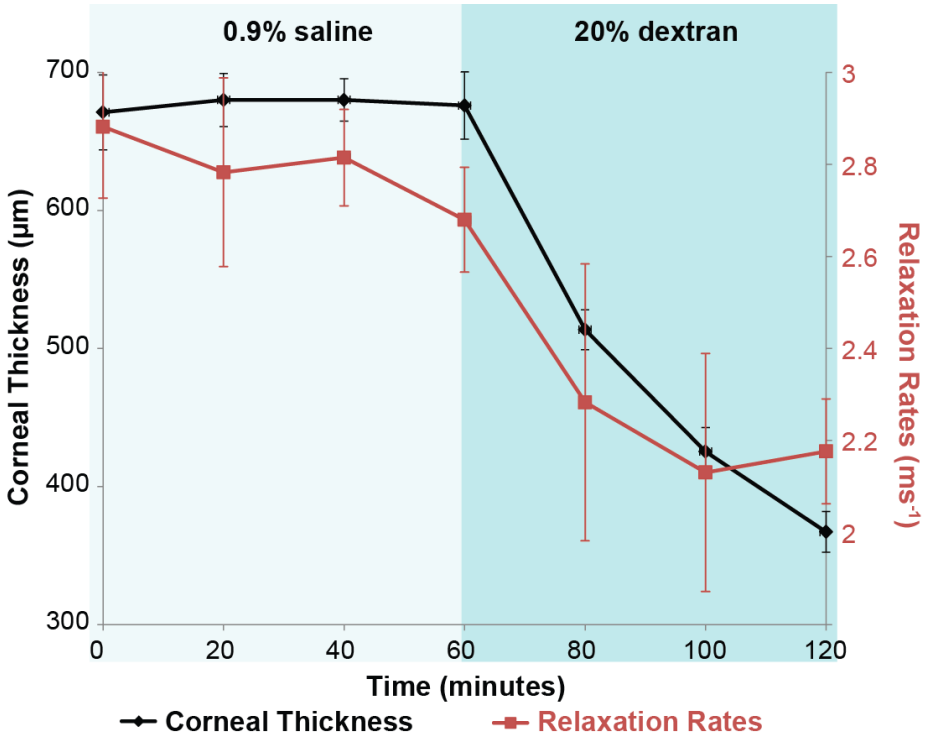

Figure 4.4: OCE measurements of average corneal thickness and relaxation rates over a time period of 120 minutes while instilling 0.9% saline and 20% dextran solutions on de-epithelialized rabbit corneas. No change ($P > 0.05$) in corneal thickness or relaxation rates is noted with 0.9% saline in the first 60 minutes across all samples, while instilling 20% dextran caused a significant decrease in corneal thickness (−44%; P = 0.01) and relaxation rates (−21%; P = 0.01). A positive correlation ($R^2 = 0.91$; P = 0.01) is observed between corneal thickness and relaxation rates. There is a decrease in relaxation rates indicating reduced corneal stiffness, with a decrease in corneal thickness.

B) Effect of CXL on corneal biomechanical properties

The baseline mean CCT of the rabbit corneas measured by structural OCT imaging was 624 ± 62 µm (n = 6 eyes) at 15 mmHg and the baseline mean relaxation rates measured by OCE imaging was 2.29 ± 0.13 ms^{-1}. Isotonic riboflavin (0.1% riboflavin dissolved in 2.5% dextran) did not affect CCT (−1%; −5 µm; 95% CI: −21 to +32; P = 0.62), but showed significantly greater relaxation rates (+10%; +0.24 ms^{-1}; 95% CI:

+0.08 to +0.4; P = 0.01) post cross-linking treatment (2.53 ± 0.1 ms^{-1}) after 60 minutes (**Figure 4.5**).

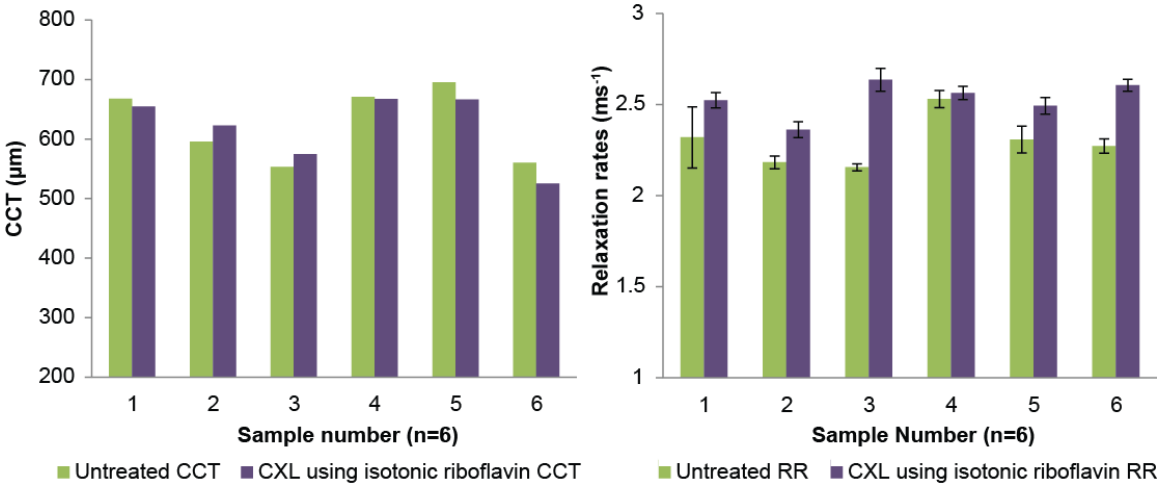

Figure 4.5: OCE measurements of central corneal thickness and relaxation rates measured ex vivo in rabbit eyes (n=6) before and after UV riboflavin treatment using isotonic riboflavin solution. Isotonic riboflavin (0.1% riboflavin dissolved in 2.5% dextran dissolved in 0.9% saline) did not affect CCT (−1%; −5 µm; 95% CI: −21 to +32); P = 0.62) but showed significantly greater relaxation rates (+10%; +0.24 ms^{-1}; 95% CI: +0.08 to +0.4; P = 0.01) after cross-linking treatment, indicating stiffer tissue biomechanical properties post-treatment.

C) Effect of tonicity and CXL on corneal biomechanical properties

The baseline mean CCT of the rabbit corneas measured by structural OCT imaging was 618 ± 57 µm (n = 7 eyes) at 15 mmHg and the baseline mean relaxation rates measured by OCE imaging was 1.91 ± 0.29 ms^{-1}. Hypertonic riboflavin (0.1% riboflavin dissolved in 20% dextran) caused a significant CCT decrease (−31%; −189 µm; 95% CI: −127 to −252; P = 0.01) after cross-linking treatment (429 ± 62 µm). CXL treatment using hypertonic riboflavin showed no significant change in relaxation rates (+6%; +0.11 ms^{-1}; 95% CI: +0.04 to +0.27; P = 0.12) (**Figure 4.6**).

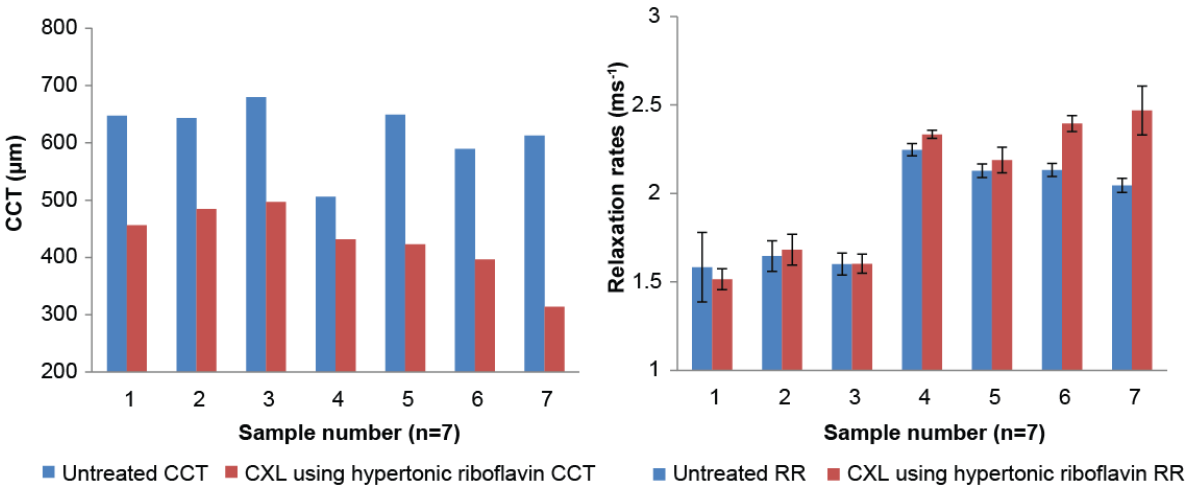

Figure 4.6: OCE measurements of central corneal thickness and relaxation rates measured ex vivo in rabbit eyes before and after UV riboflavin treatment using hypertonic riboflavin solution. Hypertonic riboflavin (0.1% riboflavin in 20% dextran dissolved in 0.9% saline) caused a tonicity-driven significant CCT decrease (n = 7; −31%; −189 µm; 95% CI: −127 to −252; P = 0.01), causing a corresponding corneal stiffness decrease (**figure 4.4**) that offset the expected stiffer material properties due to CXL treatment, resulting in no net change in corneal material properties by OCE (RR: +6%; +0.11 ms^{-1}; 95% CI: +0.04 to +0.2; P = 0.12) after cross-linking treatment using hypertonic riboflavin.

Discussion

Our results show 0.9% saline and 2.5% dextran solutions were hypotonic to the corneal stroma, while the rest (5% dextran, 10% dextran and 20% dextran solutions) were hypertonic for a time period over 200 minutes in de-epithelialized *ex vivo* corneas under controlled room environmental conditions, where temperature is ~23^{0}C and relative humidity is ~60% and used within 36 hrs after enucleation. Using this tonicity information, we applied 0.9% saline (hypotonic solution) to increase corneal thickness, followed by 20% dextran (hypertonic solution) to decrease corneal thickness in order to quantify the influence of hydration on corneal biomechanical properties using OCE imaging. There is a decrease in relaxation rates consistent with reduced stiffness with a

decrease in corneal thickness. Therefore, thick swollen corneas are stiffer and there is decreasing stiffness with decreasing corneal thickness.[122]

Following CXL treatment using isotonic riboflavin solution (riboflavin dissolved in 2.5% dextran solution), higher relaxation rates implies stiffer (10%) corneal material properties. Previous studies using other biomechanical testing techniques such as extensiometry,[59] inflation testing,[27] optical coherence elastography,[106-109] ultrasound elastography,[110] commercial devices such as the Ocular Response Analyzer[123, 124] (ORA), Brillouin spectroscopy,[28] etc., have also shown stiffer corneal properties with cross-linking treatment. However, CXL treatment using hypertonic riboflavin (riboflavin dissolved in 20% dextran) showed a tonicity driven corneal thinning with hypertonic riboflavin resulting in a stiffness decrease that offset the expected stiffer material properties due to CXL treatment, resulting in little change in corneal material properties after hypertonic CXL treatment. This demonstrates corneal hydration is an important factor in the measurement of corneal biomechanics that can confound short-term effects due to CXL treatment.

In *ex vivo* conditions, after the globe is enucleated and the cornea is de-epithelialized, the endothelial pump function is also slowly reduced. The best way to control and maintain *ex vivo* corneal thickness is to alter the stromal tonicity dynamics in controlled room environmental conditions. In this study, a solution with osmolality between 312.8 mmol/kg (2.5% dextran) and 314.4 mmol/kg (5% dextran) would be isotonic to the corneal stroma, and 2.5% dextran solution best controlled and maintained *ex vivo* corneal thickness for over 200 minutes time period in controlled room environmental conditions. The osmolality of 2.5% dextran solution (312.8 mmol/kg) obtained in this study is higher in comparison with Brubaker's[125] stromal osmolality (304 mosm~mmol/kg) measured from the interstitial fluid (extra cellular matrix) in living rabbit corneal stroma. The difference in the osmolality measures could be attributed to the

method used to measure the osmolalities, wherein Brubaker used the freezing point depression method[125], while we used the vapor pressure depression method (built into the Wescor vapor osmometer). Stahl and colleagues[126] suggest the freezing point depression method is not suitable for measuring viscous solutions and can result in a significant change from the actual value.

Stiffer properties in swollen thick corneas can be due the accumulation of fluid in the stromal extra cellular matrix. In *ex vivo* corneas, the reduced endothelial pump function creates an imbalance in the pump-leak mechanism resulting in corneal swelling with slow fluid accumulation in the stroma. Driven by the negative swelling pressure of the glycosaminoglycans present in the stromal extracellular matrix, the cornea swells and saturates to a new steady-state level, causing the corneal thickness to become much greater than previously known physiologically normal values (from ~400 µm[104] *in vivo* to 600-750 µm in *ex vivo* conditions). There is an increased amount of tension acting on the cornea surface when so much fluid accumulates within the corneal stroma resulting in stiffer material properties when measured in this condition. Following the instillation of a hypertonic agent (20% dextran solution), the fluid drains out, and the cornea is no longer swollen and the stiffness also decreases. These results are consistent with previous studies by Kling et al.[67] and Dias et al.[66] However, these results are limited only to intact *ex vivo* corneas wherein the corneal endothelial pump function is not optimum and the epithelium is also debrided. Further *in vivo* studies are needed to better understand the influence of hydration on corneal stiffness in physiologically normal ranges.

To conclude, this study demonstrates the influence of tonicity and cross-linking treatment on the corneal biomechanical properties individually and together. Corneal thickness and stiffness are correlated positively. Cross-linking treatment induces an increase in stiffness. Decrease in corneal thickness due to the application of hypertonic

riboflavin during the cross-linking treatment, results in a decrease in stiffness that offsets the stiffness increase due to cross-linking treatment. This is a short-term effect resulting due to the influence of hydration.

CHAPTER FIVE

DEPTH DEPENDENT BIOMECHANICAL PROPERTIES OF THE RABBIT CORNEAS USING DYNAMIC OPTICAL COHERENCE ELASTOGRAPHY IMAGING

Srilatha Vantipalli, [1] Jiasong Li,[2] Manmohan Singh,[2] Salavat R Aglyamov,[3] Alan R Burns,[1] Kirill V. Larin,[2, 4] Michael D. Twa[5]

[1]College of Optometry, University of Houston, 505 J. Davis Armistead Bldg., Houston, TX 77204; [2]Department of Biomedical Engineering, University of Houston, 3605 Cullen Blvd, Houston, TX 77204; [3]Department of Biomedical Engineering, University of Texas at Austin, Austin, TX, 78712; [4]Interdisciplinary Laboratory of Biophotonics, Tomsk State University, Tomsk 634050, Russia; [5]School of Optometry, The University of Alabama at Birmingham, 1716 University Blvd, Birmingham, AL 35233

Preface

The purpose of this chapter is to evaluate the depth dependent tissue properties of the stromal bed and implement a cross-linking treatment in the posterior cornea. Quantifying posterior corneal tissue properties will allow us to better understand the effects of experimental cross-linking in the deep stroma and this information will contribute to future applications in lamellar keratoplasty and refractive surgery through modification of deep corneal biomechanical properties. Elastography imaging methods will be used to measure the deep corneal tissue material properties by applying minute forces using an air pulse stimulator and capturing the microscopic tissue displacement using highly sensitive optical coherence elastography (OCE) imaging. A non-UV based collagen cross-linking technique will be performed to increase the stiffness of the deep cornea by using rose bengal stain and green light (RGX). This will provide the corneal depth dependent biomechanical properties and a cross-linking technique to increase stiffness in the deep stroma. Comparisons with the efficacy of UV riboflavin cross-linking (UV CXL) treatment in the deep stroma will be performed. Additional comparisons with collagen cross-linking treatments performed on the full thickness corneal stroma are also performed.

.

Abstract

Purpose: There are structural and biochemical differences between the anterior and posterior corneal stroma. It is not advisable to use conventional UV-Riboflavin cross-linking (UV CXL) in the deep corneal stroma due to potential UV-induced endothelial cell toxicity. Here we evaluate the biomechanical properties of the deep corneal stroma and the effect of Rose Bengal Green Light Cross-linking (RGX) treatment as a safer alternative to UV CXL treatment on the deep corneal stroma.

Methods: Optical coherence elastography (OCE) measurements were made at the corneal apex in vitro on 10 rabbit eyes: at the stromal surface after de-epithelialization, at 2/3rd corneal thickness in the deep stroma after trephination, and after RGX treatment in the deep stroma. RGX was performed (n=5) using 0.1% rose bengal solution for 20min (one drop every 5min) and 10min green light irradiation (565nm, 0.25W/cm^2) and UV CXL treatment (Dresden Protocol) was performed (n=5) in the deep stroma. Dynamic tissue deformation responses were produced using a focal micro air pulse stimulator (150µm spot size, 0.8ms duration, and force ranging 2 to 10Pa (0.02 to 0.08mmHg)) and surface deformation was recorded using a phase-sensitive swept-source optical coherence tomography (OCT) imaging system at fixed IOP (15mmHg). The recovery response of tissue deformation responses were quantified by an exponential decay constant termed as the relaxation rate (RR). Additionally, OCE measurements were obtained after RGX (n=6) and UV CXL (n=6) treatments were performed on the full thickness stromal surface.

Results: Mean relaxation rate pre-treatment was 1.68ms^{-1} with an average corneal thickness of 683µm. Relaxation rate at a depth of 2/3rd corneal thickness (185µm) reduced significantly (−22%; Mean difference: −0.38ms^{-1}; 95% CI: −0.24 to −0.51; P=0.01). Relaxation rates were greater (+22%; +0.32ms^{-1}; 95% CI: +0.18 to +0.47; P=0.01) after RGX treatment in the deep stroma (1.78ms^{-1}) than in untreated tissue

(1.46ms^{-1}). After UV CXL treatment, relaxation rates (1.63ms^{-1}) at a depth of 2/3rd corneal thickness (303µm) was greater (+44%; +0.49ms^{-1}; 95% CI: +0.29 to +0.70; P=0.01) than in untreated tissue (1.14ms^{-1}). Relaxation rates increased after conventional UV CXL (+10%; +0.24ms^{-1}; 95% CI: +0.08 to +0.40; P=0.01) and RGX (+8%; +0.20ms^{-1}; 95% CI: +0.21 to +0.37; P=0.03) treatments on the stromal surface.

Conclusions: Untreated full thickness stroma is stiffer than the untreated deep stroma. Higher relaxation rates demonstrate an increase in stiffness in the deep cornea following RGX treatment. This shows promise for future applications in lamellar keratoplasty and refractive surgery through modification of deep corneal biomechanical properties. The treatment effect was higher with UV CXL treatment (44%) compared to RGX treatment (22%) at 2/3rd corneal depth. Both treatment effects were greater in the deep stroma compared to the full thickness stroma (RGX: 8%; UV CXL: 10%)

Introduction

Keratoconus is characterized by loss of corneal structural rigidity.[56, 127] Collagen cross-linking is an emerging treatment for keratoconus that can slow disease progression by increasing corneal stiffness using riboflavin and UV light.[53] UV riboflavin cross-linking (UV CXL) is performed routinely by removing the epithelium and inducing the effect in the anterior stroma (~200um).[52, 54, 69] Combining collagen cross-linking treatment in the deep stroma with corneal transplantation procedures to treat keratoconus like anterior lamellar keratoplasty or refractive surgeries like LASIK or photorefractive keratectomy (PRK) is proposed as a prophylactic measure to increase the posterior corneal stiffness and prevent future ectasia.[65] However, UV CXL treatment is not safe for use in the deep corneal stroma due to endothelial cell UV toxicity.[70] In this study, we apply a newly described[29, 71] non-UV cross linking based on rose bengal stain and green light (RGX) to increase the stiffness of the deep cornea. Cherfan et al.[29] and Wang et al.[71] have previously shown an increase in corneal stiffness with RGX treatment applied on de-epithelialized stroma with limited penetration of rose bengal dye (a depth of 100 µm into the corneal stroma). Using rose bengal green light cross-linking treatment, will provide a new approach to increase the stiffness in the deep stroma without the damaging effects of UV radiation on the endothelium.

The efficacy of cross-linking treatment in the posterior cornea is unknown with either the RGX technique or with the conventional UV riboflavin cross-linking method. The corneal stromal architecture differs structurally as a function of depth (inhomogeneous).[7, 128, 129] Previous studies suggest that the anterior stroma is rigid over the posterior stroma owing to a densely-packed, greater degree of anterior lamellar interweaving[7, 130] and this rigidity is suggested to be responsible for corneal structural stability.[128] [11] Biomechanical testing techniques investigating the depth dependent

corneal material properties also show posterior stroma is weaker than the anterior stroma.[28, 114, 131, 132]

Apart from the mechanical variations, differences exist in the stromal composition between the anterior and posterior stroma.[133-136] The anterior stromal lamellae branch obliquely into each other, forming a well interwoven collagen lamellar network,[5, 7] while the posterior lamellae are arranged parallel to each other and parallel to the corneal surface.[3] The anterior lamellae are thinner, narrower, while the posterior lamellae are thicker and wider.[8] Dermatan sulfate and keratan sulfate are proteoglycans with covalently attached glycosaminoglycans side chains predominantly present in the stromal ground substance.[12] Dermatan sulfate is more abundant in the anterior stroma, while keratan sulfate is more abundant in the posterior stroma.[136] Keratan sulfate readily absorbs more water than dermatan sulfate and this is suggested to be the reason for higher posterior stromal swelling.[11, 128, 136] Because of these differences in the structural organization and composition across the stromal depth, the stiffness change in the deep stroma with cross-linking treatments, as compared to the stiffness increase in the conventional corneal cross-linking treatments can be more or less.

To address this, we use optical coherence elastography (OCE) imaging to measure the deep stromal biomechanical properties. OCE imaging involves non-invasively quantifying biomechanical properties using a high speed, high resolution, phase-sensitive optical coherence tomography (OCT) imaging system to capture the tissue's response to mechanical loading using a micro air-pulse stimulator that creates a localized short-duration focal stimulation.[50] We have previously used elastography imaging methods to capture the biomechanical properties after collagen cross-linking treatments of the rabbit corneas *ex vivo*.[107, 109, 137] This chapter evaluates the deep stromal biomechanical properties in *ex vivo* rabbit cornea and the effect of RGX cross-linking in the deep stroma using elastography imaging methods. Comparisons with the

efficacy of UV riboflavin cross-linking (UV CXL) treatment in the deep stroma will be performed. Additional comparisons with collagen cross-linking treatments performed on the full thickness corneal stroma post-epithelial debridement are also performed.

Methods

All experiments were conducted on freshly enucleated mature albino whole rabbit eyes obtained from Pel-Freeze Biologicals within 12 hours stored in Dulbecco's Modified Eagle's Medium and used within 36 hrs after enucleation. Rabbit eyes were prepared for OCE imaging by identifying the globe's anatomical orientation. Whole globes were placed in a holder and cannulated at the equator perpendicular to each other using two 19 mm gauge needles. Intra-ocular pressure was controlled by continuously monitoring the internal pressure using one of the needles connected to a pressure sensor ((Model 41X; Keller Instruments) and fed into the computer. The other needle attached to an automated computer-controlled micro infusion/withdrawal syringe (filled with 0.9% saline solution) pump (NE-500 programmable syringe pump, New Era Pump Systems, Inc.) was used to adjust the pressure in a continuous closed feedback loop to maintain the desired IOP inside the eyes throughout the experiments. The corneal epithelium was manually debrided using a blunt spatula. Baseline structural OCT imaging of the debrided cornea was performed to obtain the CCT, prior to OCE measurements.

Baseline optical coherence elastography (OCE) was performed using a high resolution, home-built phase-stabilized swept source optical coherence tomography imaging system and a micro air pulse stimulator that produced focal tissue surface stimulation. **Figure 4.1** shows the schematic of the OCE set-up. Our previous publications[50, 120, 121] provide a detailed description of the imaging system. The imaging system utilizes a swept source laser illuminator (HSL2000, Santec, Inc., Torrance, California) with a central wavelength of 1310 ± 75 nm, A-scan rate of 30 kHz, and an

output power of 36 mW. The system enables axial spatial resolution of ~11 µm, lateral spatial resolution of ~16 µm and high phase stability of ~16 milliradians, corresponding to a displacement sensitivity of ~3 nm in air.[121] The custom built air pulse stimulator gives a focal controlled air pulse with a localized spatiotemporal Gaussian profile having a force amplitude ranging 2 to 10 Pa (0.02 to 0.08 mmHg) delivered over 0.8 ms duration through a 150 µm diameter port at an angle of incidence of 45° to the apical surface. The distance between the air-pulse stimulator and the cornea was maintained constant (~200 µm) by manually controlling the z-axis stage.

The OCT imaging system and the air pulse stimulator delivery port were co-localized to capture the response ~0.4 mm away from the stimulated location.[120] Air pulse stimulation at the corneal apex produced a localized surface deformation made up of an initial negative surface displacement of the cornea, followed by a time-dependent recovery of the tissue to its original position. This low-amplitude (micrometer-scale) localized tissue displacement was a complex viscoelastic response occurring over a ~5 ms time period. The OCT-recorded phase profile was unwrapped and converted from phase displacement to amplitude using

$$d(t) = \frac{\lambda}{2\pi n} \times \varphi(t), \qquad (1)$$

where d was the amplitude (µm), λ was the central wavelength of the OCT system (µm), n was refractive index ($n_{air} = 1$), and φ was phase (radians). A variance-weighted Fourier fit was applied to filter the low-frequency oscillations. The exponential decay rate at which the corneal anterior surface recovered back to its initial position from the point of maximum displacement was calculated by fitting an exponential function using

$$y(t) = \left(a\, e^{(-bt)}\right) + c \qquad (2)$$

where a was amplitude (µm), and b was decay constant (ms^{-1}) starting at the point of maximum displacement amplitude until the surface recovers back to its original position.

The primary outcome measure was the exponential decay constant (*b*) termed Relaxation Rate (RR).

Deep stromal cross-linking treatments

Following baseline OCE measurements, a Barron Radial Vacuum Trephine was used to manually trephine the central 8mm cornea to a targeted depth of 2/3rd corneal thickness.

i. Rose bengal green light cross-linking treatment

Rose bengal green light cross-linking was performed in the deep stroma (n = 5) by instilling 0.1% rose bengal dye (diluted in 0.9% saline) every 5 minutes for 20 minutes. After 20 minutes, the cornea was exposed to green light (565 nm, 0.25 W/cm^2) for 10 minutes. The structural OCT and OCE measurements were performed before and after treatment in the deep stroma to obtain the central corneal thickness and the relaxation rates. **Figure 5.1** shows the experimental steps involved in performing Rose Bengal Green Light Cross-linking treatment in the deep stroma.

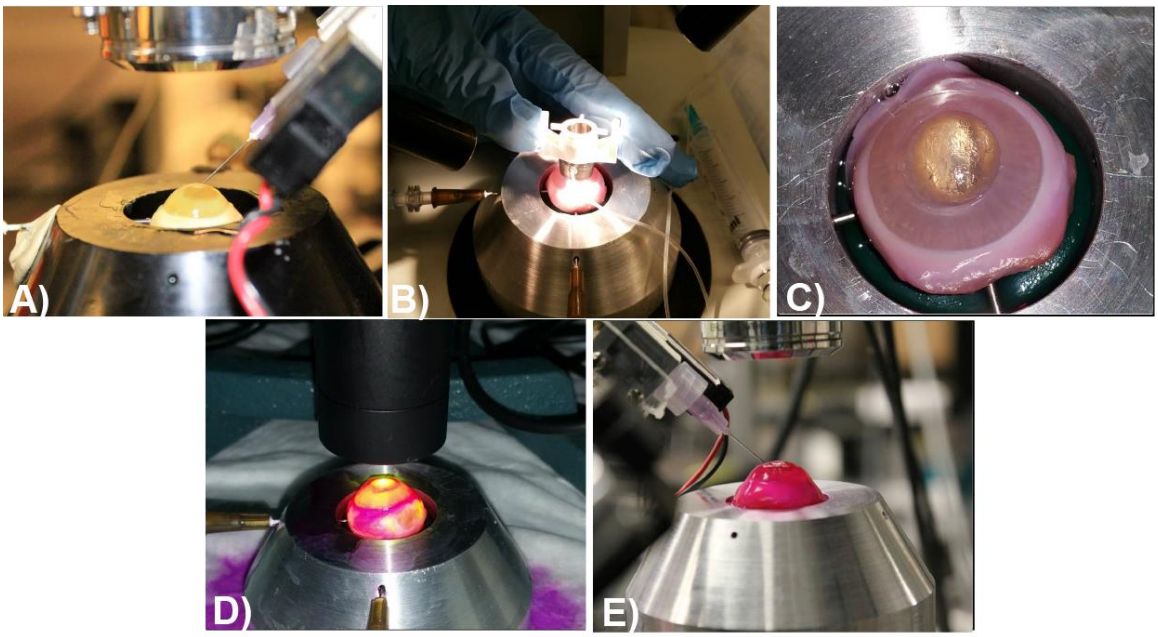

Figure 5.1: Experimental steps involved in performing Rose Bengal Green Light Cross-linking (RGX) treatment at 2/3rd corneal depth in pressure controlled rabbit eyes. A) Set-up for OCT imaging and air pulse stimulation on the corneal surface. **B)** Trephination to 2/3rd corneal thickness using Barron Radial Vacuum Trephine. **C)** Central 8mm deep corneal stroma after trephination before setting-up for imaging. **D)** RGX treatment in the deep corneal stroma performed applying 0.1% rose bengal solution for 20 minutes (one drop every 5 min) and 10 min green light irradiation (565 nm, 0.25 W/cm^2). **E)** Set-up of elastography imaging after cross-linking in the deep stroma.

ii. UV riboflavin cross-linking treatment

UV riboflavin cross-linking treatment was performed in the deep stroma (n = 5) by instilling riboflavin solution (0.1% riboflavin dissolved in 20% dextran) every 5 minutes for 30 minutes, followed by UV irradiation (365 nm, 3 mW/cm^2) for 30 minutes while instilling riboflavin solution. Structural OCT images and OCE responses were measured before and treatment in the deep stroma.

Full thickness RGX and UV CXL treatments

Following the epithelial debridement and baseline OCE measurements, rose bengal green light cross-linking (n = 6) and conventional UV riboflavin cross-linking (n = 6) treatment was performed on the stromal surface. UV CXL was performed using isotonic riboflavin solution (0.1% riboflavin in 2.5% dextran dissolved in 0.9% saline solution) to maintain corneal thickness during treatment and minimize the effects of hydration on corneal stiffness. Structural OCT images and OCE responses were captured again after the treatment.

Penetration depth of rose bengal dye into the stroma

Ex vivo fresh mature rabbit globes (n = 11) were obtained and prepared as described above. The superior and nasal limbus was marked to track the corneal orientation throughout the experiment. After epithelial debridement using a blunt spatula, the baseline central corneal thickness (CCT) measurements were obtained using the Anterior Segment Spectral Domain OCT (RTVue; Carl Zeiss). Rose Bengal dye (0.1% dye dissolved in 0.9% saline) was instilled on the exposed stromal surface (n = 5) every 5 minutes for 20 minutes. The vehicle (0.9% saline) was instilled every 5 minutes for 20 minutes in the control eyes (n = 6). CCT measurements were repeated after rose bengal dye/vehicle instillation. The cornea was then dissected out, leaving ~1-2 mm limbus surrounding the cornea. The superior and nasal limbal positions were marked by making extra cuts. Radial cuts were made at diagonal locations (at 45°, 135°, 225° and 325°) to flatten the cornea and a central 5mm wide corneal strip (vertical strip extending along the superior-inferior axis) was cut. This corneal strip was placed in a cryomold, adding optimal cutting temperature (OCT) compound and then flash frozen in liquid nitrogen for 10 seconds. These samples were cut into 5 µm thick sections using a cryostat (Bright model OTF cryostat with freezing microtome) and the corneal sections were imaged on a deconvolution microscope (DeltaVision imaging system, Applied Precision Inc.).

All images (controls and rose bengal dye-instilled) were captured at a fixed exposure time in order to compare the fluorescence intensities between the controls and rose bengal dye instilled images in the TRITC channel (Excitation wavelength: 555 nm; Emission wavelength: 617nm). TRITC channel was chosen as rose bengal dye shows maximum absorption with 562 nm maximal excitation.[29] Following the TRITC channel imaging, DAPI (4',6-diamidino-2-phenylindole, Sigma-Aldrich) was applied to visualize the presence of any residual epithelial cells post-debridement and highlight the endothelial cell margins. Each image was deconvolved to improve the resolution and reduce blur using SoftWorx software (Applied Precision).

Image analyses was performed by obtaining 50 consecutive line profiles of fluorescence intensities separately from the top, middle and bottom locations within an image in the TRITC and averaged separately for each of the samples among the controls and the rose bengal dye instilled corneal sections. The average depth of rose bengal dye diffusion was calculated as the depth until 10% maximum fluorescence intensities were recorded. Corneal thickness was obtained as the distance between the initial TRITC channel peak corresponding to the anterior stromal border and the second DAPI channel peak corresponding with the endothelium.

Results

Full thickness and deep stromal biomechanical properties

Baseline mean corneal thickness after epithelial debridement was 721 µm with 95% confidence interval (CI): 672 to 770 from pooling the data (n = 10) prior to performing RGX and UV CXL treatments. After manual trephination to 2/3rd corneal thickness, the corneal thickness was 244 µm with 95% CI: 192 to 296. Relaxation rates reduced significantly (−22%; Mean difference: −0.38 ms^{-1}; 95% CI: −0.24 to −0.51; P = 0.01) at 2/3rd corneal thickness from 1.67 ms^{-1} with 95% CI: 1.54 to 1.81 measured

anteriorly after epithelial debridement to 1.3 ms^{-1} with 95% CI: 1.13 to 1.47 measured in the deep stroma. **Figure 5.2** shows the distribution of corneal thickness and relaxation rates obtained before and after manual trephination using OCE imaging.

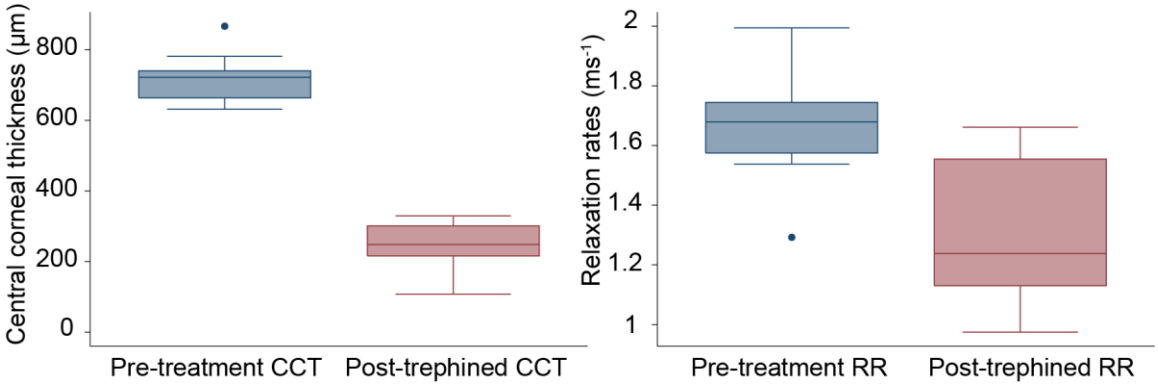

Figure 5.2: Distribution of corneal thickness and relaxation rates obtained before and after manual trephination using structural OCT and OCE imaging. Corneal thickness was 721 µm and after manual trephination to 2/3rd corneal thickness, the remaining 1/3rd corneal thickness was 244 µm. Relaxation rates reduced significantly (−22%; −0.38 ms^{-1}; 95% CI: −0.24 to −0.51; P = 0.01) at 2/3rd corneal thickness. Corneal stiffness reduced after manual trephination to 2/3rd corneal thickness.

Deep stromal RGX treatment

Relaxation rate at the corneal surface post-epithelial debridement was 1.68 ms^{-1} with 95% CI: 1.33 to 2.02 having an average central corneal thickness of 683 µm with 95% CI: 624 to 742. Relaxation rate at 2/3rd corneal depth after trephination was 1.46 ms^{-1} with 95% CI: 1.19 to 1.73, having an average deep stromal thickness of 185 µm with 95% CI: 121 to 248. After rose bengal green light cross-linking treatment in the deep stroma, mean relaxation rate was 1.78 ms^{-1} with 95% CI: 1.39 to 2.19 having an average thickness of 169 µm with 95% CI: 80 to 258.

The effect of RGX cross-linking at 2/3rd corneal thickness showed higher relaxation rates (n = 5) in all the treated eyes. Relaxation rates were significantly greater

(+22%; +0.32 ms^{-1}; 95% CI: +0.18 to +0.47; P = 0.01) after RGX treatment at 2/3rd corneal depth consistent with stiffer material properties. No significant corneal thickness change (−9%; −16 µm; 95% CI: −40 to +72; P = 0.47) was observed before and after RGX treatment at 2/3rd corneal depth. **Figure 5.3** shows the distribution of CCT and relaxation rates after epithelial debridement, after trephination and after RGX treatment for all the samples. **Table 5.1** gives the magnitude of the effect of rose bengal green light cross-linking treatment in relaxation rates for all the samples.

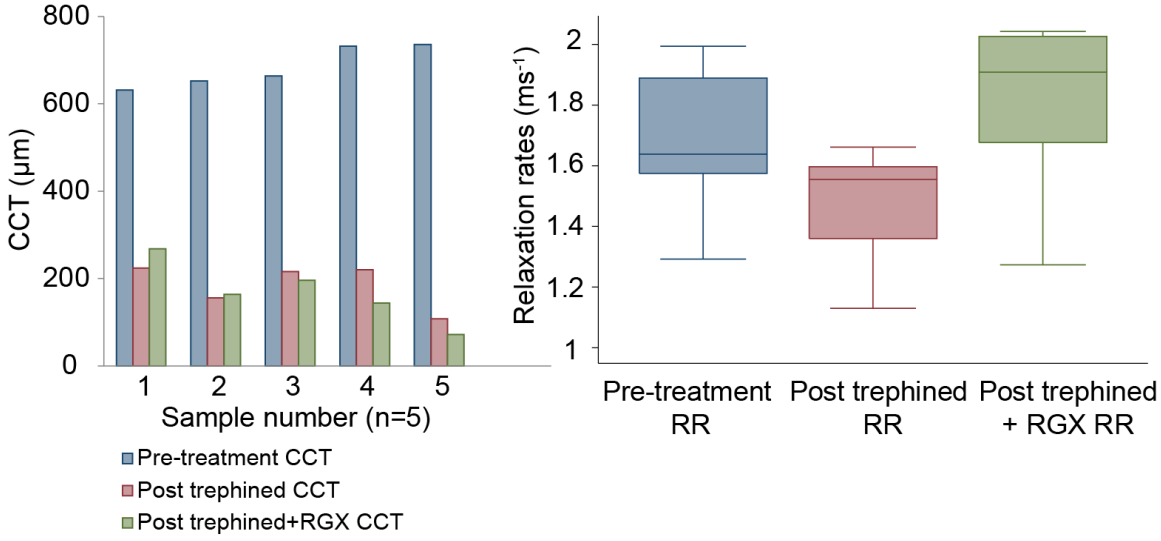

Figure 5.3: Distribution of CCT and relaxation rates after epithelium debridement, after trephination and after RGX treatment. No significant corneal thickness change (9%; −16 µm; 95% CI: −40 to +72; P = 0.47) was observed before and after RGX treatment at 2/3rd corneal depth. Relaxation rates were significantly (P = 0.01) greater (+22%; +0.32 ms^{-1}; 95% CI: +0.18 to +0.47) after RGX treatment at 2/3rd corneal depth. RGX cross-linking at 2/3rd corneal thickness showed stiffer corneal material properties after treatment in all the samples.

Table 5.1: OCE measurements after rose bengal green light cross-linking at 2/3rd corneal depth

Sample	RR before RGX*at 2/3rd corneal depth	RR after RGX*at 2/3rd corneal depth	Mean Difference	Percent increase
	Mean ± SD* ms^{-1}	Mean ± SD* ms^{-1}	ms^{-1}	%
1	1.66 ± 0.05	2.04 ± 0.01	0.38	23
2	1.60 ± 0.04	1.91 ± 0.09	0.31	19.5
3	1.55 ± 0.05	2.03 ± 0.01	0.47	30
4	1.36 ± 0.02	1.68 ± 0.05	0.31	23
5	1.13 ± 0.01	1.27 ± 0.04	0.14	13

*Rose Bengal Green Light Cross-linking; *Standard deviation

Comparison with deep stromal UV CXL treatment

Mean relaxation rate at the corneal surface post-epithelial debridement was 1.67 ms^{-1} with 95% CI: 1.56 to 1.78, having an average central corneal thickness of 759 µm with 95% CI: 673 to 845. Mean relaxation rate at 2/3rd corneal depth after trephination was 1.14 ms^{-1} with 95% CI: 0.98 to 1.29, having an average deep stromal thickness of 303 µm with 95% CI: 277 to 329. After UV riboflavin cross-linking treatment in the deep stroma, mean relaxation rate was 1.63 ms^{-1} with 95% CI: 1.34 to 1.92, having an average thickness of 238 µm with 95% CI: 224 to 251.

The effect of UV CXL cross-linking at 2/3rd corneal thickness showed higher relaxation rates (n = 5) in all the treated eyes. Relaxation rates were significantly greater (+44%; +0.49 ms^{-1}; 95% CI: +0.29 to +0.7; P = 0.01) after UV CXL treatment at 2/3rd corneal depth indicating stiffer material properties and corneal thickness significantly reduced (−22%; −65 µm; 95% CI: −26 to −104; P = 0.01) after UV CXL treatment at 2/3rd corneal depth driven by higher osmolality of riboflavin solution. **Figure 5.4** shows the distribution of CCT and relaxation rates after epithelium debridement, after trephination

and after UV CXL treatment for all the samples. The treatment effect was higher with UV CXL treatment (44%) than with RGX treatment (22%) at 2/3rd corneal depth.

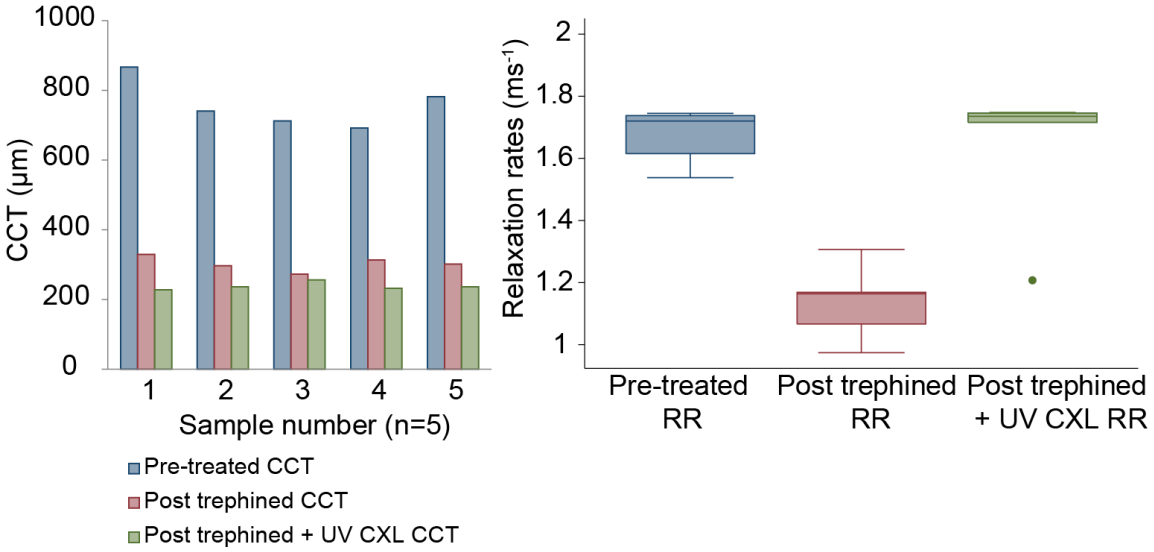

Figure 5.4: Distribution of CCT and relaxation rates after epithelium debridement, after trephination and after UV CXL treatment. Corneal thickness significantly reduced (−22%; −65 µm; 95% CI: −26 to −104; P = 0.01) after UV CXL treatment at 2/3rd corneal depth driven by higher osmolality of riboflavin solution. Relaxation rates were significantly greater (+44%; +0.49 ms^{-1}; 95% CI: +0.29 to +0.7; P = 0.01) after UV CXL treatment at 2/3rd corneal depth. UV CXL cross-linking at 2/3rd corneal thickness showed stiffer corneal material properties after treatment in all the samples. The treatment effect was higher with UV CXL treatment (44%) than with RGX treatment (22%) at 2/3rd corneal depth.

Comparison with full thickness RGX and UV CXL treatment

Baseline mean relaxation rate after epithelial debridement was 2.4 ms^{-1} with 95% CI: 2.19 to 2.61, having an average central corneal thickness of 522 µm with 95% CI: 448 to 596 in the rabbit eyes (n=6). After rose bengal green light cross-linking treatment, the mean relaxation rate was 2.6 ms^{-1} with 95% CI: 2.38 to 2.82 having an average thickness of 436 µm with 95% CI: 399 to 478. The effect of RGX cross-linking showed

significantly greater relaxation rates (+8%; +0.2 ms^{-1}; 95% CI: +0.21 to +0.37; P = 0.03) indicating stiffer material properties, with a significantly reduced corneal thickness (−15%; −83 µm; 95% CI: −40 to −126; P = 0.01) in all the treated eyes. **Figure 5.5** shows the distribution of CCT and relaxation rates after RGX treatment for all the samples.

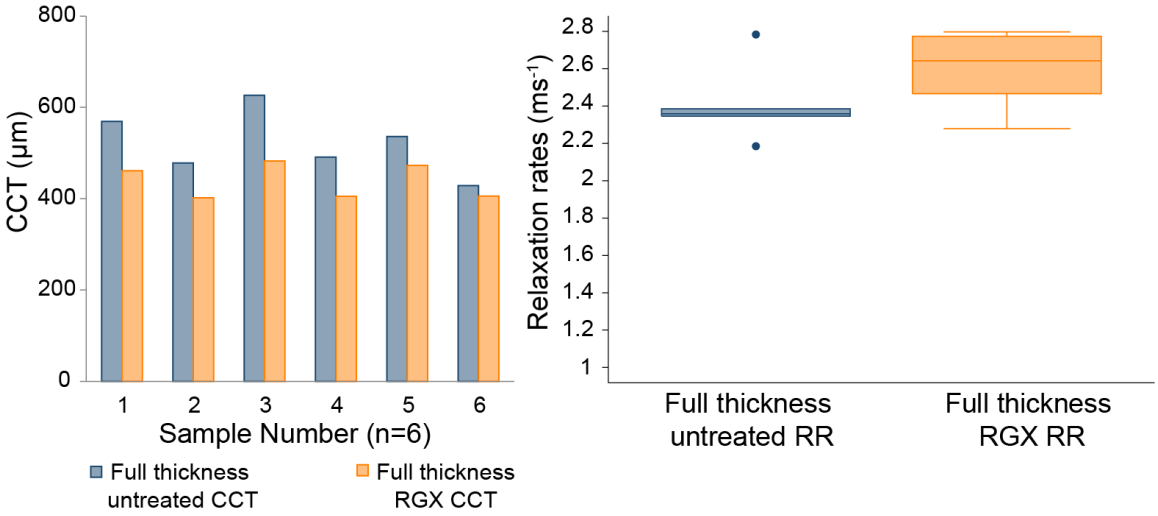

Figure 5.5: Distribution of CCT and relaxation rates after RGX treatment. The effect of RGX cross-linking showed significantly greater relaxation rates (+8%; +0.2 ms^{-1}; 95% CI: +0.21 to +0.37; P = 0.03) with a significantly reduced corneal thickness (−15%; −83 µm; 95% CI: −40 to −126; P = 0.01) in all the treated eyes. Although the effect is less as compared to RGX treatment in the deep stroma (22%), RGX treatment in the cornea shows stiffer material properties.

The baseline mean CCT of the rabbit corneas (n = 6 eyes) measured by structural OCT imaging was 624 µm with 95% CI: 559 to 688 at 15 mmHg and the baseline mean relaxation rates measured by OCE imaging was 2.29 ms^{-1} with 95% CI: 2.15 to 2.43. Full thickness UV CXL treatment did not affect CCT (−1%; −5 µm; 95% CI: −21 to +32; P = 0.63), but showed significantly greater relaxation rates (+10%; +0.24 ms^{-1}; 95% CI: +0.08 to +0.4; P = 0.01) after cross-linking treatment (2.53 ms^{-1}) indicating stiffer material properties. **Figure 5.6** shows the distribution of CCT and relaxation rates

after UV CXL treatment for all the samples. The treatment effect was higher with UV CXL treatment (10%) than with RGX treatment (8%).

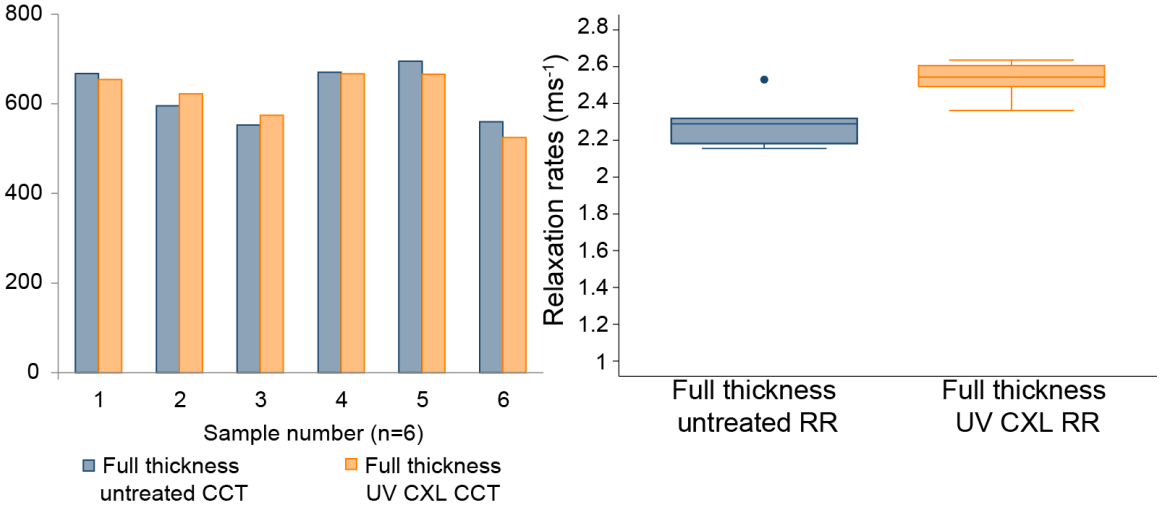

Figure 5.6: Distribution of CCT and relaxation rates after UV CXL treatment. Full thickness UV CXL treatment did not affect CCT (−1%; −5 µm; 95% CI: −21 to +32; P = 0.63), but showed significantly greater relaxation rates (+10%; +0.24 ms^{-1}; 95% CI: +0.08 to +0.4; P = 0.01) after cross-linking treatment (2.53 ms^{-1}). The treatment effect was higher with UV CXL treatment (10%) than with RGX treatment (8%) however lower as compared to UV CXL (44%) or RGX treatment (22%) in the deep stroma.

Penetration depth of rose bengal dye into the stroma

Baseline mean corneal thickness after de-epithelialization was 833 µm in the 0.9% saline treated eyes and 732 µm in the rose bengal dye treated eyes. Significant corneal swelling is observed after treating de-epithelialized rabbit corneas with 0.9% saline for 20 minutes (n=6; +27 µm; 95% CI: +19 to +36; P = 0.01) and 0.1% rose bengal dye dissolved in 0.9% saline (n=5; 36 µm; 95% CI: +22 to +50; P = 0.01) for 20 minutes measured using SD-OCT imaging. After freezing and cutting, the average thickness of the 5µm-thick corneal sections measured from the deconvolution microscopy images in the controls is 837 ± 78 (mean ± SD) and in the rose bengal dye is 624 ± 133 µm. In the control samples, the mean maximum fluorescence intensity is

124.8 ± 12.24, which is the same as background noise (auto fluorescence). In rose bengal dye instilled samples, the mean maximum fluorescence intensity is 1587.9 ± 762.6, while the mean minimum fluorescence intensity across is 114.9 ± 6.2, indicating the presence of rose bengal dye fluorescence in the treated sample as captured during imaging. **Figure 5.7** shows the individual fluorescence intensity profiles for each sample of vehicle (0.9% saline) and rose bengal dye depicting the diffusion profile.

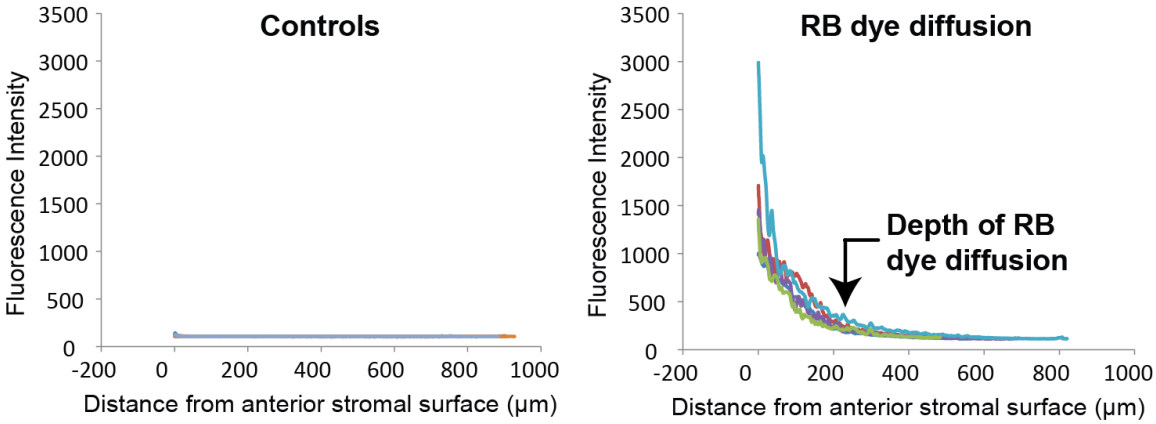

Figure 5.7: The individual fluorescence intensity profiles for each sample of vehicle (0.9% saline) and rose bengal (RB) dye showing their diffusion profile. The average corneal sections thickness measured from deconvolution microscopy images in the controls is 837 ± 78 µm and in the rose bengal dye is 624 ± 133 µm. In control samples, the mean maximum fluorescence intensity is 124.8 ± 12.24, which is the same as background noise (auto fluorescence). In rose bengal dye instilled samples, the mean maximum fluorescence intensity is 1587.9 ± 762.6, while the mean minimum fluorescence intensity across is 114.9 ± 6.2, indicating the presence of rose bengal dye fluorescence in the treated sample as captured during imaging. The average depth of rose bengal dye diffusion was up to 34 ± 7% (a depth of 210 ± 9 µm from the anterior de-epithelialized stromal surface) of the corneal thickness in all the samples.

The average depth of rose bengal dye diffusion was up to 34 ± 7% (a depth of 210 ± 9 µm from the anterior de-epithelialized stromal surface) of the corneal thickness in all the samples. **Figure 5.8** shows two deconvolution microscopy images showing

sections of rabbit corneas instilled with a) PBS and b) rose bengal dye on their anterior surface showing the diffusion of rose bengal dye into the corneal stroma.

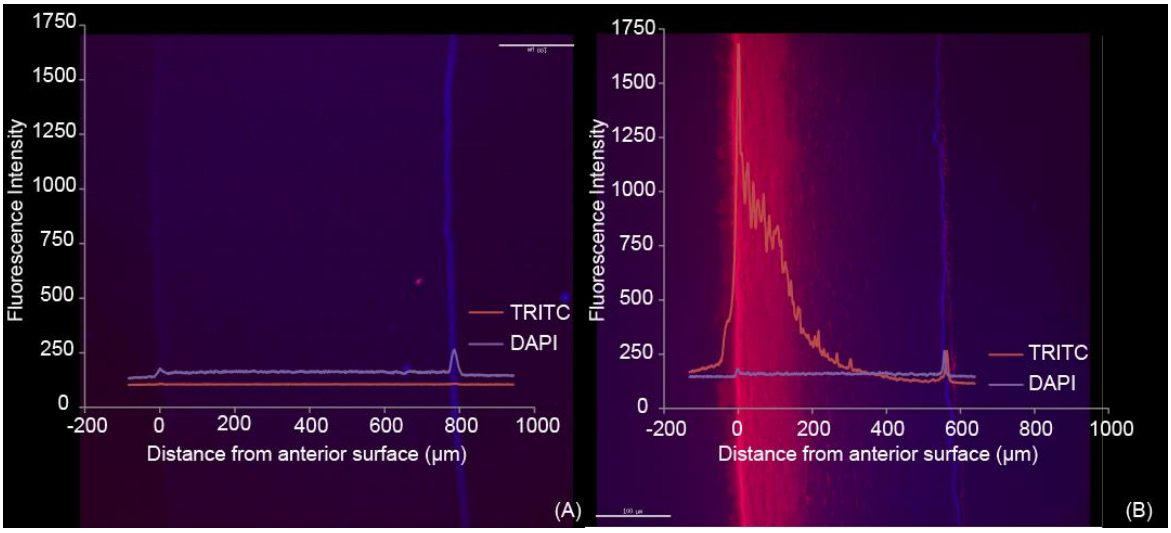

Figure 5.8: Two typical deconvolution microscopy images of rabbit corneal sections instilled with A) 0.9% saline and B) 0.1% rose bengal dye on their anterior surface, overlaid by the fluorescence intensities from TRITC and DAPI channels. The fluorescence intensities from the TRITC channel show the diffusion of rose bengal dye into the corneal stroma and DAPI channel shows the DAPI stain highlighting the endothelial cells. Scale bar: 100 µm. **A)** Control sample showing the saline instilled corneal section and **B)** RB dye instilled sample showing the diffusion of rose bengal dye to 1/3rd corneal depth.

Discussion

In this study, we used optical coherence elastography to quantify the biomechanical properties of the full thickness stroma and post-trephined deep stroma, and demonstrated the effect of RGX cross-linking in the deep stroma by showing stiffer corneal properties after RGX treatment in ex vivo rabbit corneas. Our results show stiffer full thickness stroma (28%) than the posterior stroma. This is in agreement with previous biomechanical studies investigating the depth dependent corneal properties. Pinsky et al.[138] conducted early mechanical testing using torsional rheometry in excised human

corneas and reported Young's moduli in full thickness stroma (9.48 ± 2.92 kPa) and decreasing stiffness for strips separated into anterior (7.71 ± 6.34 kPa), center (1.99 ± 0.45 kPa) and posterior stroma (1.31 ± 1.01 kPa). Randleman et al.[131] conducted strip extensiometry and reported that the posterior stroma is 50% weaker as compared to anterior stroma in excised human corneas. Thomasy and colleagues[72] used atomic force microscopy and reported higher elastic moduli for anterior stroma (1.1 ± 0.6 kPa) than posterior stroma (0.38 ± 0.22 kPa) in rabbit corneas. Previous results and ours together are consistent with the structural evidence showing variation in the organization and composition of anterior and posterior stroma. [5, 7 3]

The differences in the measured magnitudes between the anterior and posterior stroma is because of the technique used to obtain the corneal biomechanical properties. While rheometry, extensiometry and atomic force microscopy are performed on excised corneas, OCE imaging is performed non-invasively in a set-up, wherein whole rabbit globes are used with intra-ocular pressure controlled and maintained throughout the experiments. There is no corneal excision or incisions made that can artificially impact the measured corneal biomechanical properties.

The corneal thickness reduction (~300 µm) due to the influence of an osmotic agent (20% dextran solution instillation in Chapter 4) resulted in ~0.6 ms^{-1} (−21%) reduction in relaxation rates, while the thickness reduction produced by removing 2/3rd portion (~475 µm) of the corneal stroma yielded ~0.4 ms^{-1} (−22%) reduction in relaxation rates. Although the tonicity-driven thickness change is lower than the trephined reduction in thickness, both produce approximately similar reduction in corneal stiffness. This shows a higher influence of hydration on the measured corneal properties and points to the importance of accounting for hydration effects in the biomechanical measurements.

We demonstrated greater corneal stiffness (+22%) due to the effect of rose bengal green light cross-linking treatment in the deep stroma. This shows promise for

future applications in lamellar keratoplasty and refractive surgery through modification of deep corneal biomechanical properties. No significant corneal thickness change is noted with RGX treatment, while a significant reduction (−22%) is observed for UV CXL treatment driven by the osmotic effect of the 20% dextran in the riboflavin solution. Corneal thickness reduction produces decreased corneal stiffness (chapter 4). However, the effect of UV CXL treatment in the deep stroma was greater (+44%) than with RGX treatment (+22%). Therefore, the increase in corneal stiffness with UV CXL treatment in the deep stroma in conditions where thickness is controlled for can be expected to be greater than the observed increase (44%). Even in the full thickness stroma, the treatment effect was higher with UV CXL treatment (10%) than with RGX treatment (8%). Previous studies by Cherfan et al.[29] and a recent study by our group in rabbit corneas,[109] and Wang et al.[71] in porcine corneas, also show similar greater effect due to UV CXL treatment over RGX treatment.

Our recent study comparing the efficacy of UV CXL and RGX treatments[109] demonstrated an increase in stiffness in the anterior ~34% with UV CXL treatment, while RGX treatment affected only the anterior ~16% of the cornea. The reason for the differences observed between the effects of cross-linking treatments can be due to a variation in the depth of diffusion of the riboflavin solution and rose bengal dye. In this study, we found an average depth of rose bengal dye diffusion up to 34 ± 7% (until a depth of 210 ± 9 µm from the anterior de-epithelialized stromal surface) of the corneal thickness (624 ± 133 µm) in all the samples. For comparison with Cherfan et al.,[29] when we correct for the ex vivo increase in thickness (from ~500 µm to ~625 µm), the depth of diffusion is approximately 160 µm, while the depth of diffusion demonstrated by Cherfan and colleagues is about 100 µm in rabbit corneas. The depth of diffusion of rose bengal dye in our study is approximately half the depth of diffusion of riboflavin solution obtained from previous studies. Wollensak et al.[139] report the depth of riboflavin solution diffusion

to be about 300 µm wherein the depth of diffusion of riboflavin solution was studied as the depth of keratocyte loss. Another study by Gallhoefer et al.,[140] demonstrated a depth of riboflavin dye penetration to be about 274 µm wherein ex vivo fluorescence assay was used to determine the depth of diffusion in ex vivo rabbit corneas. As the corneal depth up to which the photosensitizer diffuses is effectively absorbed by the UV or green light radiation during cross-linking treatment, depth of diffusion is an important factor to weigh in while considering the efficacy of cross-linking treatments.

CHAPTER SIX

IN VIVO REPEATABILITY AND SHORT-TERM REPRODUCIBILITY OF OPTICAL COHERENCE ELASTOGRAPHY IN RABBIT CORNEA

Srilatha Vantipalli,[1] Manmohan Singh,[2] Jiasong Li,[2] Salavat R Aglyamov,[3] Kirill V. Larin,[2,4] Michael D. Twa[5]

[1]College of Optometry, University of Houston, 505 J. Davis Armistead Bldg., Houston, TX 77204; [2]Department of Biomedical Engineering, University of Houston, 3605 Cullen Blvd, Houston, TX 77204; [3]Department of Biomedical Engineering, University of Texas at Austin, Austin, TX, 78712; [4]Interdisciplinary Laboratory of Biophotonics, Tomsk State University, Tomsk 634050, Russia; [5]School of Optometry, The University of Alabama at Birmingham, 1716 University Blvd, Birmingham, AL 35233

Preface

Dynamic optical coherence elastography (OCE) is a non-invasive method to quantify corneal tissue material properties. We demonstrated the use of this technique previously to quantify the corneal biomechanical properties *in vitro* in rabbit corneas. The purpose of this study was to investigate the feasibility of using this OCE system as an *in vivo* method to derive the corneal material properties by assessing the repeatability and short term reproducibility of the measurements made *in vivo* on normal rabbit corneas.

Abstract

Purpose: Optical coherence elastography is an emerging technique to assess soft tissue biomechanics. We investigated the feasibility, repeatability, and short-term reproducibility of *in vivo* dynamic optical coherence elastography (OCE) imaging to obtain corneal biomechanical properties for the rabbit eye.

Methods: *In vivo* dynamic OCE was performed on anesthetized Dutch belted rabbits (n=20 eyes from 16 animals) using phase-sensitive optical coherence tomography (OCT) combined with focal mechanical tissue stimulation using a micro air-pulse stimulator (150µm spot size; 0.8ms duration; force ranging 2 to 10Pa (0.02 to 0.08mmHg)) at the corneal apex. Tissue surface deformation was quantified as a time-dependent viscoelastic recovery response (relaxation rate). Within-session repeated measures were recorded at different cannulated IOP levels (10, 20, 30, 40mmHg) and were repeated before and after animal re-positioning (10mmHg). Measurement precision was quantified as 95% limits of agreement (LoA), intraclass correlation coefficient (ICC), coefficient of variation (CV) and coefficient of repeatability (CR).

Results: Relaxation rates showed no significant difference within-session and between sessions and showed good limits of agreement (within-session: 10mmHg: mean ± LoA (ms^{-1}) = −0.01 ± 0.09; 20mmHg: −0.01 ± 0.1; 30mmHg: +0.02 ± 0.1; 40mmHg: +0.02 ± 0.1; between session: 0.01 ± 0.17. Excellent ICC (>0.97) with 95% confidence interval: 0.8 to 0.9, CV (<4.84%) and CR (<0.21ms^{-1}) were obtained for within and between session measures.

Conclusions: The viscoelastic recovery response during dynamic OCE was repeatable *in vivo* with excellent precision over a range of IOPs. This precision (0.01 ms^{-1}) is far less than the change observed with tissue cross-linking (0.28ms^{-1} from previous *in vitro* studies). The excellent observed measurement precision is critical for *in vivo* application

of OCE in clinical settings for the diagnosis, treatment and management of corneal diseases.

Introduction

Elastography imaging is used to derive tissue biomechanical properties by quantifying a tissue's dynamic response to precise mechanical loading. Elastography has been implemented as a clinical diagnostic tool[33, 34] for detecting liver cirrhosis,[35] breast cancer,[36, 37] prostate cancer[141] and thyroid cancer[39] with a goal of reducing the need for invasive procedures, e.g., fine-needle aspirations and biopsies. However, measuring and quantifying corneal biomechanical properties *in vivo* remains a long-standing challenge. Traditional destructive mechanical test methods e.g. strip extensiometry[20] or rheometry,[24] have been augmented by several novel clinical techniques to quantify corneal material properties such as dynamic corneal imaging by indentation,[82] surface wave elastometry,[142] ultrasound-based elastography (e.g. supersonic shear wave imaging[44]), and Brillouin spectroscopy.[143]

Current techniques for evaluating corneal biomechanical properties *in vivo,* such as the Ocular Response Analyzer[78] (ORA) or the Corneal Visualization Scheimpflug Technology[79] (CorVis ST), use an air pulse of high volume, long duration (8 ms), and large amplitude and diameter to create a global corneal deformation. We built a micro air-pulse stimulator that creates a localized short-duration (0.8 ms) focal stimulation and combined it with phase-stabilized optical coherence tomography imaging (OCT).[50] This approach is non-contact and provides the capability to obtain spatially localized corneal material properties. High-resolution imaging and fast acquisition speeds with phase-sensitive OCT provides an advantage over other imaging modalities (ultrasound, CT, MRI) to capture the subtle tissue changes induced by this dynamic mechanical stimulation. We implement optical coherence elastography[51] (OCE) to derive the tissue biomechanical properties through high-resolution phase-sensitive OCT[144] imaging of dynamically induced microscopic tissue motion created using the air-pulse stimulator[145] Previous reviews[9, 10] show the recent advances in the development and applications of

different OCE technologies. We demonstrated the application of dynamic OCE to quantify the corneal biomechanical properties previously *ex vivo* in mouse,[11, 146] rabbit,[107, 137] and porcine[147, 148] eyes. However, several factors influence the tissue response to stimulation while adapting elastography imaging from *ex vivo* to *in vivo* applications,[149] for e.g., instrument related factors: positioning; physiological parameters: breathing, heart rate, cardiac cycle, ocular pulse,[150] corneal hydration control and environmental conditions: room temperature, humidity, or random error due to other factors.

There are a number of potential sources of variability that could influence the *in vivo* repeatability of dynamic OCE imaging in the cornea including variation in corneal properties, motion artifacts due to fixational eye movements, breathing, heart rate, ocular pulsations, etc., positioning, hydration, etc. Quantifying their possible influence is critical to assess the viability of this technique for future clinical measurements. Previous development of *in vivo* elastography imaging methods for other tissues were improved by using gating mechanisms to prevent the influence of breathing and cardiac cycles. Cardiac gating is used with *in vivo* myocardial elastography to filter out motion effects during the cardiac cycle.[151] Similarly, respiratory gating is used during *in vivo* magnetic resonance elastography imaging of the liver.[152]

The purpose of this study is twofold: 1) to investigate the feasibility of performing *in vivo* dynamic OCE to obtain rabbit corneal biomechanical properties and 2) to evaluate the repeatability and short-term reproducibility of *in vivo* dynamic OCE measurements.

Methods

Animals

All experimental and animal care procedures were approved by the Institutional Animal Care and Use Committee (IACUC) of the University of Houston and were in

accordance with the Association for Research in Vision and Ophthalmology (ARVO) Statement for the Use of Animals in Ophthalmic and Vision Research. Dutch Belted male rabbits (n = 20 eyes from 16 animals; average weight: 2 kgs; age: 12-16 weeks) were used to determine the *in vivo* repeatability and short-term reproducibility of corneal tissue material properties measured using OCE. Rabbits were anesthetized with an intramuscular injection of ketamine (50 mg/kg body weight; Vedco, St. Joseph, MO) and xylazine (5 mg/kg body weight; Vedco). Dextran solution (2.5%) was instilled on the corneal surface every 5 minutes to prevent dehydration.

Optical Coherence Elastography Measurements

The OCE system is a combination of a home-built phase-stabilized swept source OCT imaging system (PhS-SSOCT) and a focused micro air pulse stimulator used to induce localized tissue surface stimulation. The OCE set-up is shown in the schematic layout (**Figure 4.1**). A detailed description of the imaging system can be found in our previous publications.[50, 121, 146] In brief, the imaging system utilizes a swept source laser illuminator (HSL2000, Santec, Inc., Torrance, California) with a central wavelength of 1310 ± 75 nm, A-scan rate of 30 kHz, and output power of 36 mW. The system has an axial spatial resolution of ~11 µm and a lateral spatial resolution of ~16 µm in the air. Phase stability is achieved by using a fiber Bragg grating (FBG) to accurately trigger the ADC (Analog to Digital Convertor) for data acquisition. This removes jitter between laser sweeping and data acquisition and increases the accuracy for phase-resolved measurements.[121] The system phase stability was ~16 milliradians, which corresponded to ~3 nm displacement sensitivity (in air).

The air pulse stimulator is a home-built device that gives a focal controlled air pulse with a localized spatiotemporal Gaussian profile having a force amplitude ranging 2 to 10 Pa (0.02 to 0.08 mmHg) delivered over 0.8 ms duration through a 150 µm diameter port at an angle of incidence of 45° to the apical surface. The stimulus

generates localized mechanical waves in tissues which disperse internally as an axial compressive force and have tangential lateral propagation (**Figure 6.1**). This low-amplitude (micrometer-scale) localized tissue displacement is a complex viscoelastic response to the air-pulse stimulation. The OCT system was used to record the time-dependent surface response at the corneal apex.[11]

The desired intraocular pressure was maintained in the rabbit's globe continuously using a computer-controlled micro-infusion/withdrawal syringe pump (NE-500 programmable syringe pump, New Era Pump Systems, Inc.) filled with 0.9% saline in a feedback loop. A pressure transducer (Model 41X; Keller Instruments) monitors the rabbit's intra-ocular pressure throughout the experiment. The input from the pressure transducer was utilized to continuously adjust the volume inside the cannulated anterior chamber by the syringe pump in an automated manner.

Experimental Procedure

The baseline central corneal thickness (CCT) was acquired from a two-dimensional structural image (B-mode) of the rabbit corneal apex comprising 500 A-scans over 6mm captured by the OCT system (**Figure 6.1**). The central 50 A-scans over a 0.5 mm lateral displacement across the corneal apex were averaged. The image intensity profile showed spiked peaks corresponding to the anterior and posterior corneal surface, which were identified manually from the 50 averaged A-scans. The distance between the peaks was measured as the central corneal thickness after correcting for the corneal refractive index (n_{cornea}=1.376)[24] using the formula,

$$CCT_{corrected} = \frac{CCT \times n_{air}}{n_{cornea}} \quad (1)$$

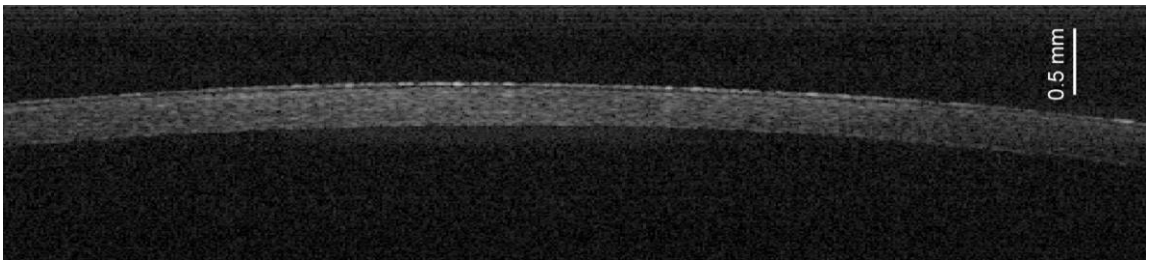

Figure 6.1: A two-dimensional structural image (B-mode) of the rabbit corneal apex comprising 500 A-scans over 6mm captured by the OCT system.

The phase signal of the tissue response to air pulse stimulation was captured at the corneal apex in M-mode using the OCT. The OCT imaging system and the air pulse stimulator delivery port were co-localized to capture the response ~0.4 mm away from the stimulated location. A 2D motorized linear stage was used to move the animal and align the eye with the air pulse stimulator delivery port and the OCT imaging system. The distance between the corneal surface and the air-pulse stimulator was maintained constant (~200 µm) by manually controlling the z-axis stage.

Repeatability conditions were defined as independent test results obtained with the same method on identical test items in the same laboratory by the same operator using the same equipment within short intervals of time (~100 ms).[153] Within-session repeatability was evaluated by obtaining two sets of repeated OCE measurements in the same session without changing the measurement location. The imaging system was used to capture 10 repeated measurements at the corneal apex at four different IOP settings: 10 mmHg (n=11), 20 mmHg (n=6), 30 mmHg (n=8) and at 40 mmHg (n=9). Short term inter-session reproducibility (n=8) was investigated by capturing 21 consecutive measurements at the corneal apex with IOP set at 10 mmHg. Following the initial measurements, another set of 21 measurements were captured after animal re-positioning. The animals were re-positioned by moving the linear stage away from the OCE set-up, lifting and replacing the animal back into its holder and re-aligning again, such that the imaging system and the air pulse stimulation were co-focused at the

corneal apex. All measurements were made within 30 minutes after anesthesia in each animal.

Analyses

The OCE-recorded tissue phase profile is made up of an initial negative surface displacement of the cornea, followed by a time-dependent recovery of the tissue back to its original position. This phase signal is unwrapped and converted from phase displacement to amplitude using the formula:

$$d(t) = \frac{\lambda}{2\pi n} \times \varphi(t), \qquad (2)$$

where d is the amplitude (µm), λ is the central wavelength of the OCT system (µm), n is refractive index (n_{air} = 1), and φ is phase (radians). **Figure 6.2** shows a typical displacement profile recorded at the corneal apex using the imaging system. A variance-weighted Fourier fit is applied to filter the low-frequency oscillations and remove the motion artifacts in the unwrapped signal (**Figure 6.2**).

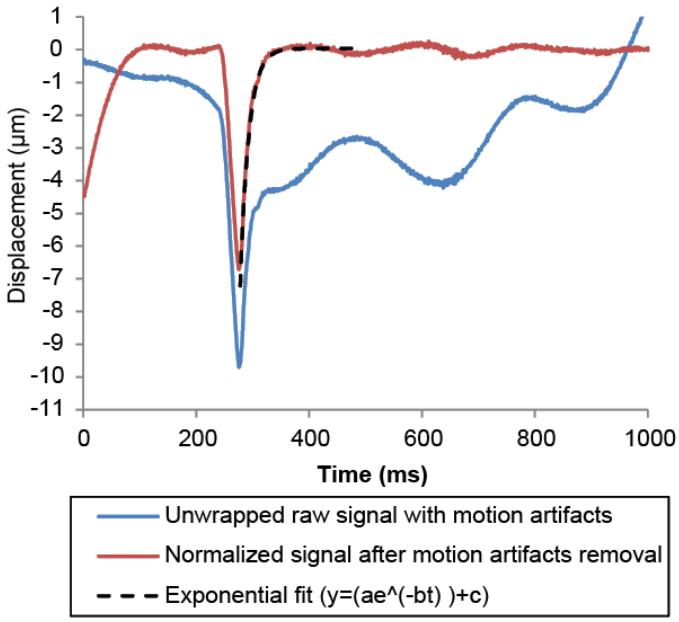

Figure 6.2: In vivo optical coherence elastography of rabbit corneal surface shows a complex viscoelastic response to mechanical stimulation. A typical displacement signal recorded at the corneal apex showing an initial deformation to maximum amplitude and recovery response (blue line). Low-frequency oscillations and motion artifacts are filtered using a Fourier fit to the raw data (red line). The decay constant (*b*) (relaxation rate) is obtained from an exponential fit (black dotted line) from the point of maximum amplitude until the phase data recovered back to the surface's initial position.

The rate at which the anterior corneal surface recovered back to its initial position from the point of maximum displacement captures the viscoelastic behavior exhibited by the cornea in response to mechanical stimulation. This recovery rate is obtained from the exponential decay function, calculated by fitting an exponential function using the formula:

$$y(t) = \left(a\, e^{(-bt)}\right) + c, \qquad (3)$$

where *a* is amplitude (µm), and *b* is decay constant (ms^{-1}) starting at the point of maximum displacement amplitude until the surface recovery back to its original position (**Figure 6.2**). The primary outcome measure of the study is the exponential decay

constant (*b*) termed Relaxation Rate. **Figure 6.3** shows an example of two typical phase signals captured between sessions, before (maroon line) and after (green line) animal re-positioning in the same eye.

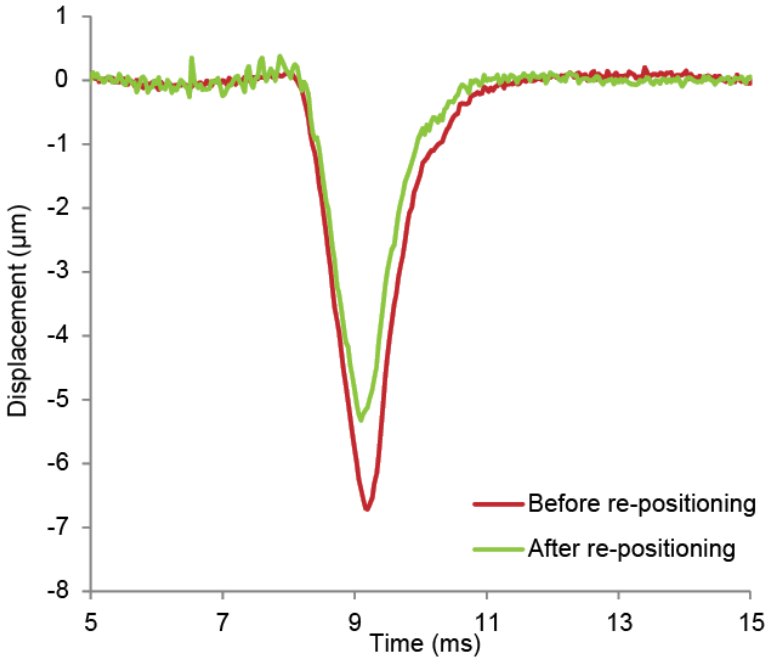

Figure 6.3: *In vivo* measurement of rabbit corneal properties using OCE shows two typical viscoelastic responses to air-pulse stimulation obtained between two sessions: before (maroon line) and after (green line) animal repositioning in the same eye.

Statistical Methods

Within-session repeatability was assessed by calculating the mean difference ($d_2 - d_1$) of 10 repeated measurements (d_1: an average of initial 5 measures; d_2: an average of latter 5 measures) made in the same location for each of the different IOP settings (10, 20, 30 and 40 mmHg). One sample two-tailed t-test was performed to test the within session relaxation rates mean difference from zero. 95% limits of agreement (LoA) (mean difference ± (1.96 x standard deviation)) were calculated as per the methods described by Bland and Altman.[154] Intra-class correlation coefficient (ICC) for a one-way random-effects model[155] with the absolute agreement was calculated using STATA v13. The coefficient of variation (CV) was calculated for the within–session relaxation rates

using $CV = 100 \times \frac{\sqrt{\frac{\sum(d_1-d_2)^2}{2n}}}{\frac{\sum(d_1+d_2)}{2n}}$. The coefficient of repeatability (CR)[156, 157] for the within-session viscoelastic recovery measures was calculated using $CR = 1.96 \times \sqrt{\frac{\sum(d_2-d_1)^2}{n-1}}$ where ($d_2 - d_1$) is the within-session relaxation rate mean difference.

Short term inter-session reproducibility was assessed by calculating the between-session mean difference, one-sample t-test 95% LoA, ICC, CR and CV for relaxation rates between sessions as described above. For each eye, the relaxation rates were compared before (d_1: 21 averaged measures) and after animal re-positioning (d_2: 21 averaged measures) at 10 mmHg.

Results

The overall mean CCT measured by structural OCT imaging was 312 ± 36 µm (n=20 eyes) in the Dutch Belted rabbits at 10 mmHg.

Within-session Repeatability

The mean difference of relaxation rates within the same session was not significantly different from zero for all the IOP settings as shown in Table 1. Levels of agreement (Table 1) are depicted in the graphs for differences against the mean of the relaxation rate measurements obtained within the same session (**Figure 6.4**) at 10 mmHg (n=11), 20 mmHg (n=6), 30 mmHg (n=8), and 40 mmHg (n=9). A significant decrease in the mean relaxation rates with an increase in IOP ($R^2 = 0.96$; $P = 0.02$) is noted (Table 1). ICC, CV, and CR calculated from the within session relaxation rate measures for all the IOP settings are shown in Table 6.1.

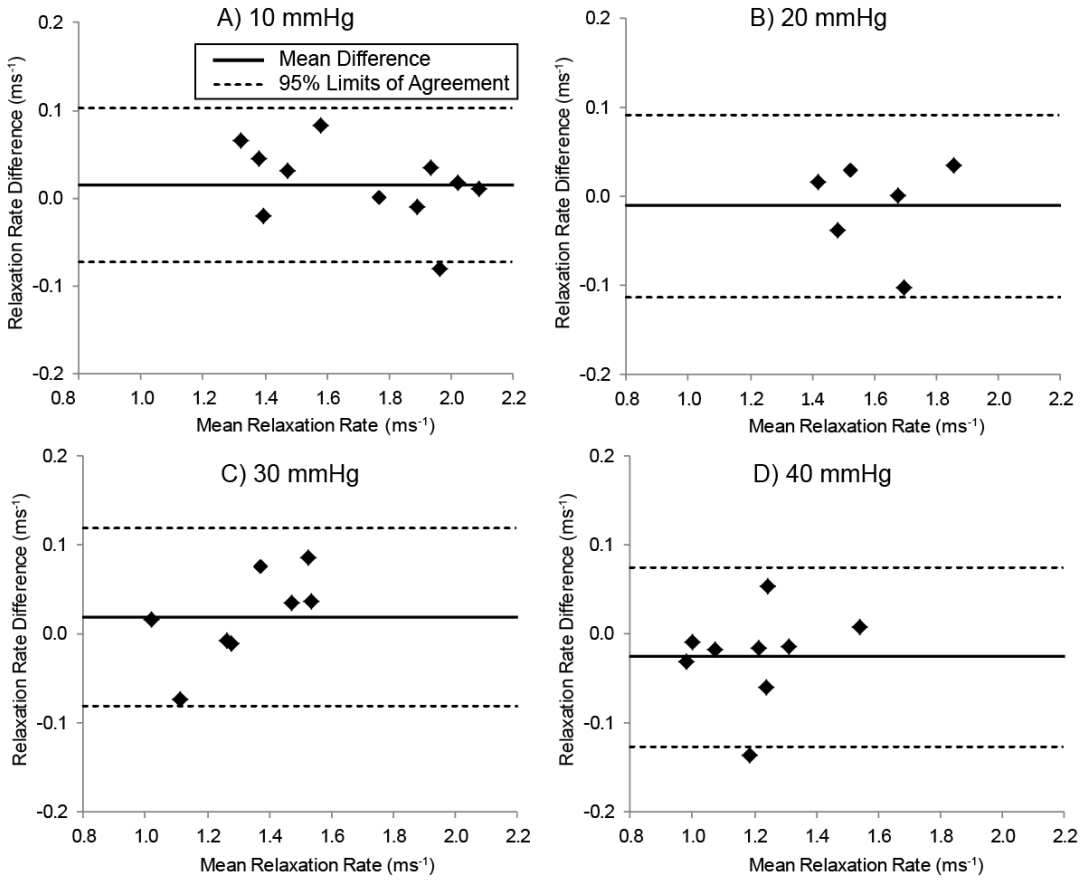

Figure 6.4: In vivo measurement of rabbit corneal biomechanical properties using OCE shows the intra-session precision of dynamic corneal recovery response (relaxation rates) measured within the same session. Residual difference against mean plots representing the difference in relaxation rates obtained within sessions in the same location measured at different IOP settings: (A) 10 mmHg (n=11), (B) 20 mmHg (n=6), (C) 30mmHg (n=8) and (D) 40mmHg (n=9). The solid line indicates the mean difference (bias) and the dashed line indicates 95% limits of agreement. There is no systematic pattern to the spread of the residual errors. Mean differences of relaxation rates for all the IOP's was not significantly different from zero (Table 6.1). 95% LoA for within-session measures at 10 mmHg: mean ± LoA (ms^{-1}) = −0.01 ± 0.09; 20 mmHg: −0.01 ± 0.1; 30 mmHg: 0.02 ± 0.1; 40 mmHg: 0.02 ± 0.1.

Short term inter-session Reproducibility

Mean difference (mean difference ± standard deviation: 0.011 ± 0.09 ms^{-1}) of relaxation rates between sessions (n=8) was not significantly different from zero (P = 0.74) (no bias). Levels of agreement (95% LoA: −0.16 to 0.18 ms^{-1}) is depicted in the graph for differences against mean for relaxation rate measurements obtained between sessions **(Figure 6.5)**. ICC for between session reproducibility is 0.98 with a 95% confidence interval of 0.90 to 0.99. CV is 3.97%. The absolute difference between two measurements made between sessions using dynamic OCE imaging can be estimated to be no more than 0.21 ms^{-1} (CR) in 95% of the occasions.

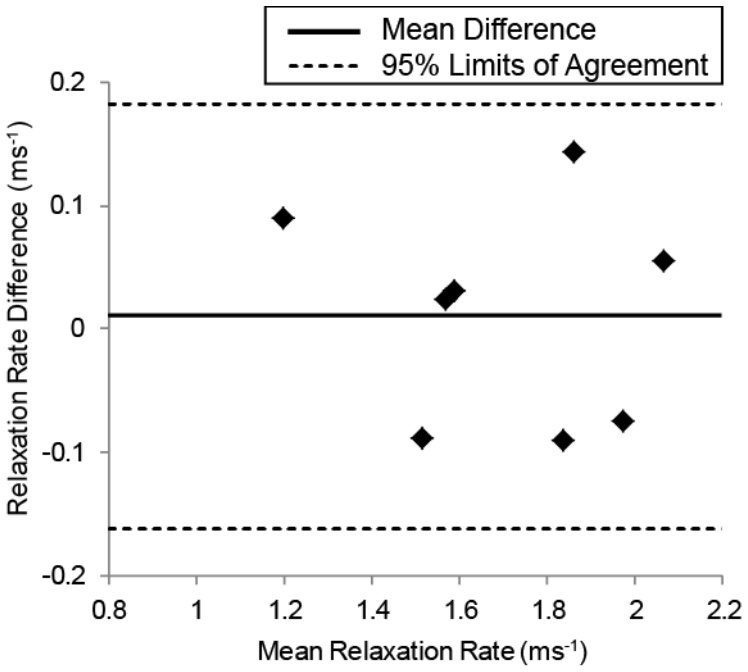

Figure 6.5: In vivo measurement of rabbit corneal material properties using OCE shows the inter-session precision of dynamic corneal recovery response (relaxation rates) measured before and after animal repositioning. The residual difference against mean plot representing the difference in relaxation rates between sessions (before and after repositioning) measured at physiological IOP settings (10mmHg) (n=8). The solid line indicates the mean difference (bias) and the dashed line indicates 95% limits of agreement. Mean difference (mean

difference ± standard deviation: 0.011 ± 0.09 ms^{-1}) of relaxation rates between sessions was not significantly different from zero (P = 0.74) (no bias)). 95% LoA was −0.16 to 0.18 ms^{-1}.

Table 6.1: In vivo precision parameters using OCE imaging in rabbit corneas

IOP	Mean ± SD*	Mean Difference ± SD*	P-value	95% LoA†	ICC‡(95% CI§)	CV ‖	CR#
mm Hg	ms^{-1}	ms^{-1}		ms^{-1}		%	ms^{-1}
	Within-session repeatability						
10	1.71 ± 0.29	0.016 ± 0.04	0.28	−0.07 to 0.10	0.99(0.98 to 0.99)	3.11	0.17
20	1.61 ± 0.16	−0.01 ± 0.05	0.65	−0.11 to 0.09	0.98(0.86 to 0.99)	2.64	0.14
30	1.32 ± 0.19	0.019 ± 0.05	0.33	−0.08 to 0.12	0.98(0.92 to 0.99)	3.90	0.17
40	1.2 ± 0.17	−0.03 ± 0.05	0.18	−0.13 to 0.08	0.97(0.90 to 0.99)	4.84	0.19
	Between session short-term reproducibility						
10	1.7 ± 0.28	0.011 ± 0.09	0.74	−0.16 to 0.18	0.98(0.90 to 0.99)	3.97	0.21

*Standard deviation, †Limits of Agreement, ‡Intra-class Correlation, §Confidence Interval, ‖Coefficient of Variability, #Coefficient of Repeatability

Discussion

Dynamic OCE enables localized measurement of *in vivo* corneal biomechanical properties. We have shown the feasibility of *in vivo* dynamic OCE imaging to obtain the viscoelastic recovery responses (relaxation rates) in rabbit corneas in this study. Variability between samples noted in the relaxation rates distributions may be due to the innate variability in tissue stiffness from animal to animal due to variation in corneal curvature, thickness, and variable dampening due to orbital fat and ocular adnexa.

Rabbit corneal biomechanical properties measured using *in vivo* dynamic OCE measurements in rabbit corneas shows good repeatability and short-term reproducibility. Other factors that we did not study which may contribute to the residual variations in the *in vivo* OCE corneal mechanical properties measurements are instrument-related

factors, physiological parameters: breathing, heart rate, cardiac cycle, ocular pulse[150] and environmental conditions: room temperature, humidity, or random error due to other factors. Despite these variations, *in vivo* OCE imaging is highly reproducible. Motion artifacts caused due to these factors appear to be too small to affect the viscoelastic recovery responses captured using OCE imaging in anesthetized rabbits.

Intra-ocular pressure *in vivo* did not have an effect on repeatability. However, intraocular pressure is an important influence on the corneal biomechanical properties causing a decrease in the viscoelastic recovery response (mean relaxation rates) with an increase in IOP (Table 6.1) ($R^2 = 0.96$; ranging from 1.2 ms^{-1} at 10 mmHg to 1.71 ms^{-1} at 40 mmHg; $P = 0.02$; 95% CI: −0.03 to −0.01). This observed decrease in relaxation rate contrasts with our previous findings with *ex vivo* porcine corneal tissue,[158] where we observed an increase in the relaxation rates (ranging from ~1 ms^{-1} at 10 mmHg to ~1.5 ms^{-1} at 30 mmHg) indicating stiffer material properties with an increase in IOP. However, in *ex vivo* tissues, this is potentially confounded by a loss of corneal hydration control. Corneal swelling can occur *ex vivo* due to degradation of the epithelial and the endothelial barriers resulting in higher (*ex vivo* porcine corneal thickness: 900-1000 µm) than physiologically normal corneal thickness (normal physiological porcine corneal thickness[159]: 650-700 µm). Conversely, an increase in IOP can push fluid out of the corneal stroma leading to corneal thinning—an effect that we and others have noted in whole globe inflation studies.[160] *In vivo*, the epithelium is intact and the functional endothelial pump maintains normal physiological corneal hydration. The effects we observed demonstrate the influence of IOP on rabbit corneal biomechanical properties at normal physiological corneal thickness (*in vivo* rabbit CCT: 312 ± 36 µm). We are conducting further *ex vivo* and *in vivo* investigations to understand better the influence of hydration and corneal thickness on corneal biomechanical properties over a range of tissue thickness values.

Direct absolute comparison of corneal biomechanical properties is not possible as current techniques use different loading mechanisms (indentation[42, 161], ultrasound[25, 44], air pulse[78, 162]) to assess distinct aspects (displacement, shear wave propagation, Brillouin shift,[143] etc.) while obtaining the corneal biomechanical properties. Therefore, the outcome variables also vary ranging several orders of magnitude. Because of these variations, only relative comparisons can be made.

We compare the coefficient of variation (CV) obtained using currently available *in vivo* devices e.g. ORA[78] or Corneal Visualization Scheimpflug Technology[79] (CorVis ST) that measure corneal material properties. Kynigopoulos et al.[163] made four consecutive measurements (within-session repeatability) using ORA in normal healthy volunteers. The coefficient of variation for Corneal Hysteresis (CH) was 12.38%, and Corneal Resistance Factor (CRF) was 10.44% which is higher than the within session CV (3.11%) obtained through *in vivo* dynamic OCE imaging. Similarly in a study by Kopito et al.,[164] the coefficient of variation of CH (9.9%) and CRF (8.1%) from 8 consecutive measurements using ORA was higher to 3.11% found in this study. Nemeth et al.[162] made three consecutive measurements using CorVis ST attaining ten parameters that together describe corneal material properties in human subjects. The coefficient of variation for 7 of the 10 parameters was greater (ranging from 4.3% to 23%) than the 3.11% found in our study. Similarly, Bak-Nielson et al.[165] attained 19 parameters to describe the corneal material properties in human subjects and the CV for 14 out of 19 parameters was greater (ranging from 3.4% to 38%) than the 3.11% found in our study. This implies that the within-session measurements made using *in vivo* dynamic OCE imaging have lower variability as compared to the ORA or CorVis ST.

Wasielica-Poslednik et al.[166] made three measurements with 1-2 minutes between each measurement (short-term between session reproducibility) using ORA and found the coefficient of variation obtained for CH (>11.8) and CRF (>8.1) higher

than that (3.97%) from between session reproducibility using OCE. This implies that *in vivo* dynamic OCE imaging has lower variability as compared to ORA for short term inter-session measurements. However, these comparisons with the ORA and CorVis ST measurements made in normal human subjects include some variability attributable to eyelid movements, tear film, blinking, eye saccades, and fixation as opposed to the dynamic OCE measurements made in anesthetized rabbits in this study.

The viscoelastic recovery response is a complex non-linear response due to unique corneal structural features e.g. inhomogeneity[115] due to the composition of its different layers and anisotropy because of the organization of collagen lamellae with preferential collagen fibril orientation.[9,10,24] The cornea, like other soft tissues, is visco-elastic, with a combination of elastic and viscous properties (due to the collagen fibers and the ground substance/extracellular matrix). Due to these attributes, corneal elastic moduli cannot be determined directly without making simplifying assumptions. Recently we used a modified Rayleigh–Lamb equation to quantitatively assess corneal viscoelasticity in *ex vivo* corneas using dynamic OCE imaging assuming free boundary conditions, corneal shape as a flat disk, corneal isotropy, and homogeneity.[167] While we acknowledge the limitations of assuming the cornea to be isotropic and homogeneous, these first-order simplifying assumptions will help us quantify the greatest factors contributing to the corneal material properties which can be improved upon in the future by advanced tissue modeling techniques. Future steps will include further development of viscoelastic mathematical modeling to account for corneal thickness, curvature, nonlinearity, viscosity, the effect of IOP, etc. that links the viscoelastic response obtained with dynamic OCE imaging to quantitative universal material properties like Young's modulus.

These preliminary *in vivo* results indicate that dynamic OCE imaging is capable of obtaining localized corneal biomechanical properties in rabbit corneas. The precision

obtained from short-term OCE reproducibility (0.01 ms^{-1}) is far less than the effect due to *in vitro* UV Riboflavin cross-linking (0.28 ms^{-1}),[145] which should provide the dynamic range needed for clinically relevant measurement of corneal biomechanical properties. The OCE measurements show a high degree of repeatability and reproducibility making it a precise technique for attaining *in vivo* viscoelastic recovery response (relaxation rate) at a specific location. Dynamic OCE imaging can be a promising tool for evaluation of biomechanical properties in a clinical set-up. Application of dynamic OCE to derive *in vivo* corneal material properties will allow us to measure and quantify the magnitude of ectatic diseases and effectiveness of UV Riboflavin cross-linking treatments and to follow the mechanical changes over time.

CHAPTER SEVEN

Conclusions and Future Directions

Conclusions

Characterizing the micro air-pulse stimulator parameters enabled a non-invasive loading mechanism to stimulate the cornea. Spatially localized air pulse stimulation allows for spatial characterization of the cornea and combining it with a phase-sensitive optical coherence tomography (OCT) as part of the optical coherence elastography (OCE) imaging system demonstrating promise in quantifying the corneal biomechanical properties while preserving the intact corneal shape and structure.

The acute effects of UV riboflavin cross-linking (CXL) treatment on the corneal ultrastructure and morphology were investigated in this dissertation by evaluating the change in collagen fibril spacing and corneal thickness after treatment. Although UV riboflavin cross-linking treatment produced an acute overall decrease in corneal thickness, no thickness difference is observed between the controls (hypertonic riboflavin only) and the CXL treated paired region (hypertonic riboflavin + UV irradiation) post-tissue processing. However, we demonstrated anterior collagen fibril spacing reduction in the CXL treated region, showing that acute CXL treatment-induced change are not only tonicity driven.

We demonstrated a way to control and maintain corneal thickness over a period of 200 minutes in controlled environmental conditions in *ex vivo* rabbit corneas and then applied optical coherence elastography imaging methods to quantify the influence of corneal hydration state and UV riboflavin cross-linking treatments on the measured corneal biomechanical properties. Corneal thickness and stiffness are correlated positively. Isotonic CXL treatment produced stiffer corneas; however, hypertonic CXL treatment produced a tonicity-driven stiffness decrease that offset the expected stiffer material properties due to CXL treatment, resulting in no change in corneal material properties. This demonstrates corneal hydration as an important factor in the

measurement of corneal biomechanics that can confound short-term effects due to CXL treatment.

We evaluated the biomechanical properties of the deep corneal stroma and the effect of a non-UV based collagen cross-linking technique: Rose Bengal Green Light Cross-linking (RGX) treatment as a safer alternative to UV riboflavin cross-linking treatment on the deep corneal stroma. This work provided the corneal depth dependent biomechanical properties and demonstrated increased stiffness in the deep stroma with RGX and CXL cross-linking treatments. We demonstrated the depth of diffusion of rose bengal dye to be approximately half the depth of diffusion of riboflavin solution obtained from previous studies.[139, 140] As the corneal depth up to which the photosensitizer diffuses is effectively absorbed by the UV or green light radiation during cross-linking treatment, depth of diffusion is an important factor to weigh in while considering the efficacy of cross-linking treatments.

Our preliminary *in vivo* results indicate that dynamic OCE imaging is capable of obtaining localized corneal biomechanical properties in rabbit corneas. The OCE measurements show a high degree of repeatability and reproducibility making it a precise technique for attaining *in vivo* viscoelastic recovery response (relaxation rate) at a specific location. Dynamic OCE imaging can be a promising tool for evaluation of biomechanical properties in a clinical set-up and will allow us to measure and quantify the magnitude of ectatic diseases and effectiveness of UV Riboflavin cross-linking treatments and to follow the mechanical changes over time in the future.

Future applications and directions

The ability to obtain point-wise measurements using the air pulse stimulator will enable the adaptation and implementation of dynamic optical coherence elastography (OCE) imaging to derive *in vivo* spatial characterization of corneal biomechanical

properties. This is an important advance because spatial variation in corneal biomechanical properties are the hallmark of ectatic conditions like keratoconus[83] or post-refractive surgical ectasia.[84] Future applications include quantifying the changes in the tissue's mechanical strength resulting from novel customized treatments protocols targeted to treat the locally affected regions during surgeries or cross-linking treatments. Biomechanical testing methods are being developed for application in the eye to characterize the biomechanical properties of ocular tissues, for e.g., sclera,[85] optic nerve head,[88, 168-170] lamina cribrosa,[171] etc. in order to understand the etiology of disease processes and provide efficient management therapies and track the efficacy of treatment. The air pulse stimulation characteristics are flexible and can be modified for future applications in other ocular tissues to stimulate and obtain biomechanical properties of the sclera (myopia),[85] lens (cataract),[86] extra-ocular muscles,[87] lamina cribrosa and optic nerve (glaucoma)[88] by re-configuring the required excitation air pulse characteristics suitable for the tissue.

UV riboflavin cross-linking procedure is FDA approved (as of April, 2016) to treat keratoconus and other ectasias. It is even more important to understand the biochemical and ultrastructural changes due to CXL treatment, in order to determine the most efficient protocol with the potential to deliver the magnitude needed to achieve maximal reduction in disease progression. We confined the investigation of ultrastructural changes due to CXL treatment in this work to only collagen fibril spacing; however, future studies should be towards evaluating the effect of CXL treatment and hydration influence on the proteoglycan-glycosaminoglycan complexes surrounding the collagen fibrils. This information can potentially aid in understanding the mechanism of CXL treatment with the goal to improve the efficacy of the cross-linking treatment and reduce the variability in the treatment outcomes. Future work should also focus towards understanding the long-term effects of cross-linking on the corneal ultrastructure. With

stromal reconstitution over time, there is high probability of treatment reversal resulting in the need for repeated CXL treatment. Is the rate of collagen regeneration affected by CXL treatment? Is repeating CXL treatment a good idea and at what stage is it indicated? These are all questions that have yet to be addressed.

The tools and techniques developed to perform OCE measurements in *ex vivo* rabbit eyes can be utilized directly to screen human donor corneas prior to corneal transplantation procedures, to evaluate their stiffness and aid in preventing future ectasias. However, additional information in the form of a normative database needs to be collected and established, before we can create an effective screening protocol. These tools and techniques developed in *ex vivo* rabbit eyes will be useful when applied to test the biomechanical strength of experimental artificial human corneas being grown on polymer scaffolds as an alternative replacement to human donor corneas during corneal transplantations.

Combining collagen cross-linking treatment in the deep stroma with corneal transplantation procedures to treat keratoconus like anterior lamellar keratoplasty or refractive surgeries like LASIK or photorefractive keratectomy (PRK) is proposed as a prophylactic measure to increase the posterior corneal stiffness and prevent future ectasia.[65] Quantifying deep corneal tissue properties will allow us to better understand the effects of experimental cross-linking in the deep stroma and this information will contribute to future applications in lamellar keratoplasty and refractive surgery through modification of deep corneal biomechanical properties.

Dynamic OCE enables localized measurement of *in vivo* corneal biomechanical properties. We have shown the feasibility of *in vivo* dynamic OCE imaging to obtain the viscoelastic recovery responses (relaxation rates) in rabbit corneas in this work. The immediate next step would be to perform OCE measurements in *ex vivo* and *in vivo* rabbit eyes to evaluate the effect of dampening due to orbital fat and ocular adnexa, the

effect of lid pressure on the cornea and the variable effect of increasing intra-ocular pressure (*ex vivo* vs. *in vivo*). Future steps will include further development of viscoelastic mathematical modeling to account for corneal thickness, curvature, nonlinearity, viscosity, the effect of IOP, etc. that links the viscoelastic response obtained with dynamic OCE imaging to quantitative universal material properties like Young's modulus.

References

1. Maurice DM. The Structure and Transparency of the Cornea. J Physiol-London 1957;136:263-&.

2. Meek KM, Leonard DW. Ultrastructure of the corneal stroma: a comparative study. Biophys J 1993;64:273-80.

3. Meek KM, Quantock AJ. The use of X-ray scattering techniques to determine corneal ultrastructure. Prog Retin Eye Res 2001;20:95-137.

4. Hanlon SD, Behzad AR, Sakai LY, Burns AR. Corneal stroma microfibrils. Exp Eye Res 2015;132:198-207.

5. Morishige N, Petroll WM, Nishida T, Kenney MC, Jester JV. Noninvasive corneal stromal collagen imaging using two-photon-generated second-harmonic signals. J Cataract Refract Surg 2006;32:1784-1791.

6. Meek KM, Boote C. The use of X-ray scattering techniques to quantify the orientation and distribution of collagen in the corneal stroma. Prog Retin Eye Res 2009;28:369-392.

7. Jester JV, Winkler M, Jester BE, et al. Evaluating Corneal Collagen Organization Using High Resolution Non Linear Optical (NLO) Macroscopy. Eye Contact Lens 2010;36:260-264.

8. Komai Y, Ushiki T. The three-dimensional organization of collagen fibrils in the human cornea and sclera. Invest Ophthalmol Vis Sci 1991;32:2244-2258.

9. Pinsky PM, van der Heide D, Chernyak D. Computational modeling of mechanical anisotropy in the cornea and sclera. J Cataract Refract Surg 2005;31:136-45.

10. Meek KM, Newton RH. Organization of collagen fibrils in the corneal stroma in relation to mechanical properties and surgical practice. J Refract Surg 1999;15:695-9.

11. Bron AJ. The architecture of the corneal stroma. Br J Ophthalmol 2001;85:379-81.

12. Michelacci YM. Collagens and proteoglycans of the corneal extracellular matrix. Braz J Med Biol Res 2003;36:1037-46.

13. Scott JE. Extracellular matrix, supramolecular organisation and shape. J Anat 1995;187 (Pt 2):259-69.

14. Lewis PN, Pinali C, Young RD, et al. Structural Interactions between Collagen and Proteoglycans Are Elucidated by Three-Dimensional Electron Tomography of Bovine Cornea. Structure 2010;18:239-245.

15. Hedblom EE. The role of polysaccharides in corneal swelling. Exp Eye Res 1961;1:81-91.

16. Hedbys BO, Dohlman CH. A new method for the determination of the swelling pressure of the corneal stroma in vitro. Exp Eye Res 1963;2:122-9.

17. Dohlman CH, Hedbys BO, Mishima S. The swelling pressure of the corneal stroma. Invest Ophthalmol 1962;1:158-62.

18. Klyce SD, Dohlman CH, Tolpin DW. In vivo determination of corneal swelling pressure. Exp Eye Res 1971;11:220-9.

19. Bonanno JA. Molecular mechanisms underlying the corneal endothelial pump. Exp Eye Res 2012;95:2-7.

20. Hoeltzel DA, Altman P, Buzard K, Choe K. Strip extensiometry for comparison of the mechanical response of bovine, rabbit, and human corneas. J Biomech Eng 1992;114:202-15.

21. Wollensak G, Spoerl E, Seiler T. Stress-strain measurements of human and porcine corneas after riboflavin-ultraviolet-A-induced cross-linking. J Cataract Refract Surg 2003;29:1780-1785.

22. Hjortdal JO. Regional elastic performance of the human cornea. J Biomech 1996;29:931-42.

23. Jue B, Maurice DM. The mechanical properties of the rabbit and human cornea. J Biomech 1986;19:847-53.

24. Nyquist GW. Rheology of the cornea: experimental techniques and results. Exp Eye Res 1968;7:183-8.

25. Dupps WJ, Jr., Netto MV, Herekar S, Krueger RR. Surface wave elastometry of the cornea in porcine and human donor eyes. J Refract Surg 2007;23:66-75.

26. Elsheikh A, Anderson K. Comparative study of corneal strip extensometry and inflation tests. Journal of the Royal Society, Interface / the Royal Society 2005;2:177-85.

27. Kling S, Remon L, Perez-Escudero A, Merayo-Lloves J, Marcos S. Corneal biomechanical changes after collagen cross-linking from porcine eye inflation experiments. Invest Ophthalmol Vis Sci 2010;51:3961-8.

28. Scarcelli G, Kling S, Quijano E, et al. Brillouin microscopy of collagen crosslinking: noncontact depth-dependent analysis of corneal elastic modulus. Invest Ophthalmol Vis Sci 2013;54:1418-25.

29. Cherfan D, Verter EE, Melki S, et al. Collagen Cross-Linking Using Rose Bengal and Green Light to Increase Corneal Stiffness. Invest Ophthalmol Vis Sci 2013;54:3426-3433.

30. Kotecha A, Elsheikh A, Roberts CR, Zhu H, Garway-Heath DF. Corneal thickness- and age-related biomechanical properties of the cornea measured with the ocular response analyzer. Invest Ophthalmol Vis Sci 2006;47:5337-47.

31. Kling S, Bekesi N, Dorronsoro C, Pascual D, Marcos S. Corneal viscoelastic properties from finite-element analysis of in vivo air-puff deformation. PLoS One 2014;9:e104904.

32. Ophir J, Cespedes I, Ponnekanti H, Yazdi Y, Li X. Elastography: a quantitative method for imaging the elasticity of biological tissues. Ultrason Imaging 1991;13:111-34.

33. Parker KJ, Doyley MM, Rubens DJ. Imaging the elastic properties of tissue: the 20 year perspective. Phys Med Biol 2011;56:R1-R29.

34. Toyono T, Usui T, Yokoo S, et al. Angiopoietin-Like 7 Is an Anti-Angiogenic Protein Required to Prevent Vascularization of the Cornea. PLoS One 2015;10.

35. Wang JH, Changchien CS, Hung CH, et al. FibroScan and ultrasonography in the prediction of hepatic fibrosis in patients with chronic viral hepatitis. J Gastroenterol 2009;44:439-46.

36. Wojcinski S, Farrokh A, Weber S, et al. Multicenter study of ultrasound real-time tissue elastography in 779 cases for the assessment of breast lesions: improved diagnostic performance by combining the BI-RADS(R)-US classification system with sonoelastography. Ultraschall Med 2010;31:484-91.

37. Geerling G, Duncker GIW. Diagnostics and Therapy for Endothelial Diseases of the Cornea - Is There Still a Gold Standard? Klin Monatsbl Augenh 2012;229:593-593.

38. Castaneda B, Hoyt K, Westesson K, et al. Performance of three-dimensional sonoelastography in prostate cancer detection: A comparison between ex vivo and in vivo experiments. 2009 IEEE International Ultrasonics Symposium, 2009:519-522.

39. Dighe M, Kim J, Luo S, Kim Y. Utility of the ultrasound elastographic systolic thyroid stiffness index in reducing fine-needle aspirations. J Ultrasound Med 2010;29:565-574.

40. Schmitt J. OCT elastography: imaging microscopic deformation and strain of tissue. Opt Express 1998;3:199-211.

41. Kennedy KM, Chin L, McLaughlin RA, et al. Quantitative micro-elastography: imaging of tissue elasticity using compression optical coherence elastography. Sci Rep 2015;5:15538.

42. Ford MR, Dupps WJ, Jr., Rollins AM, Roy AS, Hu Z. Method for optical coherence elastography of the cornea. J Biomed Opt 2011;16:016005.

43. Ahmad A, Huang PC, Sobh NA, et al. Mechanical contrast in spectroscopic magnetomotive optical coherence elastography. Phys Med Biol 2015;60:6655-68.

44. Tanter M, Touboul D, Gennisson JL, Bercoff J, Fink M. High-Resolution Quantitative Imaging of Cornea Elasticity Using Supersonic Shear Imaging. IEEE Trans Med Imaging 2009;28:1881-1893.

45. Li C, Guan G, Cheng X, Huang Z, Wang RK. Quantitative elastography provided by surface acoustic waves measured by phase-sensitive optical coherence tomography. Opt Lett 2012;37:722-4.

46. Nguyen TM, Arnal B, Song S, et al. Shear wave elastography using amplitude-modulated acoustic radiation force and phase-sensitive optical coherence tomography. J Biomed Opt 2015;20:016001.

47. Manapuram RK, Aglyamov S, Menodiado FM, et al. Estimation of shear wave velocity in gelatin phantoms utilizing PhS-SSOCT. Laser Phys Lett 2012;22:1439-1444.

48. Wang S, Larin KV. Optical coherence elastography for tissue characterization: a review. J Biophotonics 2015;8:279-302.

49. Kennedy BF, Kennedy KM, Oldenburg AL, et al. Optical Coherence Elastography. In: Drexler W, Fujimoto GJ, editors. Optical Coherence Tomography: Technology and Applications. Cham: Springer International Publishing, 2015:1007-1054.

50. Wang S, Larin KV, Li J, et al. A focused air-pulse system for optical-coherence-tomography-based measurements of tissue elasticity. Laser Phys Lett 2013;10:075605.

51. Dupps WJ, Jr., Wilson SE. Biomechanics and wound healing in the cornea. Exp Eye Res 2006;83:709-20.

52. Wollensak G, Spoerl E, Seiler T. Riboflavin/ultraviolet-a-induced collagen crosslinking for the treatment of keratoconus. Am J Ophthalmol 2003;135:620-7.

53. Hersh PS, Greenstein SA, Fry KL. Corneal collagen crosslinking for keratoconus and corneal ectasia: One-year results. J Cataract Refract Surg 2011;37:149-160.

54. Tomkins O, Garzozi HJ. Collagen cross-linking: Strengthening the unstable cornea. Clin Ophthalmol 2008;2:863-7.

55. Meek KM, Tuft SJ, Huang Y, et al. Changes in collagen orientation and distribution in keratoconus corneas. Invest Ophthalmol Vis Sci 2005;46:1948-56.

56. Radner W, Zehetmayer M, Skorpik C, Mallinger R. Altered organization of collagen in the apex of keratoconus corneas. Ophthalmic Res 1998;30:327-32.

57. Hafezi F, Kanellopoulos J, Wiltfang R, Seiler T. Corneal collagen crosslinking with riboflavin and ultraviolet A to treat induced keratectasia after laser in situ keratomileusis. J Cataract Refract Surg 2007;33:2035-40.

58. Wollensak G, Spoerl E, Seiler T. Riboflavin/ultraviolet-a-induced collagen crosslinking for the treatment of keratoconus. Am J Ophthalmol 2003;135:620-7.

59. Wollensak G, Spoerl E, Seiler T. Stress-strain measurements of human and porcine corneas after riboflavin-ultraviolet-A-induced cross-linking. J Cataract Refract Surg 2003;29:1780-5.

60. Spoerl E, Huhle M, Seiler T. Induction of cross-links in corneal tissue. Exp Eye Res 1998;66:97-103.

61. Brummer G, Littlechild S, McCall S, Zhang Y, Conrad GW. The role of nonenzymatic glycation and carbonyls in collagen cross-linking for the treatment of keratoconus. Invest Ophthalmol Vis Sci 2011;52:6363-6369.

62. Malik NS, Moss SJ, Ahmed N, et al. Ageing of the human corneal stroma: structural and biochemical changes. Biochim Biophys Acta 1992;1138:222-228.

63. Sady C, Khosrof S, Nagaraj R. Advanced Maillard reaction and crosslinking of corneal collagen in diabetes. Biochem Biophys Res Commun 1995;214:793-797.

64. O'Brart DP. Corneal collagen cross-linking: a review. J Optom 2014;7:113-124.

65. Randleman JB, Khandelwal SS, Hafezi F. Corneal Cross-Linking. Surv Ophthalmol 2015.

66. Dias J, Ziebarth NM. Impact of Hydration Media on Ex Vivo Corneal Elasticity Measurements. Eye Contact Lens 2015;41:281-6.

67. Kling S, Marcos S. Effect of hydration state and storage media on corneal biomechanical response from in vitro inflation tests. J Refract Surg 2013;29:490-7.

68. Kling S, Marcos S. Contributing factors to corneal deformation in air puff measurements. Invest Ophthalmol Vis Sci 2013;54:5078-85.

69. Kohlhaas M, Spoerl E, Schilde T, et al. Biomechanical evidence of the distribution of cross-links in corneas treated with riboflavin and ultraviolet A light. J Cataract Refract Surg 2006;32:279-83.

70. Wollensak G, Sporl E, Reber F, Pillunat L, Funk R. Corneal endothelial cytotoxicity of riboflavin/UVA treatment in vitro. Ophthalmic Res 2003;35:324-328.

71. Wang T, Peng YB, Shen NC, et al. Photochemical activation increases the porcine corneal stiffness and resistance to collagenase digestion. Exp Eye Res 2014;123:97-104.

72. Thomasy SM, Raghunathan VK, Winkler M, et al. Elastic modulus and collagen organization of the rabbit cornea: epithelium to endothelium. Acta biomaterialia 2014;10:785-91.

73. Ojeda JL, Ventosa JA, Piedra S. The three-dimensional microanatomy of the rabbit and human cornea. A chemical and mechanical microdissection-SEM approach. J Anat 2001;199:567-76.

74. Henriksson JT, McDermott AM, Bergmanson JP. Dimensions and morphology of the cornea in three strains of mice. Invest Ophthalmol Vis Sci 2009;50:3648-54.

75. Goes RM, Barbosa FL, De Faria ESSJ, Haddad A. Morphological and autoradiographic studies on the corneal and limbal epithelium of rabbits. Anat Rec (Hoboken) 2008;291:191-203.

76. Kaye GI, Pappas GD. Studies on the cornea. I. The fine structure of the rabbit cornea and the uptake and transport of colloidal particles by the cornea in vivo. J Cell Biol 1962;12:457-79.

77. Van Horn DL, Sendele DD, Seideman S, Buco PJ. Regenerative capacity of the corneal endothelium in rabbit and cat. Invest Ophthalmol Vis Sci 1977;16:597-613.

78. Luce DA. Determining in vivo biomechanical properties of the cornea with an ocular response analyzer. J Cataract Refract Surg 2005;31:156-62.

79. Hon Y, Lam AKC. Corneal Deformation Measurement Using Scheimpflug Noncontact Tonometry. Optom Vis Sci 2013;90:E1-E8.

80. McKnight AL, Kugel JL, Rossman PJ, et al. MR elastography of breast cancer: preliminary results. AJR Am J Roentgenol 2002;178:1411-7.

81. Liang X, Orescanin M, Toohey KS, Insana MF, Boppart SA. Acoustomotive optical coherence elastography for measuring material mechanical properties. Opt Lett 2009;34:2894-6.

82. Grabner G, Eilmsteiner R, Steindl C, et al. Dynamic corneal imaging. J Cataract Refract Surg 2005;31:163-74.

83. Gefen A, Shalom R, Elad D, Mandel Y. Biomechanical analysis of the keratoconic cornea. J Mech Behav Biomed Mater 2009;2:224-36.

84. Kerautret J, Colin J, Touboul D, Roberts C. Biomechanical characteristics of the ectatic cornea. J Cataract Refract Surg 2008;34:510-3.

85. McBrien NA, Jobling AI, Gentle A. Biomechanics of the sclera in myopia: extracellular and cellular factors. Optom Vis Sci 2009;86:E23-30.

86. Pedrigi RM, Humphrey JD. Computational model of evolving lens capsule biomechanics following cataract-like surgery. Ann Biomed Eng 2011;39:537-48.

87. Yoo L, Reed J, Shin A, Demer JL. Atomic force microscopy determination of Youngs modulus of bovine extra-ocular tendon fiber bundles. J Biomech 2014;47:1899-903.

88. Downs JC, Roberts MD, Burgoyne CF. Mechanical environment of the optic nerve head in glaucoma. Optom Vis Sci 2008;85:425-35.

89. Hayes S, Boote C, Kamma-Lorger CS, et al. Riboflavin/UVA collagen cross-linking-induced changes in normal and keratoconus corneal stroma. PLoS One 2011;6:e22405.

90. Andreassen TT, Simonsen AH, Oxlund H. Biomechanical properties of keratoconus and normal corneas. Exp Eye Res 1980;31:435-441.

91. McCall AS, Kraft S, Edelhauser HF, et al. Mechanisms of corneal tissue cross-linking in response to treatment with topical riboflavin and long-wavelength ultraviolet radiation (UVA). Invest Ophthalmol Vis Sci 2010;51:129-138.

92. Hayes S, Kamma-Lorger CS, Boote C, et al. The Effect of Riboflavin/UVA Collagen Cross-linking Therapy on the Structure and Hydrodynamic Behaviour of the Ungulate and Rabbit Corneal Stroma. PLoS One 2013;8.

93. Gautieri A, Redaelli A, Buehler MJ, Vesentini S. Age- and diabetes-related nonenzymatic crosslinks in collagen fibrils: candidate amino acids involved in Advanced Glycation End-products. Matrix Biol 2014;34:89-95.

94. Tanaka S, Avigad G, Brodsky B, Eikenberry EF. Glycation induces expansion of the molecular packing of collagen. J Mol Biol 1988;203:495-505.

95. Wollensak G, Wilsch M, Spoerl E, Seiler T. Collagen fiber diameter in the rabbit cornea after collagen crosslinking by riboflavin/UVA. Cornea 2004;23:503-507.

96. Meek KM, Fullwood NJ, Cooke PH, et al. Synchrotron x-ray diffraction studies of the cornea, with implications for stromal hydration. Biophys J 1991;60:467-74.

97. Hanlon SD, Patel NB, Burns AR. Assessment of postnatal corneal development in the C57BL/6 mouse using spectral domain optical coherence tomography and microwave-assisted histology. Exp Eye Res 2011;93:363-370.

98. Russin WA, Trivett CL. Vacuum-Microwave Combination for Processing Plant Tissues for Electron Microscopy. In: Giberson RT, Demaree RS, editors. Microwave Techniques and Protocols. Totowa, NJ: Humana Press, 2001:25-35.

99. Connon CJ, Meek KM, Newton RH, et al. Hyaluronidase treatment, collagen fibril packing, and normal transparency in rabbit corneas. J Refract Surg 2000;16:448-455.

100. Freund DE, McCally RL, Farrell RA, et al. Ultrastructure in anterior and posterior stroma of perfused human and rabbit corneas. Relation to transparency. Invest Ophthalmol Vis Sci 1995;36:1508-1523.

101. Slack JW, Kangas TA, Edelhauser HF, Geroski DH, Mcdermott ML. Comparison of Corneal Preservation Media for Corneal Hydration and Stromal Proteoglycan Loss. Cornea 1992;11:204-210.

102. Mergler S, Pleyer U. The human corneal endothelium: new insights into electrophysiology and ion channels. Prog Retin Eye Res 2007;26:359-378.

103. Spoerl E, Wollensak G, Seiler T. Increased resistance of crosslinked cornea against enzymatic digestion. Curr Eye Res 2004;29:35-40.

104. Chan T, Payor S, Holden BA. Corneal Thickness Profiles in Rabbits Using an Ultrasonic Pachometer. Invest Ophthalmol Vis Sci 1983;24:1408-1410.

105. Giraud JP, Pouliquen Y, Offret G, Payrau P. Statistical morphometric studies in normal human and rabbit corneal stroma. Exp Eye Res 1975;21:221-229.

106. Dorronsoro C, Pascual D, Perez-Merino P, Kling S, Marcos S. Dynamic OCT measurement of corneal deformation by an air puff in normal and cross-linked corneas. Biomed Opt Express 2012;3:473-487.

107. Twa MD, Li J, Vantipalli S, et al. Spatial characterization of corneal biomechanical properties with optical coherence elastography after UV cross-linking. Biomed Opt Express 2014;5:1419-27.

108. Ford MR, Roy AS, Rollins AM, Dupps WJ. Serial biomechanical comparison of edematous, normal, and collagen crosslinked human donor corneas using optical coherence elastography. J Cataract Refract Surg 2014;40:1041-1047.

109. Li JS, Singh M, Han ZL, et al. A comparison study of Riboflavin/UV-A and Rose-Bengal/Green light cross-linking of the rabbit corneas using optical coherence elastography. Proc Spie 2016;9693.

110. Nguyen TM, Aubry JF, Touboul D, et al. Monitoring of Cornea Elastic Properties Changes during UV-A/Riboflavin-Induced Corneal Collagen Cross-Linking using Supersonic Shear Wave Imaging: A Pilot Study. Invest Ophthalmol Vis Sci 2012;53:5948-5954.

111. Bueno JM, Gualda EJ, Giakoumaki A, et al. Multiphoton microscopy of ex vivo corneas after collagen cross-linking. Invest Ophthalmol Vis Sci 2011;52:5325-31.

112. Elsheikh A, Wang DF, Brown M, et al. Assessment of corneal biomechanical properties and their variation with age. Curr Eye Res 2007;32:11-19.

113. Nash IS, Greene PR, Foster CS. Comparison of Mechanical-Properties of Keratoconus and Normal Corneas. Exp Eye Res 1982;35:413-424.

114. Winkler M, Chai D, Kriling S, et al. Nonlinear optical macroscopic assessment of 3-D corneal collagen organization and axial biomechanics. Invest Ophthalmol Vis Sci 2011;52:8818-27.

115. Maurice DM. The structure and transparency of the cornea. J Physiol 1957;136:263-86.

116. Mishima S, Maurice DM. The effect of normal evaporation on the eye. Exp Eye Res 1961;1:46-52.

117. Cohen SR, Polse KA, Brand RJ, Mandell RB. Humidity effects on corneal hydration. Invest Ophthalmol Vis Sci 1990;31:1282-7.

118. Metha AB, Crane AM, Rylander HG, 3rd, Thomsen SL, Albrecht DG. Maintaining the cornea and the general physiological environment in visual neurophysiology experiments. J Neurosci Methods 2001;109:153-66.

119. Li J, Wang S, Singh M, et al. Air-pulse OCE for assessment of age-related changes in mouse corneain vivo. Laser Phys Lett 2014;11:065601.

120. Li J, Wang S, Manapuram RK, et al. Dynamic optical coherence tomography measurements of elastic wave propagation in tissue-mimicking phantoms and mouse cornea in vivo. J Biomed Opt 2013;18:121503.

121. Manapuram RK, Manne VGR, Larin KV. Development of phase-stabilized swept-source OCT for the ultrasensitive quantification of microbubbles. Laser Phys Lett 2008;18:1080-1086.

122. Twa MD, Vantipalli S, Sing M, Li JS, Larin KV. Influence of corneal hydration on optical coherence elastography. Proc Spie 2016;9693.

123. Vinciguerra P, Albe E, Mahmoud AM, et al. Intra- and postoperative variation in ocular response analyzer parameters in keratoconic eyes after corneal cross-linking. J Refract Surg 2010;26:669-676.

124. Goldich Y, Marcovich AL, Barkana Y, et al. Clinical and corneal biomechanical changes after collagen cross-linking with riboflavin and UV irradiation in patients with progressive keratoconus: results after 2 years of follow-up. Cornea 2012;31:609-614.

125. Brubaker RF, Kupfer C. Microcryoscopic determination of the osmolality of interstitial fluid in the living rabbit cornea. Invest Ophthalmol 1962;1:653-60.

126. Stahl U, Willcox M, Stapleton F. Osmolality and tear film dynamics. Clin Exp Optom 2012;95:3-11.

127. Andreassen TT, Simonsen AH, Oxlund H. Biomechanical properties of keratoconus and normal corneas. Exp Eye Res 1980;31:435-41.

128. Muller LJ, Pels E, Vrensen GF. The specific architecture of the anterior stroma accounts for maintenance of corneal curvature. Br J Ophthalmol 2001;85:437-443.

129. Winkler M, Shoa G, Xie Y, et al. Three-dimensional distribution of transverse collagen fibers in the anterior human corneal stroma. Invest Ophthalmol Vis Sci 2013;54:7293-301.

130. Petsche SJ, Pinsky PM. The role of 3-D collagen organization in stromal elasticity: a model based on X-ray diffraction data and second harmonic-generated images. Biomech Model Mechanobiol 2013;12:1101-13.

131. Randleman JB, Dawson DG, Grossniklaus HE, McCarey BE, Edelhauser HF. Depth-dependent cohesive tensile strength in human donor corneas: implications for refractive surgery. J Refract Surg 2008;24:S85-9.

132. Dias JM, Ziebarth NM. Anterior and posterior corneal stroma elasticity assessed using nanoindentation. Exp Eye Res 2013;115:41-46.

133. Freund DE, McCally RL, Farrell RA, et al. Ultrastructure in anterior and posterior stroma of perfused human and rabbit corneas. Relation to transparency. Invest Ophthalmol Vis Sci 1995;36:1508-23.

134. Morishige N, Takagi Y, Chikama T, Takahara A, Nishida T. Three-Dimensional Analysis of Collagen Lamellae in the Anterior Stroma of the Human Cornea Visualized by Second Harmonic Generation Imaging Microscopy. Invest Ophthalmol Vis Sci 2011;52:911-915.

135. Abahussin M, Hayes S, Cartwright NEK, et al. 3D Collagen Orientation Study of the Human Cornea Using X-ray Diffraction and Femtosecond Laser Technology. Invest Ophthalmol Vis Sci 2009;50:5159-5164.

136. Castoro JA, Bettelheim AA, Bettelheim FA. Water gradients across bovine cornea. Invest Ophthalmol Vis Sci 1988;29:963-968.

137. Wang S, Larin KV. Shear wave imaging optical coherence tomography (SWI-OCT) for ocular tissue biomechanics. Opt Lett 2014;39:41-4.

138. Petsche SJ, Chernyak D, Martiz J, Levenston ME, Pinsky PM. Depth-Dependent Transverse Shear Properties of the Human Corneal Stroma. Invest Ophthalmol Vis Sci 2012;53:873-880.

139. Wollensak G, Spoerl E, Wilsch M, Seiler T. Keratocyte apoptosis after corneal collagen cross-linking using riboflavin/UVA treatment. Cornea 2004;23:43-49.

140. Gallhoefer NS, Spiess BM, Guscetti F, et al. Penetration depth of corneal cross-linking with riboflavin and UV-A (CXL) in horses and rabbits. Vet Ophthalmol 2015.

141. Castaneda B, Hoyt K, Westesson K, et al. Performance of three-dimensional sonoelastography in prostate cancer detection: a comparison between ex vivo and in vivo experiments. Ultrasonics Symposium (IUS), 2009 IEEE International: IEEE, 2009:519-522.

142. Dupps WJ, Jr., Netto MV, Herekar S, Krueger RR. Surface wave elastometry of the cornea in porcine and human donor eyes. J Refract Surg 2007;23:66-75.

143. Scarcelli G, Pineda R, Yun SH. Brillouin optical microscopy for corneal biomechanics. Invest Ophthalmol Vis Sci 2012;53:185-90.

144. Schwarz W, Keyserlingk DG. [On the fine structure of the human cornea with special reference to the problem of transparency]. Z Zellforsch Mikrosk Anat 1966;73:540-8.

145. Muller LJ, Pels E, Vrensen GF. The specific architecture of the anterior stroma accounts for maintenance of corneal curvature. Br J Ophthalmol 2001;85:437-43.

146. Lucio A, Smith RL. Architecture of the corneal stroma of the hen. Acta Anat (Basel) 1984;120:196-201.

147. Li J, Han Z, Singh M, Twa MD, Larin KV. Differentiating untreated and cross-linked porcine corneas of the same measured stiffness with optical coherence elastography. J Biomed Opt 2014;19:110502-110502.

148. Han ZL, Aglyamov SR, Li JS, et al. Quantitative assessment of corneal viscoelasticity using optical coherence elastography and a modified Rayleigh-Lamb equation. J Biomed Opt 2015;20.

149. Kolen AF, Miller NR, Ahmed EE, Bamber JC. Characterization of cardiovascular liver motion for the eventual application of elasticity imaging to the liver in vivo. Phys Med Biol 2004;49:4187-206.

150. Stalmans I, Harris A, Vanbellinghen V, Zeyen T, Siesky B. Ocular pulse amplitude in normal tension and primary open angle glaucoma. J Glaucoma 2008;17:403-407.

151. Pernot M, Fujikura K, Fung-Kee-Fung SD, Konofagou EE. ECG-gated, mechanical and electromechanical wave imaging of cardiovascular tissues in vivo. Ultrasound Med Biol 2007;33:1075-85.

152. Huwart L, Peeters F, Sinkus R, et al. Liver fibrosis: non-invasive assessment with MR elastography. NMR Biomed 2006;19:173-9.

153. ISO B. 5725-1: 1994. Accuracy (trueness and precision) of measurement methods and results--part;1.

154. Bland JM, Altman DG. Statistical Methods for Assessing Agreement between Two Methods of Clinical Measurement. Lancet 1986;1:307-310.

155. Shrout PE, Fleiss JL. Intraclass correlations: uses in assessing rater reliability. Psychol Bull 1979;86:420-8.

156. Bartlett JW, Frost C. Reliability, repeatability and reproducibility: analysis of measurement errors in continuous variables. Ultrasound Obstet Gynecol 2008;31:466-75.

157. Vaz S, Falkmer T, Passmore AE, Parsons R, Andreou P. The Case for Using the Repeatability Coefficient When Calculating Test–Retest Reliability. PLoS One 2013;8:e73990.

158. Li JS, Singh M, Vantipalli S, et al. Assessment of the biomechanical properties of porcine cornea after UV cross-linking at different intraocular pressures. Proc Spie 2015;9327.

159. Faber C, Scherfig E, Prause JU, Sorensen KE. Corneal thickness in pigs measured by ultrasound pachymetry in vivo. Scand J Lab Anim Sci 2008;35:39-43.

160. Kling S, Marcos S. Effect of hydration state and storage media on corneal biomechanical response from in vitro inflation tests. J Refract Surg 2013;29:490-497.

161. Yoo L, Reed J, Shin A, et al. Characterization of Ocular Tissues Using Microindentation and Hertzian Viscoelastic Models. Invest Ophthalmol Vis Sci 2011;52:3475-3482.

162. Nemeth G, Hassan Z, Csutak A, et al. Repeatability of ocular biomechanical data measurements with a Scheimpflug-based noncontact device on normal corneas. J Refract Surg 2013;29:558-63.

163. Kynigopoulos M, Schlote T, Kotecha A, et al. Repeatability of intraocular pressure and corneal biomechanical properties measurements by the ocular response analyser. Klin Monatsbl Augenh 2008;225:357-60.

164. Kopito R, Gaujoux T, Montard R, et al. Reproducibility of viscoelastic property and intraocular pressure measurements obtained with the Ocular Response Analyzer. Acta Ophthalmol (Copenh) 2011;89:e225-e230.

165. Bak-Nielsen S, Pedersen IB, Ivarsen A, Hjortdal J. Repeatability, Reproducibility, and Age Dependency of Dynamic Scheimpflug-Based Pneumotonometer and Its Correlation With a Dynamic Bidirectional Pneumotonometry Device. Cornea 2015;34:71-77.

166. Wasielica-Poslednik J, Berisha F, Aliyeva S, Pfeiffer N, Hoffmann EM. Reproducibility of ocular response analyzer measurements and their correlation with central corneal thickness. Graefes Arch Clin Exp Ophthalmol 2010;248:1617-1622.

167. Han Z, Aglyamov SR, Li J, et al. Quantitative assessment of corneal viscoelasticity using optical coherence elastography and a modified Rayleigh–Lamb equation. J Biomed Opt 2015;20:020501-020501.

168. Burgoyne CF, Downs JC. Premise and prediction-how optic nerve head biomechanics underlies the susceptibility and clinical behavior of the aged optic nerve head. J Glaucoma 2008;17:318-28.

169. Sigal IA, Ethier CR. Biomechanics of the optic nerve head. Exp Eye Res 2009;88:799-807.

170. Downs JC. Optic nerve head biomechanics in aging and disease. Exp Eye Res 2015;133:19-29.

171. Downs JC, Roberts MD, Sigal IA. Glaucomatous cupping of the lamina cribrosa: A review of the evidence for active progressive remodeling as a mechanism. Exp Eye Res 2011;93:133-140.